University of Crete

Master Thesis

Coupled Accelerating Airy Waves in Fiber Optics

Author:
Gkoutsoulas Michail

Supervisor:
Efremidis Nikolaos

A thesis submitted in fulfilment of the requirements for the degree of Master of Science

in the

Department of Applied Mathematics

November 12, 2015

"The most exciting phrase to hear in science, the one that heralds new discoveries, is not 'Eureka!' but 'That's funny...'."

Isaac Asimov

UNIVERSITY OF CRETE

Abstract

Faculty Of Sciences and Engineering
Department of Applied Mathematics

Master of Science

Coupled Accelerating Airy Waves in Fiber Optics

by Gkoutsoulas Michail

More than three decades ago Berry and Balazs proposed theoretically that the Schrödinger equation describing a free particle admits a nonspreading Airy wave packet solution. This Airy packet corresponds to a family of orbits represented by a parabola. Although the most exotic feature of this Airy packet sparked the idea behind this thesis; to copropagate signal pulse along with an accelerating Airy (control) pulse. Our goal was to show that depending on Airy$'s$ parameters we can control the evolution of the spectrum and the temporal location of the signal pulse. So by properly assuming an Airy pulse we can accelerate or decelerate a signal pulse while we can manipulate the signal pulse to follow Airy$'s$ parabolic trajectory. The corresponding simulations both in the real and in the spectral space were discussed.

Acknowledgements

I would like to express my gratitude to my supervisor Nikolaos Efremidis for the useful comments, remarks and engagement through the learning process of this master thesis. Furthermore I would like to thank Vasileios Paltoglou for introducing me to the topic as well for the support on the way. I would like to thank my loved ones, who have supported me throughout entire process, both by keeping me harmonious and helping me putting pieces together. I will be grateful forever for your love.

Contents

I dedicate my dissertation work to my family and friends. . .

Chapter 1

General Introduction about Optical Fibers

1.1 Brief Historical Perspective

Though the very important discovery that light's guidance is due to the total reflection inside an optic fibre was made in the early 1900, technical problems didn't made easy to create efficient enough optic fibres in order to study relative to the optics physical phenomena. The complexity of nonlinear phenomena was added to the technical problems making the creation of less lossy optic fibres urgent. Although uncladded fibers were built from 1920's it wasn't until 1957 when van Heel and Hopkins and Kapany proposed that the usage of dielectric cladding was essential in the optics field. [1–3]

A very important contribution to the field of fiber optics was made when it was suggested the existence of soliton-like pulses as an interaction between the dispersive and nonlinear effects [4] while they propagate in optic fibres . This had a radical contribution in the generation and control of ultra short pulses . Pulse compression along with optical-switching methods were developed in the 1980s and lead to the exploitation of nonlinear effects developed in fiber optics.[5–9]

Later the usage of rare-earth elements in optic fibers contribute significantly in the growth of optic amplifiers that lead to the generation of a new type of amplifiers with specific advantages. Optical fibers doped with Erbium were in particular interest because they operate in the wavelength region 1.55 μm and thus are significantly important for fiber optic lightwave systems [10]. Although the innovative breakthrough, that doped optic fibers led to the employment of two nonlinear effects named Raman scattering and four-wave mixing, that occur

in optic fibers, led to one very special category of amplifiers which is independent of rare-earth elements and created in the early 2000. It's special characteristic is that it can operate in any spectral region. That was very important for the telecommunication companies because since then the only optic fibres that existed were able to operate in a very specific spectral region [11].

The creation of such very efficient amplifiers made it easier to study more complex phenomena than optical solitons such as dispersion managed solitons and dissipative solitons [12–15]. The development of new fibers where the structural changes affect both their dispersive and nonlinear properties was crucial importance to the growth of fibres which have two wavelengths where the group velocity dispersion is equal to zero. That changes in the group velocity dispersion are very important if someone consider the critical role of (GVD) in the propagation of pulses; different spectral components of the beam travel at different speeds which leads to the pulse broadening.

1.2 Propagation in Optic Fibers

In order to describe at first and then to understand the nonlinear phenomena in optical fibers, we should consider the theory of electromagnetic wave propagation in dispersive nonlinear media. Later we will show the equations that govern the wave propagation in single-mode fibers. Beginning from Maxwell's equations and using the theory of pulse propagation in non dispersive media under the slow varying envelope approximation we will show how under particular assumptions Maxwell's equations lead to Non Linear Schrödinger equation.

1.2.1 Maxwell's Equations

As we already know the equations that govern both all the electromagnetic phenomena and the propagation of optical beams in fibers are Maxwell's Equations and can be written in the following form [16]

$$\nabla \times \mathbf{E} = -\frac{\partial \mathbf{B}}{\partial t} \tag{1.1}$$

$$\nabla \times \mathbf{H} = \mathbf{J} + \frac{\partial \mathbf{D}}{\partial t} \tag{1.2}$$

$$\nabla \cdot \mathbf{D} = \rho_f \tag{1.3}$$

$$\nabla \cdot \mathbf{B} = 0 \tag{1.4}$$

where **E** and **H** are electric and magnetic field vectors respectively and **D**, **B** are the corresponding electric and magnetic flux densities. The current density vector **J** and the charge density ρ_f represent the sources for the electromagnetic field. In the absence of free charges in a medium such as optical fibers **J**=0 and ρ_f=0 too.

The flux densities **D** and **B** arise in response to the electric and magnetic fields **E** and **H** propagating inside the medium and are related to them through the constitutive relations

$$\mathbf{D} = \epsilon_0 \mathbf{E} + \mathbf{P} \tag{1.5}$$

$$\mathbf{B} = \mu_0 \mathbf{H} + \mathbf{M} \tag{1.6}$$

where ϵ_0 is the vacuum permittivity, μ_0 is the vacuum permeability, and **P** and **M** are the induced electric and magnetic polarizations. For a non-magnetic medium such as optic fibers, $\mathbf{M} = 0$.

We can use Maxwell's equations to derive the wave equation that describes light propagation in optical fibers. Wave equation can be obtained simply by taking the curl of Eq. (1.1) and using Eqs. (1.2),(1.3),(1.4)

$$\nabla \times \nabla \times \mathbf{E} = \nabla \times \left(-\frac{\partial \mathbf{B}}{\partial t} \right) = \nabla \times \left(-\frac{\partial \left(\mu_0 \mathbf{H} + \mathbf{M} \right)}{\partial t} \right) = \nabla \times \left(-\mu_0 \frac{\partial \mathbf{H}}{\partial t} - \frac{\partial \mathbf{M}}{\partial t} \right) =$$

$$= -\nabla \times \mathbf{H} \mu_0 \frac{\partial}{\partial t} - \nabla \times \frac{\partial \mathbf{M}}{\partial t} = -\left(\mathbf{J} + \frac{\partial \mathbf{D}}{\partial t} \right) \mu_0 \frac{\partial}{\partial t} = -\mu_0 \frac{\partial^2 \mathbf{D}}{\partial t^2} = -\mu_0 \epsilon_0 \frac{\partial^2 \mathbf{E}}{\partial t^2} - \mu_0 \frac{\partial^2 \mathbf{P}}{\partial t^2}$$

By assuming $\mu_0 \epsilon_0 = -\frac{1}{c^2}$ we finally obtain that

$$\nabla \times \nabla \times \mathbf{E} = -\frac{1}{c^2} \frac{\partial^2 \mathbf{E}}{\partial t^2} - \mu_0 \frac{\partial^2 \mathbf{P}}{\partial t^2} \tag{1.7}$$

where c is the speed of light in vacuum. To complete the description, a relation between the induced polarization **P** and the electric field **E** is needed. If we include only the third-order nonlinear effects governed by $\chi^{(3)}$, the induced polarization consists of two parts such that [17–19].

$$\mathbf{P}(r,t) = \mathbf{P}_L(r,t) + \mathbf{P}_{NL}(r,t) \tag{1.8}$$

where the linear $\mathbf{P}_L$ and the nonlinear part $\mathbf{P}_{NL}$ are related to the electric field by the general relations

$$\mathbf{P}_L(r,t) = \epsilon_0 \int_{-\infty}^{t} \chi^{(1)(t-t')} \cdot \mathbf{E}(r,t')\, dt' \tag{1.9}$$

$$\mathbf{P}_{NL}(r,t) = \epsilon_0 \int_{-\infty}^{t} dt_1 \int_{-\infty}^{t} dt_2 \int_{-\infty}^{t} dt_3 \times \chi^{(3)}(t-t_1, t-t_2, t-t_3) \vdots \mathbf{E}(r,t_1)\,\mathbf{E}(r,t_2)\,\mathbf{E}(r,t_3) \tag{1.10}$$

The relations are valid in the electric-dipole approximation and assume that the medium response is local.

Equations (1.7)-(1.10) can describe in general the third-order nonlinear effects in optical fibers. However due to their complexity, several approximations are needed. A significant simplification is to treat the nonlinear polarization $\mathbf{P}_{NL}$ in Eq. (1.8) as small perturbation to the total induced polarization. This is because the nonlinear effects are relatively weak in silica fibers. So to begin with we can set $\mathbf{P}_{NL} = 0$. Because Eq. (1.7) is then linear in $\mathbf{E}$, it is useful to write in the frequency domain as

$$\nabla \times \nabla \times \tilde{\mathbf{E}}(r,\omega) = \epsilon(\omega) \frac{\omega^2}{c^2} \tilde{\mathbf{E}}(r,\omega) \tag{1.11}$$

where $\tilde{\mathbf{E}}(r,\omega)$ is the Fourier transform of $\mathbf{E}(r,t)$ defined as

$$\tilde{\mathbf{E}}(r,\omega) = \int_{\infty}^{\infty} \mathbf{E}(r,t) \exp(i\omega t) dt \tag{1.12}$$

The frequency-dependent dielectric constant appearing in Eq. (1.11) is defined as

$$\epsilon(\omega) = 1 + \tilde{\chi}^{(1)}(\omega) \tag{1.13}$$

where $\tilde{\chi}^1(\omega)$ is the Fourier transform of $\chi^1(t)$. As $\tilde{\chi}^1(\omega)$ is in general complex, so is $\epsilon(\omega)$. It's real and imaginary parts can be related to the refractive index $n(\omega)$ and the absorption coefficient $\alpha(\omega)$ by using the definition

$$\epsilon = (n + iac/2\omega)^2 . \tag{1.14}$$

From Eqs. (1.13),(1.14), n and α are related to $\chi^{(1)}$ by the relations

$$n(\omega) = 1 + \frac{1}{2} Re\left[\tilde{\chi}^{(1)}(\omega)\right] \tag{1.15}$$

$$\alpha(\omega) = \frac{\omega}{nc} Im\left[\tilde{\chi}^{(1)}(\omega)\right], \tag{1.16}$$

where Re and Im stand for the real and imaginary parts, respectively.

Two further simplifications can be made before solving Eq. (1.11). First, because of low optical losses in fibers in the wavelength region of interest, the imaginary part $\epsilon(\omega)$ is small in comparison to the real part. Thus, we can replace $\epsilon(\omega)$ by $n^2(\omega)$ and include fiber loss in a perturbative manner. Second, as $n(\omega)$ is often independent of the spatial coordinates in both the core and cladding of step-index fiber one can prove that

$$\nabla \times \nabla \times \mathbf{E} = \nabla(\nabla \cdot \mathbf{E}) - \nabla^2 \mathbf{E}$$

From Eq. (1.3) we can obtain that $\nabla \mathbf{D} = \epsilon_0 \nabla \cdot \mathbf{E} = \rho_f$. But $\nabla(\rho_f) = 0$ so we can finally obtain the following that

$$\nabla \times \nabla \times \mathbf{E} = \nabla(\nabla \cdot \mathbf{E}) - \nabla^2 \mathbf{E} = -\nabla(\rho_f) - \nabla^2 \mathbf{E} = -\nabla^2 \mathbf{E} \tag{1.17}$$

So by direct substituting Eq. (1.17) to Eq. (1.11) we can obtain an equation at the following form

$$\nabla^2 \tilde{\mathbf{E}} + n^2(\omega) \frac{\omega^2}{c^2} \tilde{\mathbf{E}} = 0 \tag{1.18}$$

1.3 Pulse-Propagation Equation

The study of most nonlinear effects in optical fibers involves the use of short pulses. When such optical pulses propagate inside a fiber, both dispersive and nonlinear effects influence their shapes and spectra. In this section we derive a basic equation that governs propagation of optical pulses in nonlinear dispersive fibers. The starting point is the wave Equation Eq. (1.7), (1.8).

$$\nabla \times \nabla \times \mathbf{E} = -\frac{1}{c^2}\frac{\partial^2 \mathbf{E}}{\partial t^2} - \mu_0 \frac{\partial^2 \mathbf{P}}{\partial t^2}$$

$$\mathbf{P}(r,t) = \mathbf{P}_L(r,t) + \mathbf{P}_{NL}(r,t)$$

and recalling that $\nabla \times \nabla \times \mathbf{E} = -\nabla^2 \mathbf{E}$ we finally have

$$-\nabla^2 \mathbf{E} = -\frac{1}{c^2}\frac{\partial^2 \mathbf{E}}{\partial t^2} - \mu_0 \frac{\partial^2 \mathbf{P}}{\partial t^2} \Rightarrow \nabla^2 \mathbf{E} - \frac{1}{c^2}\frac{\partial^2 \mathbf{E}}{\partial t^2} = \mu_0 \frac{\partial^2 \mathbf{P}}{\partial t^2} \Rightarrow \nabla^2 \mathbf{E} - \frac{1}{c^2}\frac{\partial^2 \mathbf{E}}{\partial t^2} =$$

$$= \mu_0 \frac{\partial^2 \mathbf{P}_L}{\partial t^2} + \mu_0 \frac{\partial^2 \mathbf{P}_{NL}}{\partial t^2}$$

So at last we have shown that the equation that governs propagation of opticl pulses in nonlinear dispersive fibers is:

$$\nabla^2 \mathbf{E} - \frac{1}{c^2}\frac{\partial^2 \mathbf{E}}{\partial t^2} = \mu_0 \frac{\partial^2 \mathbf{P}_L}{\partial t^2} + \mu_0 \frac{\partial^2 \mathbf{P}_{NL}}{\partial t^2} \tag{1.19}$$

1.4 Nonlinear Pulse Propagation

Due to it's complexity equation Eq. (1.19) needs some more simplifications to be made before it is actually been solved. To begin with $\mathbf{P}_{NL}$, is treated as a small perturbation to $\mathbf{P}$. This is justified because nonlinear changes in the refractive index are very small in practise. Second, the optical field is assumed to maintain its polarization along the fiber length so that a scalar approach is valid. Although in practise this is not really the case, such an approximation seems to work quite well in practice. In the slowly varying envelope approximation adopted here, it is useful to separate the rapidly varying part of the electric field by writing it in the form

$$\mathbf{E}(r,t) = \frac{1}{2}\hat{x}\left[E(r,t)\exp(-i\omega_0 t) + c.c\right] \tag{1.20}$$

where $\hat{x}$ is the polarization unit vector and $E(r,t)$ is a slowly varying function of time. The polarization components $\mathbf{P}_L$ and $\mathbf{P}_{NL}$ can also be expressed in a similar way by writing

$$\mathbf{P}_L(r,t) = \frac{1}{2}\hat{x}\left[P_L(r,t)\exp(-i\omega_0 t) + c.c\right] \tag{1.21}$$

$$\mathbf{P}_{NL}(r,t) = \frac{1}{2}\hat{x}\left[P_{NL}(r,t)\exp(-i\omega_0 t) + c.c\right] \tag{1.22}$$

To obtain the wave equation for the slowly varying amplitude $E(r,t)$, it is more convenient to work in the Fourier domain. This is generally not possible as Eq. (1.19) is nonlinear because of the intensity dependence of the dielectric constant. In one approach ϵ_{NL} is treated as as constant during the derivation of the propagation equation. The approach is justified in view of the slowly varying envelope approximation and the perturbative nature of P_{NL}. We begin from Eq. (1.20) while using Eq. (1.22) to direct substitute them to Eq. (1.19) while for the Fourier transform of $E(r,t)$ we obtain the following formation

$$\tilde{E}(r,\omega-\omega_0) = \int_{-\infty}^{\infty} E(r,t)\, exp\left[i(\omega-\omega_0)t\right] dt \tag{1.23}$$

is found to satisfy the *Helmholtz* equation:

$$\nabla^2\tilde{E} + \epsilon(\omega)\, k_0^2\tilde{E} = 0 \tag{1.24}$$

where $k_0 = \frac{\omega}{c}$ and $\epsilon(\omega)$ is the dielectric constant. The dielectric constant can be used to define the refractive index $\hat{n}$ and the absorption coefficient $\hat{\alpha}$. However, both $\hat{n}$ and $\hat{\alpha}$ become intensity dependent because of the nonlinear dependence of the dielectric constant to the intensity of the refractive index.

To solve Equation Eq. (1.24) we will use the method of separation of variables while we assume a solution in the following form:

$$\tilde{E}(r,\omega-\omega_0) = F(x,y)\,\tilde{A}(z,\omega-\omega_0)\exp(i\beta_0 z), \tag{1.25}$$

where $\tilde{A}(z,\omega)$ is a slowly varying function of z and β_0 is the wave number to be determined later. After direct substitution of Eq. (1.25) to Eq. (1.24) we have:

$$\nabla^2\tilde{E} = \frac{\partial^2 E}{\partial x^2} + \frac{\partial^2 E}{\partial y^2} + \frac{\partial^2 E}{\partial z^2}$$

$$= \frac{\partial^2 F}{\partial x^2}\tilde{A}\left(z, \omega - \omega_0\right)\exp\left(i\beta_0 z\right)$$

$$+\frac{\partial^2 F}{\partial y^2}\tilde{A}\left(z, \omega - \omega_0\right)\exp\left(i\beta_0 z\right)$$

$$+\frac{\partial^2 \tilde{A}}{\partial z^2}F\left(x, y\right)\exp\left(i\beta_0 z\right)$$

$$+2i\beta_0\frac{\partial \tilde{A}}{\partial z}F\left(x, y\right)\exp\left(i\beta_0 z\right) - \beta_0^2 F\left(x, y\right)\tilde{A}\left(z, \omega - \omega_0\right)\exp\left(i\beta_0 z\right)$$

After we have done all these calculations we can now return to Eq. (1.24) equation to direct substitute and simplify our equations a bit.

$$\frac{\partial^2 F}{\partial x^2} + \frac{\partial^2 F}{\partial y^2} + \left[\epsilon\left(\omega\right)k_0^2 - \tilde{\beta}0^2\right]F = 0 \tag{1.26}$$

$$\frac{\partial^2 \tilde{A}}{\partial z^2} + 2i\beta_0\frac{\partial \tilde{A}}{\partial z} + \left(\tilde{\beta}^2 - \beta_0^2\right)\tilde{A} = 0 \tag{1.27}$$

where in Eq. (1.27) we should neglect the second derivative $\partial^2\tilde{A}/\partial z^2$ since $A\left(\tilde{z}, \omega\right)$ is assumed to be a slowly varying function of z. The dielectric constant $\epsilon\left(\omega\right)$ in Eq. (1.26) can be approximated by

$$\epsilon = \left(n + \Delta n\right)^2 \approx n^2 + 2n\Delta n \tag{1.28}$$

where Δn is a small perturbation.

Equation (1.26) can be solved using first-order perturbation theory [20]. To begin with we will substitute ϵ with n^2 and obtain the modal distribution $F\left(x, y\right)$ and the corresponding wave number $\beta\left(\omega\right)$. Next, by including the effect of Δn in Eq. (1.26) while using the first-order perturbation theory someone can conclude that Δn does not affect the modal distribution $F\left(x, y\right)$. However the eigenvalue $\tilde{\beta}$ becomes

$$\tilde{\beta}\left(\omega\right) = \beta\left(\omega\right) + \Delta\beta\left(\omega\right) \tag{1.29}$$

Using Eqs. (1.20) and Eq. (1.25) the electric field $\mathbf{E}\left(r, t\right)$ can be written as

$$\mathbf{E}\left(r, t\right) = \frac{1}{2}\hat{x}\left\{F\left(x, y\right)A\left(z, t\right)\exp\left[i\left(\beta_0 z - \omega_0 t\right)\right] + c.c\right\}, \tag{1.30}$$

where $A(z,t)$ is the slowly varying pulse envelope . The Fourier transform $\tilde{A}(z,\omega-\omega_0)$ of $A(z,t)$ satisfies Eq. (1.27) which can be written as

$$2i\beta_0\frac{\partial\tilde{A}}{\partial z}+\left(\beta^2-\beta_0^2\right)\tilde{A}=0\Rightarrow 2\beta_0\frac{\partial\tilde{A}}{\partial z}=i\left(\tilde{\beta}^2-\beta_0^2\right)\tilde{A}$$

which under the assumption $\tilde{\beta}^2-\beta_0^2\approx 2\beta_0\left(\tilde{\beta}-\beta_0\right)$ can be written as

$$\frac{\partial\tilde{A}}{\partial z}=\frac{i}{2\beta_0}\left[2\beta_0\left(\tilde{\beta}-\beta_0\right)\right]\tilde{A}$$

which using Eq. (1.29)can be written in the following form

$$\frac{\partial\tilde{A}}{\partial z}=i\left[\beta(\omega)+\Delta\beta(\omega)-\beta_0\right]\tilde{A} \tag{1.31}$$

From this last equation someone can conclude that each spectral component within the pulse envelope acquires, as it propagates, down the fiber, a phase shift whose magnitude is both frequency and intensity dependent.

At this point we can go back to the time domain by taking the inverse Fourier transform of Eq. (1.31) and obtain the propagation equation for $A(z,t)$. However, as an exact functional form of $\beta(\omega)$ is rarely known, it is useful to expand $\beta(\omega)$ in a Taylor series around the carrier frequency ω_0 as

$$\beta(\omega)=\beta_0+(\omega-\omega_0)\beta_1+\frac{1}{2}(\omega-\omega_0)^2\beta_2+\frac{1}{6}(\omega-\omega_0)^3\beta_3+\cdots, \tag{1.32}$$

where $\beta_0\equiv\beta(\omega_0)$ and the higher order terms are defined as

$$\beta_m=\left(\frac{d^m\beta}{d\omega^m}\right)_{\omega=\omega_0} \tag{1.33}$$

We can obtain a similar formula for $\Delta\beta(\omega)$ can be written as

$$\Delta\beta(\omega)=\Delta\beta_0+(\omega-\omega_0)\Delta\beta_1+\frac{1}{2}(\omega-\omega_0)^2\Delta\beta_2+\frac{1}{6}(\omega-\omega_0)^3\Delta\beta_3+\cdots, \tag{1.34}$$

where $\Delta\beta_0=\Delta\beta_0(\omega_0)$ and the higher order terms are defines as

$$\Delta\beta_m=\left(\frac{d^m\Delta\beta}{d\omega^m}\right)_{\omega=\omega_0} \tag{1.35}$$

After neglecting the cubic and the higher order terms in Eq. (1.32) and assume that $\Delta\beta = \Delta\beta_0$ Eq. (1.31) can be written as

$$\frac{\partial \tilde{A}}{\partial z} = i\left[\beta_0 + \beta_1(\omega-\omega_0) + \frac{1}{2}\beta_2(\omega-\omega_0)^2 + \Delta\beta - \beta_0\right]\tilde{A} \Rightarrow$$

$$\frac{\partial \tilde{A}}{\partial z} = i\left[\beta_1(\omega-\omega_0) + \frac{1}{2}\beta_2(\omega-\omega_0)^2 + \Delta\beta\right]\tilde{A}$$

so Eq. (1.31) can finally be written as

$$\frac{\partial \tilde{A}}{\partial z} - i\left[\beta_1(\omega-\omega_0) + \frac{1}{2}\beta_2(\omega-\omega_0)^2 + \Delta\beta\right]\tilde{A} = 0, \tag{1.36}$$

Calculating the inverse Fourier transform of $A(z,t)$ we can obtain the following equation:

$$A(z,t) = \frac{1}{2\pi}\int_{-\infty}^{\infty}\tilde{A}(z,\omega-\omega_0)\,exp\left[-i(\omega-\omega_0)t\right]d\omega. \tag{1.37}$$

Using the inverse Fourier transform mentioned above someone can conclude that firstly

$$\mathcal{F}^{-1}\left\{(\omega-\omega_0)\tilde{A}(z,\omega-\omega_0)\right\} = i\frac{\partial A(z,t)}{\partial t} \tag{1.38}$$

$$\mathcal{F}^{-1}\left\{(\omega-\omega_0)^2\tilde{A}(z,\omega-\omega_0)\right\} = -\frac{\partial^2 A(z,t)}{\partial t^2} \tag{1.39}$$

Thus combining Eqs. (1.36) - (1.39) we obtain the propagation equation for $A(z,t)$

$$\frac{\partial A}{\partial z} + \beta_1\frac{\partial A}{\partial t} + \frac{i\beta_2}{2}\frac{\partial^2 A}{\partial t^2} = i\Delta\beta_0 A \tag{1.40}$$

The $\Delta\beta_0$ term on the right side of the last equation includes the effects of fiber loss and nonlinearity. Using $\beta(\omega) \approx n(\omega)\omega/c$ and assuming that $F(x,y)$ does not vary much over the pulse bandwidth Eq. (1.40) can be written as

$$i\frac{\partial A}{\partial z} + \beta_1\frac{\partial A}{\partial t} + \frac{\beta_2}{2}\frac{\partial^2 A}{\partial t^2} + \frac{\alpha}{2}A = i\gamma(\omega_0)|A|^2 A, \tag{1.41}$$

where in Eq. (1.41) the amplitude A is assumed to be normalized such that $|A|^2$ represents the optical power. This equation is related to the nonlinear Schrödinger (NLS) equation and it can be reduced to that form under certain conditions. Eq. (1.41) includes the effects of fiber losses through α, of chromatic dispersion through β_1 and β_2 and of nonlinearity through γ. By neglecting the contribution of the third order dispersion term and under some more assumptions Eq. (1.41)

can finally be written as

$$\frac{\partial A}{\partial z} - i\frac{\beta_2}{2}\frac{\partial^2 A}{\partial t^2} - i\frac{\alpha}{2}A + \gamma\left(\omega_0\right)|A|^2 A = 0, \tag{1.42}$$

To summarize the effects of the phenomena we mentioned just before, beginning from parameter β_1; pulse envelope moves at the group velocity $v_g \equiv 1/\beta_1$, while the effects of group-velocity dispersion GVD are governed by β_2. The β_2 term can be positive or negative from which we can derive two different cases as mention later the normal and anomalous dispersion whereas β_2 is positive or negative respectively. The right term in Eq. (1.41) is responsible for the nonlinear phenomena we can observe and governs the self-phase modulation or simply (SPM).

1.5 Nonlinear Effects

1.5.1 Chromatic Dispersion

Although Chromatic Dispersion is not a nonlinear phenomenon it has a huge affect on how the nonlinear effects interact with the pulses through it's propagation. Assuming that the propagation constant is called β. Applying the *Taylor* series on β in respect of ω around a frequency ω_0 where the pulse spectrum is located we have:

$$\beta(\omega) = \beta_0 + \beta_1\left(\omega - \omega_0\right) + \frac{1}{2}\beta_2\left(\omega - \omega_0\right)^2 \tag{1.43}$$

Parameter β_2 stands for group velocity dispersion and as we mention before it is responsible for the broadening of the pulse. Eq. (1.1) becomes really important when pulse's wavelength is such that the group velocity dispersion equal to zero. This wavelength is called $zero - dispersion\ wavelength$. Although β_2 is equal to zero, dispersion effects still exhibit at this region.

To understand better the propagation of the pulse at this regime we should include in Eq. (1.1) the third order term. The β_3 order that appears is called third order dispersion (TOD) parameter. That kind of higher order effects can lead to distort of ultra short pulses both in linear and nonlinear regimes[21],[22].

Non-linear effects taking place in the optic fibers can exhibit interestingly enough properties depending on the sign of the β_2 parameter. We can name two cases. In the first one the group velocity dispersion parameter β_2 is positive

whereas in the second case β_2 is negative. The first case is called the normal dispersion case while the second one is the anomalous. An important feature of Chromatic Dispersion is that different spectral components of the beam travel at different speeds. So in the normal dispersion regime the high frequency components of the pulse(blue-shifted) travel slower than the low frequency components(red-shifted) of the same pulse. On the other hand when the pulse propagates on the anomalous regime the low frequency components tend to travel faster than the high frequency components.

The anomalous dispersion regime is in particular interest because it is the case in which the existence of solitons is supported as an interaction between the dispersion and the nonlinear effects. Whereas our pulses propagate through the normal or anomalous dispersion regime it is a common phenomenon that the faster travelling pulse will walk through the slower moving pulse as a result of the mismatch in their group velocities. As a result the group velocity dispersion plays a critical role in such nonlinear phenomena [23] .

1.5.2 Raman Scattering Effect

While a category of elastic nonlinear effects can occur inside optical fibers an other category of stimulated inelastic scattering exists . In contrast with the elastic in the inelastic phenomena the optical field transfers part of its energy to the nonlinear medium . Those inelastic phenomena are separated in two main categories, the stimulated Raman scattering (SRS) and the stimulated Brillouin scattering (SBS) depending on the type of photons that are participating. Thus the optical photons participate in SRS and are in our particular interest while acoustic photons participate in SBS. An other basic difference between SRS and SBS is that SRS scatters light in both directions (forward and backward) while SBS only in forward direction . A brief description of SRS can be given using a quantum mechanical example. In this example a photon of the pump pulse is annihilated to create a photon at a lower frequency (belonging to Stokes wave) and a photon with the right energy and momentum to conserve the energy and the momentum. SRS effect occurring inside optical fibers was used to develop new types of amplifiers which did not require doped fibers as the amplifiers that were used in the past .

1.5.3 Optical Kerr Effect

The dependence of the refractive index of an optic fiber to the optical intensity rises the Optical Kerr Effect [24], [25]. The nonlinear phase shift induced by an intense high power pump beam is used to change the transmission of a weak probe through a nonlinear medium. As a result phase modulation due to intensity dependant refractive index gives birth to a variety of nonlinear effects such as Self Phase modulation (SPM), Cross Phase Modulation (XPM) among others. At this point we should point out that the optical Kerr Effect is only noticeable with the use of very intense pump pulses [26],[27].

1.5.4 Self-Phase Modulation

The intensity dependence of the refractive index is responsible for many nonlinear effects where the most important of them is the SPM and the XPM. Self induced modulation is related with the self induced phase shift that a pulse is submitted to while it's propagation in an optical fiber. Such as GVD so is SPM related with pulse broadening as well the formation of solitons [28], [29] while pulse propagates on the anomalous dispersion regime inside optic fibers. Here a very beneficial example of the interaction between the Group Velocity Dispersion and the Self-Phase Modulation is the copropagation of a soliton and an other nondispersive pulse. As we are going to see in our simulations the compression of the pulse is easy to archived in the anomalous dispersion regime where the linear induced chirp of the chromatic dispersion is combined with the opposite sign of the nonlinear induced chirp of the Self Phase Modulation.

1.5.5 Cross Phase Modulation

Another phenomenon powered from the Kerr effect is the Cross Phase Modulation [1]. While Self-Phase modulation is related to the self induced phase shift of a pulse the Cross-Phase modulation is the induced phase shift that is due to the reaction of two propagating pulses in the optic fiber and is a direct result of different wavelengths, direction etc. It is well known that the cross phase modulation is responsible for asymmetric broadening of the co propagating pulses. An other common thing about XPM is that for pulses with equal intensities but with different wavelengths the effect of the XPM on the nonlinear phase shift is twice the effect of SPM. An important feature of XPM is that the pulses need to

travel with the same group velocities , otherwise XPM will not be able to affect on the co-propagating pulses and the pulses will just slide past each other while propagating.

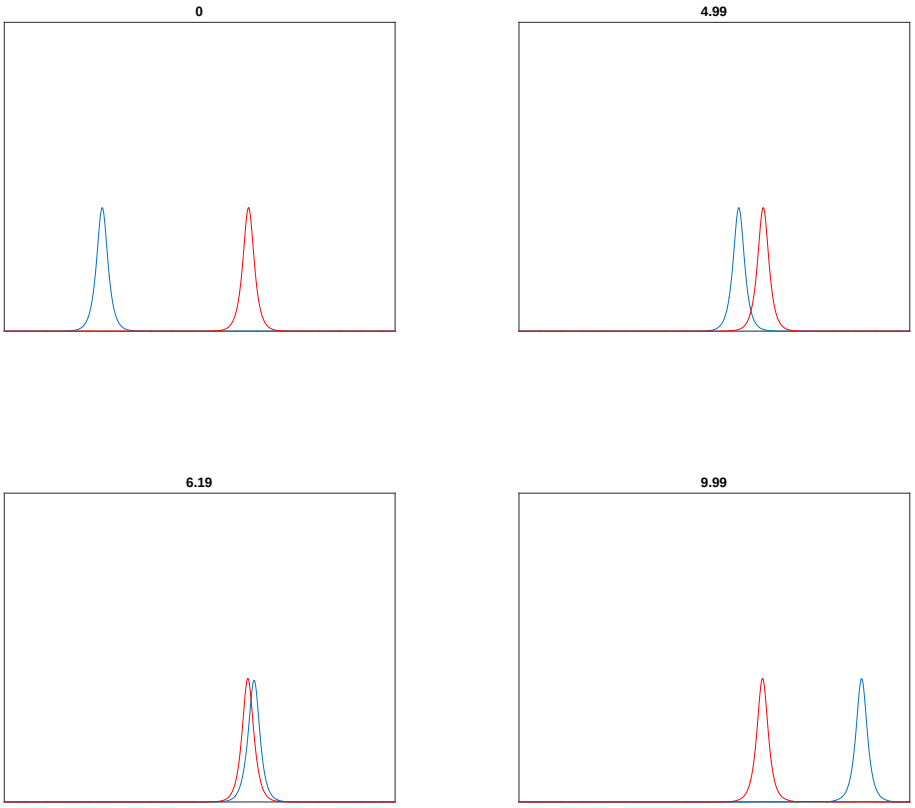

FIGURE 1.1: In the upper row we depict the evolution of two fundamental solitons propagating in the anomalous dispersion regime until they met up. An initial chirp was given to see how they will react if we stimulate a collision between them. In the lower row we show the evolution of those two solitons after they collide. It is clear that the difference in the group velocity makes possible the pass by of the chirped one through the other.

1.6 Numerical Methods

The NLS equation i.e.Eq. (1.41) is a nonlinear partial differential equation and a lot of research has been done to obtain analytic solutions. Although in some cases due to its complexity an analytic solution is not always possible. As a result a numerical approximation of the problem is often necessary. A numerical approach also will help us understand the corresponding nonlinear effects in optical fibers. For this reason a variety of numerical methods have been developed [30–60]. Those numerical methods are separated in two major categories; the finite-difference methods and the pseudospectral methods.

While each method has its advantages and disadvantages compared with the other the pseudospectral split-step Fourier method has been more popular to solve the pulse propagation problem in nonlinear dispersive media. The reason for the success of this method is due to its speed compared with finite-difference method. This advantage occurs to the speed of the finite-Fourier transform (FFT) algorithm [61].

1.6.1 Split-Step Fourier Method

To determine how the split-step Fourier method [32], [33] works it will be useful to begin from a linear equation rather than Eq. (1.42) which is nonlinear. So we will begin with an equation in the following form

$$\frac{\partial u}{\partial z} = (L + M)\, u \tag{1.44}$$

The exact solution of Eq. (1.44) over a distance h can be written in the following form

$$u\,(x, h) = e^{h(L+M)} u\,(x, 0)\,, \tag{1.45}$$

Now we consider two split equations

$$v_t = Lv \tag{1.46}$$

and

$$v_t = Mv \tag{1.47}$$

whose solutions can be written $e^{hL} v\,(x, 0)$ and $e^{hM} v\,(x, 0)$. The complexity of Eq. (1.44) may not help us to obtain a solution although the split equations gave us the ability to approximate the the factor $e^{h(L+M)}$ by a sequence of split operators as

$$e^{h(L+M)} = e^{\beta_n hM} e^{\alpha_n hL} \cdots e^{\beta_1 hM} e^{\alpha_1 hL} \tag{1.48}$$

where coefficients α_j and β_j are constants. Expanding the factor $e^{h(L+M)}$ through Taylor series we obtain the following result

$$e^{h(L+M)} = 1 + h\,(L + M) + \frac{1}{2} h^2\,(L + M)^2 + \cdots \tag{1.49}$$

As anyone can see the simplest split-step scheme is when we take $\alpha_1 = \beta_1 = 1$ and other coefficients to be zero. In this case we get the first order splitting.

$$S_1(h) = e^{hM}e^{hL} = e^{h(L+M)} + O\left(h^2\right) \tag{1.50}$$

A slightly more complex case would be the second order splitting. Thus the values of the coefficients α_j and β_j would change. In order to determine those coefficients we are going to follow the procedure below. Firstly for the second order splitting we assume that we have at most 4 coefficients that may differ from zero: $\alpha_1,\ \alpha_2,\ \beta_1,\ \beta_2$ while all the other α_j, β_j will be equal to zero. More specifically Eq. (1.50) will obtain the following form

$$e^{h(L+M)} = e^{\beta_2 hM}e^{\alpha_2 hL}e^{\beta_1 hM}e^{\alpha_1 hL} \tag{1.51}$$

Now by expanding each term through Taylor series we have firstly for $e^{\beta_2 hM}$

$$e^{\beta_2 hM} \approx 1 + h\beta_2 M + \frac{h^2}{2}\beta_2^2 M^2 + O\left(h^3\right)$$

secondly for $e^{\alpha_2 hL}$

$$e^{\alpha_2 hL} \approx 1 + h\alpha_2 L + \frac{h^2}{2}\alpha_2^2 L^2 + O\left(h^3\right)$$

while similar equations are arising for β_1, α_1 respectively. So if we now calculate the products $e^{\beta_2 hM}e^{\alpha_2 hL}$, first, and then, $e^{\beta_1 hM}e^{\alpha_1 hL}$ we will have

$$e^{\beta_2 hM}e^{\alpha_2 hL} = 1 + h\alpha_2 L = \frac{h^2}{2}\alpha_2^2 L^2 + h\beta_2 M + h^2\beta_2 M\alpha_2 L + \frac{h^2}{2}\beta_2^2 M + O\left(h^3\right)$$

while a similar equation occurs when we follow the relative procedure for the $e^{\beta_1 hM}e^{\alpha_1 hL}$ product.

$$e^{\beta_1 hM}e^{\alpha_1 hL} = 1 + h\alpha_1 L + \frac{h^2}{2}\alpha_1^2 L^2 + h\beta_1 M + h^2\beta_1 M\alpha_1 L + \frac{h^2}{2}\beta_1^2 M^2 + O\left(h^3\right)$$

Now by substituting back to Eq. (1.51) the products that we have calculated just before we obtain that

$$\begin{aligned} &e^{\beta_2 hM}e^{\alpha_2 hL}e^{\beta_1 hM}e^{\alpha_1 hL} \\ &= \left(1 + h\beta_2 M + \frac{h^2}{2}\beta_2^2 M^2 + O\left(h^3\right)\right)\left(1 + h\alpha_2 L + \frac{h^2}{2}\alpha_2^2 L^2 + O\left(h^3\right)\right) \end{aligned}$$

$$= 1 + h\alpha_2 L + \frac{h^2}{2}\alpha_2^2 L^2 + h\beta_2 M + h^2\beta_2 M\alpha_2 L + \frac{h^2}{2}\beta_2^2 M^2 + h\alpha_1 L +$$

$$h^2\alpha_1\alpha_2 L^2 + h^2\alpha_1\beta_2 LM + \frac{h^2}{2}\alpha_1^2 L^2 + h\beta_1 M + h^2\beta_1 M\alpha_2 L + h^2\beta_1\beta_2 M^2$$

$$+ h^2\beta_1 M\alpha_1 L + \frac{h^2}{2}\beta_1^2 M^2$$

$$= 1 + h\left(\alpha_2 L + \beta_2 M + \alpha_1 L + \beta_1 M\right) + \frac{h^2}{2}\left\{\alpha_2^2 L + 2\beta_2 M\alpha_2 L\right\}$$

$$+\frac{h^2}{2}\left\{\beta_2^2 M^2 + 2\alpha_1\alpha_2 L^2 + 2\alpha_1\beta_2 LM + \alpha_1^2 L^2 + 2\beta_1\alpha_2 ML\right\}$$

$$+ \frac{h^2}{2}\left\{+2\beta_1\beta_2 M^2 + 2\beta_1\alpha_1 ML + \beta_1^2 M^2\right\} \tag{1.52}$$

Now by comparing Eq. (1.51) witg Eq. (1.49) we are able to export a system of equations that will lead us to $\alpha_1,\ \beta_1,\ \alpha_2,\ \beta_2$ coefficients. More analytically

$$(\alpha_2 + \alpha_1)^2 = 1$$

$$(\beta_2 + \beta_1)^2 = 1$$

$$\beta_2\alpha_2 + \beta_1\alpha_2 + \beta_1\alpha_1 = \frac{1}{2}$$

$$\alpha_1\beta_2 = \frac{1}{2}$$

We can easily conclude that $\beta_2 = 1$, $\beta_1 = 0$ and $\alpha_2 = \alpha_1 = \frac{1}{2}$ which leads finally to

$$S_2(h) = e^{\frac{1}{2}hL}e^{hM}e^{\frac{1}{2}hL} = e^{h(L+M)} + O\left(h^3\right) \tag{1.53}$$

It is easy to understand that the complexity of higher order split-step will make the algebra much more difficult. A more efficient way was proposed by Yoshida . The idea is to symmetrically assemble a few lower-order schemes together to obtain a higher-order one. Specifically to obtain a fourth-order split-step scheme $S_4(h)$, we express $S_4(h)$ as a symmetric product of three second-order schemes:

$$S_4(h) = S_2(c_1 h)\, S_2(c_0 h)\, S_1(c_2 h) \tag{1.54}$$

where c_0, c_1 are real constants. To determine c_0 and c_1 , we use a standard formula

$$e^X e^Y e^X = e^{2X+Y+\frac{1}{6}[Y,Y,X]-\frac{1}{6}[X,X,Y]+\cdots}, \tag{1.55}$$

where X and Y are any operators $[X,Y] \equiv XY - YX, [X,X,Y] \equiv [X,[X,Y]]$, *etc.*. This formula can be obtained by repeated application of the Baker-Campbell-Hausdorff formula for the operator $e^X e^Y$:

$$e^X e^Y = e^{X+Y+\frac{1}{2}[X,Y]+\frac{1}{12}([X,X,Y]+[Y,Y,X])+\frac{1}{24}[X,Y,Y,X]+\cdots} \tag{1.56}$$

Now we can express S_2 in the following form

$$S_2(h) = e^{h(L+M)+h^3 A_3+h^5 A_5+\cdots} \tag{1.57}$$

where

$$A_3 = \frac{1}{12}[M,M,L] - \frac{1}{24}[L,L,M] \tag{1.58}$$

Combining Eqs. (1.51), (1.54) we obtain the following formation for Eq. (1.51):

$$S_4(h) = e^{c_1 h(L+M)+c_1^3 h^3 A_3} e^{c_0 h(L+M)+c_0^3 h^3 A_3} e^{c_1 h(L+M)+c_1^3 h^3 A_3}$$

which leads to

$$S_4(h) = e^{(2c_1+c_0)h(L+M)+\left(2c_1^3+c_0^3\right)h^3 A_3+O\left(h^5\right)} \tag{1.59}$$

From this last formula we obtain two equations from which we will export a solution for both c_0 and c_1

$$c_0 + 2c_1 = 1, `c_0^3 + 2c_1^3 = 0 \tag{1.60}$$

thus by direct substituting $c_0 = 1 - 2c_1$ we obtain for the third order equation

$$(1-2c_1)^3 + 2c_1^3 = 0 \Rightarrow -6c_1^3 + 12c_1^2 - 6c_1 + 1 = 0 \Rightarrow c_1 = \frac{1}{2 - 2^{\frac{1}{3}}}$$

If this scheme is unfolded into a product of individual split operators of the form Eq. (1.48) then this fourth-order scheme is such that n=4 and

$$\begin{aligned} &\alpha_1 = \frac{1}{2}c_1, && \alpha_2 = \frac{1}{2}(1-c_1), && \alpha_3 = \frac{1}{2}(1-c_1), && \alpha_4 = \frac{1}{2}c_1 \\ &\beta_1 = c_1, && \beta_2 = 1-2c_1, && \beta_3 = c_1, && \beta_4 = 0 \end{aligned} \tag{1.61}$$

Similarly higher order split-steps can occur although that would not mean that

those schemes are necessarily better. Moreover as we have seen even from the fourth-order scheme the algebra teens to be complicated enough. As a result the complexity of the calculation in higher order schemes along with the high accuracy of second-order makes higher order seems less attractive.

So as we mentioned before at the beginning of this subsection the example we used referred to a linear equation. In the case of a nonlinear equation as for example Eq. (1.42) we consider that

$$u_t = M(u) + N(u) \tag{1.62}$$

where at least on of the operators M, N, is nonlinear in u, where M is a differential operator that includes the dispersion and losses terms within a linear medium and N is a nonlinear operator that accounts for the the effect of fiber nonlinearities on pulse propagation. More analytically

$$M = -\frac{i\beta_2}{2}\frac{\partial^2}{\partial T^2} - \frac{\alpha}{2} \tag{1.63}$$

$$N = i\gamma |u|^2 \tag{1.64}$$

In general dispersion and nonlinear effects act together along the fiber. The approximation behind the split-step Fourier method is that we assume the dispersive and nonlinear effects act independently during the propagation of the optical field in a small distance h. Thus propagation from z to $z + h$ is obtained in two steps. In the first step, nonlinearity acts alone and $M = 0$ in Eq. (1.57). In the second step, dispersion acts alone, and $N = 0$ in Eq. (1.57). As we have done in the linear case we begin by splitting Eq. (1.57) in two equations which need to be solved

$$v_t = M(v) \tag{1.65}$$

and

$$v_t = N(v) \tag{1.66}$$

The idea behind the split-step methods to solve nonlinear equations is actually a common practise which let us to formally extend the previous split-step schemes we have shown for linear equations directly to nonlinear equations. For example the extension of the Strang splitting scheme (second-order scheme) is that starting from the initial condition $u(x, 0)$, we first integrate the M-operator

equation Eq. (1.65) by half $h/2$ to get an intermediate solution $v_1(x)$. Then starting from $v_1(x)$, we integrate the N-operator Eq. (1.66) by one step h to get an other intermediate solution $v_2(x)$. Lastly, starting from $v_2(x)$, we integrate the M-operator again by half a step $h/2$. The resulting function is then our numerical approximation $S_2(x)\,u(x,0)$ for the nonlinear solution $u(x,h)$. Extension for higher order schemes such as $S_4(x)$ is similar.

The main advantage of the split-step Fourier method is its implementation is very easy in practise. We show the algebra for second and fourth order split-step methods as for higher order schemes the algebra seems to be more and more complex. Although higher order schemes would be more useful to archive better computational efficiency. Also the use of an adaptive step size along z can also be very helpful but only for certain problems. Another advantage is that they preserve some important properties of the original propagation equations. For instance as $|u^2|$ is a constant we can conclude that $\int |u^2|\,dx$ is a conserved quantity in the implementation of the split-step methods because each split-step operator integration is power invariant. This power conservation can be important for the long-time evolution simulations.

The split-step methods are particularly suitable for NLS-type equations. Besides the fact that the split-step Fourier method was first used in the early 70's and other methods such as Finite-Difference Methods were applied too, the advantages of the split-step schemes such as the ease of the implementation along with the variety of the optical problems that it can be applied give a main advantage to split-step schemes comparing with other numerical methods. Although an appropriate choice of step size z along with x are essential to maintain the required accuracy.

Chapter 2

Self-accelerating Airy waves in Optics

2.1 The Infinite-Energy Airy Waves

We begin by assuming the (1+1)D free particle Schrödinger equation in the following form:

$$i\frac{\partial u}{\partial \xi} + \frac{1}{2}\frac{\partial^2 u}{\partial s^2} = 0 \tag{2.1}$$

where $s = x/x_0$ represents a dimensionless transverse coordinate, x_0 is an arbitrary transverse scale, $\xi = z/kx_0^2$ is a normalized propagation distance (with respect to the Rayleigh range), $k = 2\pi n/\lambda_0$ is the wavenumber of the optical wave. As Berry and Balazs [62] have shown the Airy function constitutes a solution with nonspreading properties through time. By nonspreading properties we mean the exotic feature of Airy to propagate without any changes at its formation as well as the ability to freely accelerate in free space. So by rewriting Eq. (2.1) in an other formation our target is to show that Airy corresponds to one solution of the NLS while it preserves its non dispersive feature or more formally that $u\left(s, \xi = 0\right) = Ai(s)$.

$$i\frac{\partial u}{\partial \xi} = -\frac{1}{2}\frac{\partial^2 u}{\partial s^2} \Rightarrow \frac{\partial u}{\partial \xi} = i\frac{1}{2}\frac{\partial^2 u}{\partial s^2} \Rightarrow u_\xi = \frac{i}{2}u_{ss}$$

To continue we calculate the Fourier transform of u_{ss}, with , which is equal to:

$$\mathcal{F}\left\{\frac{i}{2}u_{ss}\right\} = \frac{i}{2}(-ik)^2\mathcal{F}\left\{u\right\} = \frac{-ik^2}{2}\mathcal{F}\left\{u\right\}$$

and thus

$$\mathcal{F}\{u_\xi\} = \frac{-i}{2}k^2\mathcal{F}\{u\} \Rightarrow \mathcal{F}\{u(k,\xi)\} = e^{\frac{-i}{2}k^2\xi}\mathcal{F}\{u(k,0)\}$$

Now from $\mathcal{F}\{u(k,\xi)\}$ by applying the inverse Fourier transform we will jump from Fourier space(k,ξ) to real space variables(s,ξ) and finally

$$u(s,\xi) = \mathcal{F}^{-1}\{\mathcal{F}\{u(k,\xi)\}\} = \mathcal{F}^{-1}\left\{e^{\frac{-i}{2}k^2\xi}\mathcal{F}\{u(k,0)\}\right\}$$

$$= \int \frac{dk}{2\pi} e^{\frac{-i}{2}k^2\xi} e^{iks}\mathcal{F}\{u(k,0)\}$$

By definition we know that Airy function is equal to

$$\mathrm{Ai}(s) = \int \frac{dp}{2\pi} e^{ip^3/3e^{ips}} \Rightarrow \mathcal{F}\{Ai(s)\} = \int ds e^{-iks} Ai(s)\&$$

$$= \int ds e^{-iks} \int \frac{dp}{2\pi} e^{ips} e^{ip^3/3} = \int ds e^{i(p-k)s} \int \frac{dp}{2\pi} e^{ip^3/3} = e^{ik^3/3} = \mathcal{F}\{u(k,0)\}$$

So now after we have calculated the $\mathcal{F}\{u(k,0)\}$ we can compute $u(s,\xi)$.

$$u(s,\xi) = \int \frac{dk}{2\pi}\mathcal{F}\{u(k,0)\}\, e^{\frac{-i}{2}k^2\xi} e^{iks} = \int \frac{dk}{2\pi} e^{i(\frac{k^3}{3} - \frac{k^2}{2}\xi + ks)}$$

After that we would like to transform this 3rd order polynomial to a canonical form. Thus we are going to follow the procedure below: We assume $k = K + \xi/2$, and by substituting this to our initial 3rd order polynomial

$$\frac{k^3}{3} - \frac{k^2}{2}\xi + ks$$

we have the following:

$$\frac{(K+\xi/2)^3}{3} - \frac{(K+\xi/2)^2}{\xi/2} + (K+\xi/2)s$$

$$= \frac{K^3}{3} + \frac{K^2\xi}{2} + \frac{K\xi^2}{4} + \frac{\xi^3}{24} - \frac{K^2\xi}{2} - \frac{K\xi^2}{2} - \frac{\xi^3}{8} + Ks + \frac{\xi s}{2}$$

$$= \frac{K^3}{3} - \frac{K\xi^2}{4} - \frac{\xi^3}{12} + Ks\frac{\xi s}{2} = \frac{K^3}{3} + K(s - \frac{\xi^2}{4}) + \frac{\xi s}{2} - \frac{\xi^3}{12}$$

To sum up we have conclude that

$$\left(\frac{k^3}{3} - \frac{k^2}{2}\xi + ks\right) = \frac{K^3}{3} + K\left(s - \frac{\xi^2}{4}\right) + \frac{\xi s}{2} - \frac{\xi^3}{12}$$

and by substituting this last equation to

$$u(s,\xi) = \int \frac{dk}{2\pi} e^{i(\frac{k^3}{3} - \frac{k^2}{2}\xi + ks)}$$

we have that

$$u(s,\xi) = \int \frac{dK}{2\pi} e^{i(K^3/3 + K(s-\xi^2/4) + \xi s/2 - \xi^3/12)}$$

$$= e^{i(\xi s/2 - \xi^3/12)} \int \frac{dK}{2\pi} e^{i(K^3/3 + K(s-\xi^2/4)} = e^{i(\xi s/2 - \xi^3/12)} Ai(s - (\xi/2)^2)$$

and finally we have

$$u(s,\xi) = \mathrm{Ai}\left[s - \left(\frac{\xi}{2}\right)^2\right] \exp\left(is\frac{\xi}{2} - \frac{i\xi^3}{12}\right) \tag{2.2}$$

From Eq. (2.2) we can can easily observe the nondispersive identity of the Airy solution since $u(s, \xi = 0) = Ai(s)$ as well as the acceleration of an Airy wave packet while it propagates through ξ. From $(\frac{\xi}{2})^2$ we can justify the ballistic trajectory of Airy.

As Berry and Balazs supposed the acceleration feature of a diffraction free Airy wave packet does not slur over Ehrenfest's theorem which describes the motion of the center of the gravity of a wave packet, [62–70] and that is because the Airy function is not square integrable which means that the center of mass cannot be defined. An ideal example of infinite energy Airy beam would be a free-falling particle which is constantly been accelerated from earth's gravitational field while neither friction or other obstacles stop it's momentum [63].

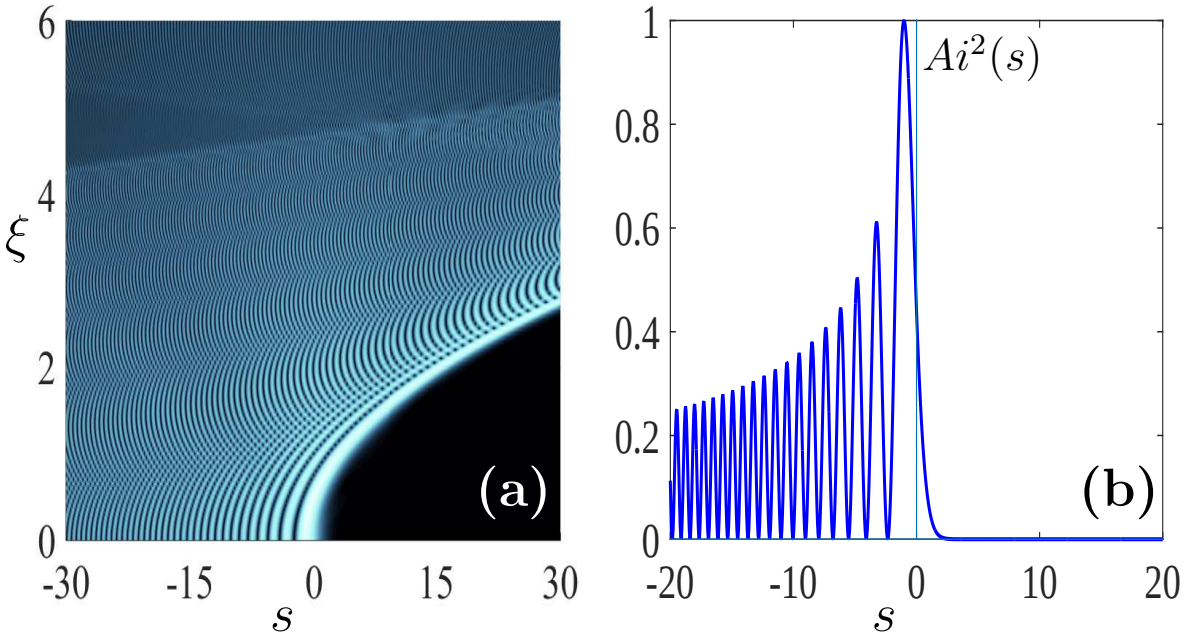

FIGURE 2.1: (a)In the figure above it is obvious both the acceleration and the ballistic trajectory of a diffraction free Airy wave while it propagates through ξ. (b)In this figure we depict the intensity profile of an infinite-energy Airy wave.

2.2 The Finite Energy Airy Waves

The main issue that we have to face with the infinite energy Airy waves are that they are not observable in practice. One way to make it physically observable is to induce an exponential function so as to be multiplied with the Airy function, in the following formation:

$$u(s,0) = \mathrm{Ai}(s)\exp(as) \tag{2.3}$$

where $a > 0$ is the decay factor which should be positive so as to preserve finite energy Airy$'$ s tail, which is necessary for the realistic representation of such waves. As we mentioned before the decay factor is necessary so as the positive branch of the Airy function to decay fast enough in order to archive convergence of Eq. (2.3).

Now we have to prove that even the the truncated Airy function we assumed in Eq. (2.3) is also a non dispersive solution of Eq. (2.1). Following the same steps as before we only have to calculate again the *Fourier* transformation of the new

initial function given by Eq. (2.3).

$$\mathcal{F}\{u(s,0)\} = \mathcal{F}\{\mathrm{Ai}(s)\exp(as)\} = \int ds e^{-iks}\,\mathrm{Ai}(s)\exp(as)$$

$$= \int ds e^{-iks}\int \frac{dp}{2\pi}e^{is(p+a)}e^{ip^3/3} = \int ds e^{is(-k+p+a)}\int \frac{dp}{2\pi}e^{ip^3/3} = e^{\frac{(a+ik)^3}{3}}$$

$$\Rightarrow u(s,\xi) = \int \frac{dk}{2\pi}\mathcal{F}\{u(k,0)\}\,e^{\frac{-i}{2}k^2\xi}e^{iks} = \int \frac{dk}{2\pi}e^{\frac{(a+ik)^3}{3}}e^{\frac{-i}{2}k^2\xi}e^{iks}$$

we assume $k+ia = K$ so the last integral is transformed to:

$$\int \frac{dk}{2\pi}e^{i[\frac{K^3}{3}-\frac{(K-ia)^2}{2}\xi+(K-ia)s]}$$

From this last equation we extract the following:

$$\frac{K^3}{3} - \frac{(K-ia)^2}{2}\xi + (K-ia)s \tag{2.4}$$

Now we assume

$$K = K_1 + \frac{\xi}{2}$$

and Eq. (2.4) becomes:

$$\frac{[K_1+\frac{\xi}{2}]^3}{3} - \frac{[K_1+\frac{\xi}{2}-ia]^2}{2}\xi + [K_1+\frac{\xi}{2}-ia]^2 s$$

$$= \frac{K_1^3}{3}+\frac{K_1^2\xi}{2}+\frac{K_1\xi^2}{4}+\frac{xi^3}{24}+\frac{a^2\xi}{2}+\frac{ia\xi^2}{2}+iaK_1\xi-\frac{\xi^3}{8}-\frac{K_1\xi^2}{2}-\frac{K_1\xi^2}{2}+K_1s+\frac{\xi s}{2}-ias$$

$$= \frac{K_1^3}{3}+K_1^2\xi-\frac{K_1\xi^2}{4}+iaK_1\xi+K_1s-\frac{xi^3}{12}+]\frac{\xi s}{2}+\frac{a^2\xi}{2}+\frac{ia\xi^2}{2}-ias$$

$$= \frac{K_1^3}{3}+K_1\left(s+ia\xi-\left(\frac{\xi}{2}\right)^2\right)-\frac{\xi^3}{12}+\frac{\xi s}{2}+\frac{a^2\xi}{2}+\frac{ia\xi^2}{2}-ias$$

Thus

$$u(s,\xi) = \int \frac{dK_1}{2\pi}e^{i[\frac{K_1^3}{3}+K_1(s+ia\xi-\frac{\xi}{2}^2)+as-\frac{a\xi^2}{2}-\frac{i\xi^3}{12}+ia^2\frac{\xi}{2}+is\frac{\xi}{2}]}$$

$$= e^{as-\frac{a\xi^2}{2}-\frac{i\xi^3}{12}+ia^2\frac{\xi}{2}+is\frac{\xi}{2}}\int \frac{dK_1}{2\pi}e^{i[\frac{K_1^3}{3}+K_1(s-(\frac{\xi}{2})^2+ia\xi]}$$

$$= e^{\left(as-\frac{a\xi^2}{2}-\frac{i\xi^3}{12}+ia^2\frac{\xi}{2}+is\frac{\xi}{2}\right)}\,\mathrm{Ai}\left(s-\left(\frac{\xi}{2}\right)^2+ia\xi\right) \tag{2.5}$$

At this point it is important to mention that if we directly substitute $\alpha = 0$, at Eq. (2.5) we will end up with exactly the same solution as in the Infinite Power Airy beam case. Although the most important parameter that we should make clear in this finite energy Airy wave is that despite the truncation function we have induced the Airy wave still freely accelerates even in free space for example in the absence of any potential that could lead to acceleration of the beam. As we observed in the infinite power Airy wave case, in this case too the term $(\frac{\xi}{2})^2$ indicates the acceleration of the Airy wave in free space through a parabolic trajectory [71]. At this point we should mention that Airy$'$ s diffraction that is noticed in Fig. 2.2 in comparison with Fig. 2.1 is due to the truncation function that we added.

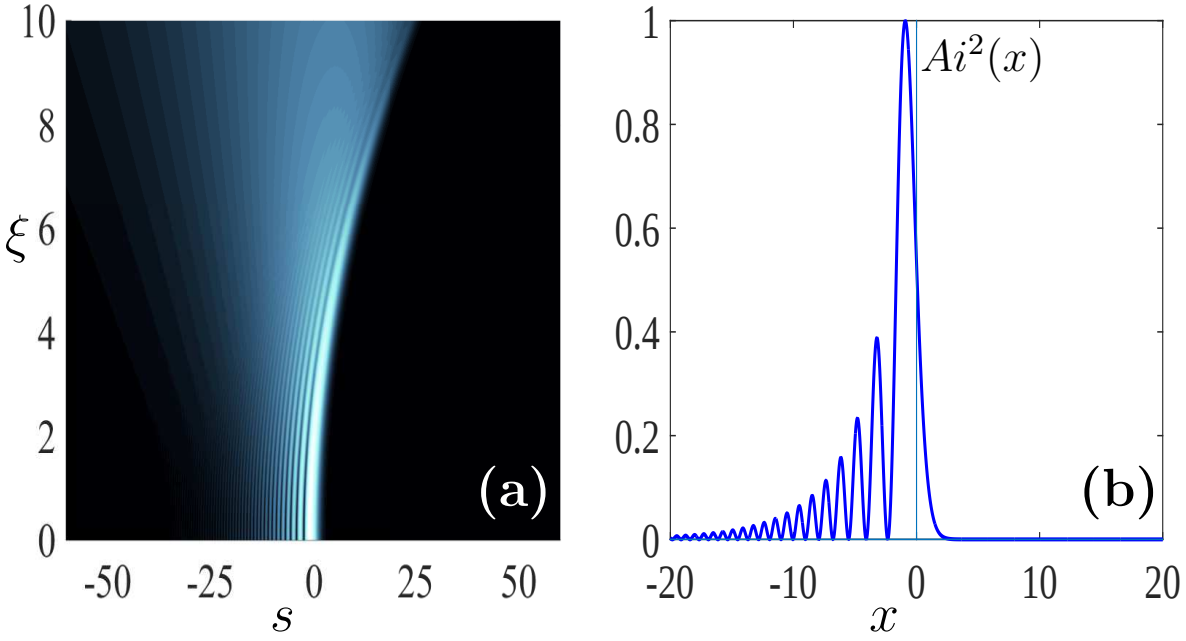

FIGURE 2.2: In figure (a) we depict the dynamics of a Finite Energy Airy wave when $a = 0.1$ while in figure (b)it's illustrated the profile energy of the corresponding truncated *Airy* wave

2.3 Creation of Caustics in periodic lattices ; fold or cusp

Nikolaos K. Efremidis and Ioannis D. Chremmos have shown the that beams with power law phases produce curved caustics which are associated with the fold and cusp type catastrophes [72]. Moreover they proved that a 2nd order power

law phase is able of self-focusing but with some spherical aberrations. But the most important aspect of those studies shows that if we construct the initial phase or wavefront of the beam we can have predefined trajectories with pure power law caustics along with aberration free focusing waves. A typical example is the Airy function that constitutes the only one dimensional dispersion free solution of the Schrödinger equation [62] which have parabolic trajectory as well. As it is shown [71, 73] an exponentially apodized function multiplied to Airy ends up with a finite energy Airy beam with reduced nondispersive features. Although this does not consist a major problem as Airy does not distort abruptly. Curved light waves like Airy beam which follows a parabolic trajectory highlighted new potentials in particle manipulation [74], filament generation [75],plasmonics [76, 77], and near field imaging [78], and optical bullet formation [79, 80]

Light beams can follow different families of curved trajectories including the general power law [81, 82]. This feature of light beams is responsible for the loss in Airy$'s$ dispersion free character. Trajectories like the ones we have described above can be analysed through the catastrophe theory [83, 84]. If we consider the coupled mode theory equation

$$i\dot{u}_n + \kappa\left(u_{n-1} + u_{n+1}\right) = 0 \tag{2.6}$$

which consists the one-dimensional potential free discrete Schrödinger equation, where $\dot{u}_n = \frac{du_n}{dz}$ z is the propagation direction and κ is the coupling coefficient between adjacent waveguides. The solution of Eq. (2.6) can be written in the following form:

$$u(x,z) = \frac{1}{2\pi}\int_{-\infty}^{\infty}\int_{0}^{2\pi} A(\xi)e^{i\Psi}dqd\xi \tag{2.7}$$

where $\Psi = \varphi(\xi) + q(x-\xi) + 2\kappa\cos(q)z$. Applying a stationary phase method to Eq. (2.6) on the integration variable q, ξ, we result in the ray equation

$$x = \xi + 2\kappa\sin(q(\xi))z \tag{2.8}$$

where $q(\xi) = \varphi'(\xi)$. Along the caustic trajectory, the phase should be stationary to the higher than first order to variations of the initial wavefront. Requiring second order stationary $\Psi_{\xi\xi}\Psi_{qq} - \Psi_{q\xi}^2 = 0$. More analytically we have:

$$\Psi_\xi = \varphi'(\xi) - q \Rightarrow \Psi_{\xi\xi} = \varphi''(\xi)$$

$$\Psi_q = (x - \xi) - 2\kappa \sin(q)z,\ \Psi_{qq} = -2\kappa \cos(q)z,\ \Psi_{q\xi} = -1 \tag{2.9}$$

$$\Psi_{\xi\xi}\Psi_{qq} - \Psi_{q\xi} = -2\kappa z \cos(q)\varphi''(\xi) - 1$$

but $q(\xi) = \varphi'(\xi)$

So we have

$$\Psi_{\xi\xi}\Psi_{qq} - \Psi_{q\xi} = -2\kappa z \cos(q(\xi))q'(\xi) - 1 = 0 \tag{2.10}$$

Then we assume $\varphi(\xi) = -\alpha(-\xi)^\beta H(-\xi)/\beta$, thus, $q(\xi) = \alpha(-\xi)^{\beta-1}H(-\xi)$

From Eq. (2.8) we have

$$x = \xi + 2\kappa z \sin(q(\xi)) \Rightarrow z = \frac{-1}{2\kappa \cos(q(\xi)q'(\xi)}$$

but

$$q(\xi) = \alpha(-\xi)^{\beta-1}H(-\xi) \Rightarrow q'(\xi) = -\alpha(\beta-1)(-\xi)^{\beta-2}H(-\xi)$$

Now by substituting $q'(\xi)$ to z we have

$$z = \frac{-1}{2\kappa \cos(a(-\xi)^{\beta-1}\alpha(\beta-1)(-\xi)^{\beta-2}} = \frac{(-\xi)^{2-\beta}}{2\alpha(\beta-1)\kappa \cos(a(-\xi)^{\beta-1})}$$

So by substituting z to x we finally have

$$x = \xi + \frac{2\kappa \sin(a(-\xi)^{\beta-1}(-\xi)^{2-\beta}}{2\alpha(\beta-1)\kappa \cos(\alpha(-\xi))^{\beta-1}} = \xi + \frac{\tan(\alpha(-\xi)^{\beta-1}}{\alpha(\beta-1)(-\xi)^{\beta-2}} \tag{2.11}$$

Then by assuming

$$0 < q(\xi) < \frac{\pi}{2} \Rightarrow \alpha(-\xi_0)^{\beta-1} < \frac{\pi}{2} \Rightarrow (-\xi_0)^{\beta-1} < \frac{\pi}{2\alpha} \Rightarrow \xi_0 < -[\frac{\pi}{2\alpha}]^{\frac{1}{\beta-1}} \tag{2.12}$$

From Eq. (2.11)we have

$$x = \xi + \frac{\tan(\alpha(-\xi)^{\beta-1})}{\alpha(\beta-1)(-\xi)^{\beta-2}}, but, \tan(\alpha(-\xi)^{\beta-1}) \approx \alpha(-\xi)^{\beta-1} \tag{2.13}$$

As a result Eq. (2.11) becomes

$$x = \xi + \frac{\alpha(-\xi)^{\beta-1}}{\alpha(\beta-1)(-\xi)^{\beta-2}} = \xi - \frac{-\xi}{\beta-1} = \frac{\xi\beta - \xi - \xi}{\beta-1} = \frac{\xi(\beta-2)}{\beta-1} \tag{2.14}$$

As we found before

$$z = \frac{-\xi^{2-\beta}}{2\alpha\kappa(\beta-1)\cos(\alpha(-\xi)^{\beta-1)}}$$

but $\cos(\alpha(-\xi)^{\beta-1}) \approx 1$, as a result

$$z = \frac{(-\xi)^{2-\beta}}{2\alpha(\beta-1)\kappa} \tag{2.15}$$

But from Eq. (2.14) we have that $\xi = \left(\frac{x(\beta-1)}{\beta-2}\right)^{\beta-2} \Rightarrow (-\xi)^{2-\beta} = \left(\frac{-x(\beta-1)}{\beta-2}\right)^{2-\beta}$
So by substituting $(-\xi)^{2-\beta} = \left(\frac{-x(\beta-1)}{\beta-2}\right)^{2-\beta}$ to Eq. (2.15) we have

$$z = \frac{\left(\frac{-x(\beta-1)}{\beta-2}\right)^{2-\beta}}{2\alpha\kappa(\beta-1)} \Rightarrow 2z\alpha(\beta-1)\kappa = \left(\frac{-x(\beta-1)}{\beta-2}\right)^{2-\beta}$$

$$\Rightarrow [2z\alpha(\beta-1)\kappa)]^{\frac{1}{2-\beta}} = \frac{-x(\beta-1)}{\beta-2}$$

$$\Rightarrow \frac{x(\beta-1)}{2-\beta} = [2z\alpha(\beta-1)\kappa)]^{\frac{1}{2-\beta}}$$

$$x = [(2-\beta)(\beta-1)]\,[2\alpha\kappa z(\beta-1)]^{\frac{1}{2-\beta}} \tag{2.16}$$

which is finally the final formation of the caustic trajectory for small values of (ξ, x).

As we can conclude from equation Eq. (2.16) both the parabolic trajectory and the acceleration $x''(z)$ of the Airy beam are obvious. Also we can see that as z is getting bigger the acceleration dicreases gradually resulting to the caustic to approach the asymptotic in the following formation: $x = \xi_0 + 2\kappa z$.

Moreover we have seen that waves which have exponent phase $1 < \beta < 2$ lead to a caustic that in terms of catastrophe theory is called a "fold". On the other

hand waves with exponent phase $\beta > 2$ we can observe radical changes at caustic's trajectory which is now can be called as a "cusp".

As we have mentioned before by redesigning the initial phase we can produce different types of caustic trajectories.
We assume $x = \gamma z^{\delta}$ while $x = \xi + 2\kappa z sin(q(\xi))$. Using $\xi = f(z) = zf'(z)$ we can calculate $q(\xi)$ by following the steps described below.

$$\xi = f(z) - zf'(z) = \gamma z^{\delta} - z\delta\gamma z^{\delta-1} = \gamma z^{\delta} - \delta\gamma z^{\delta} = \gamma z^{\delta}(1-\delta)$$

From Eq. (2.8) we know that $x = \xi + 2\kappa z \sin(q(\xi)) \Rightarrow \gamma z^{\delta} = \gamma z^{delta}(1-\delta) + 2\kappa z \sin(q(\xi)) \Rightarrow \delta\gamma z^{\delta} = 2\kappa z \sin(q(\xi)) \Rightarrow q(\xi) = \arcsin\left[\frac{\delta\gamma}{2\kappa}\left(\frac{\xi}{(1-\delta)\gamma}\right)^{\frac{\delta-1}{\delta}}\right]$

$$q(\xi) = \arcsin\left[\frac{\delta\gamma^{\frac{1}{\delta}}}{2\kappa}\right]\left(\frac{\xi}{1-\delta}\right)^{\frac{\delta-1}{\delta}} \tag{2.17}$$

The optical wavefront that generates the caustic extends from ξ_0 to 0 where $q(\xi_0) = \frac{\pi}{2}$
From this last equation we have

$$q(\xi_0) = \frac{\pi}{2} \Rightarrow \arcsin\left[\frac{\delta\gamma^{\frac{1}{\delta}}}{2\kappa}\right]\left(\frac{\xi_0}{1-\delta}\right)^{\frac{\delta-1}{\delta}} = \frac{\pi}{2} \Rightarrow \frac{\pi}{2}\frac{\delta\gamma^{\frac{1}{\delta}}}{2\kappa}\left(\frac{\xi_0}{1-\delta}\right)^{\frac{\delta-1}{\delta}} = \frac{\pi}{2}$$

$$\Rightarrow \gamma^{\frac{1}{\delta}} = \frac{2\kappa}{\delta}\left[\frac{(1-\delta)}{\xi_0}\right]^{\frac{\delta-1}{\delta}}$$

$$\gamma = \left(\frac{2\kappa}{\delta}\right)^{\delta}\left[\frac{1-\delta}{\xi_0}\right]^{\delta-1} \tag{2.18}$$

Now if we go back to our initial power law caustic trajectory equation $x = \gamma z^{\delta}$ and substitute γ from Eq. (2.18) then we have

$$z^{\delta} = \frac{1}{\gamma} = \left[\frac{1}{\left(\frac{2\kappa}{\delta}\right)^{\delta}\left[\frac{1-\delta}{\xi_0}\right]^{\delta-1}}\right] = \frac{-\xi_0\delta}{2\kappa(\delta-1)} \tag{2.19}$$

2.4 Design of Airy trajectory under the usage of Linear Index Potential

As shown in [85], an optically induced linear index potential is capable of enhancement or reduction of Airy beam acceleration trajectory which can be realized by changing the index gradient transversely . In this section we will present the formation of linear longitiudinal (z - axis) index potential that we assumed in order to design the trajectory that the Airy wave follows.

$$iu_z + \frac{1}{2}u_{xx} - \frac{d(z)x}{2}u = 0 \tag{2.20}$$

where $\frac{d(z)x}{2}$ is the transversely linear index potential with a gradient d(z). After we transform Eq. (2.19) to *Fourier* space we have the following:

$$\hat{u} = \int_{-\infty}^{\infty} e^{-ikx}u(x)dx \Rightarrow \frac{\partial \hat{u}}{\partial k} = \int_{-\infty}^{\infty} -ixe^{-ikx}u(x)dx$$

$$= -i\int_{-\infty}^{\infty} xe^{-ikx}u(x)dx \Rightarrow \frac{\partial \hat{u}}{\partial k}i \Rightarrow \frac{\partial \hat{u}}{\partial k}i = \mathcal{F}\{xu(x)\}$$

As a result Eq. (2.19) is transformed to:

$$i\hat{u}_z + \frac{(-ik)^2}{2}\hat{u} - i\frac{d(z))}{2}\hat{u}_k = 0 \Rightarrow -u_z - \frac{ik^2\hat{u}}{2} + \frac{d(z)}{2}\hat{u}_k = 0$$

which is finally equal to:

$$\hat{u} - \frac{d(z)}{2}\hat{u}_k = -i\frac{k^2}{2}\hat{u} \tag{2.21}$$

which can be modified to the following formation which consist the characteristic system

$$\frac{dz}{1} = -\frac{dk}{\left(\frac{dz}{2}\right)} = -\frac{d\hat{u}}{\left(\frac{i}{2}k^2\hat{u}\right)} \tag{2.22}$$

To solve the system above we will begin with :

$$\frac{dz}{1} = -\frac{dk}{\left(\frac{dz}{2}\right)} \Rightarrow -\frac{1}{2}d(z)dz = dk$$

$$\Rightarrow \int_{\kappa}^{\kappa(z)} dk = -\frac{1}{2}\int_0^z d(s)ds \Rightarrow \kappa(z) = \kappa - \frac{1}{2}D(z)$$

where $D(z) = \int_0^z d(s)ds$

Next we are going to solve the other set of equations:

$$\frac{dz}{1} = -\frac{d\hat{u}}{\left(\frac{ik^2u}{2}\right)} \Rightarrow \left(\frac{-ik^2}{2}\right)dz = \frac{d\hat{u}}{\hat{u}} \Rightarrow \frac{dz}{1} = -\frac{d\hat{u}}{\left(\frac{ik^2u}{2}\right)} \Rightarrow \left(\frac{-ik^2}{2}\right)dz = \frac{d\hat{u}}{\hat{u}}$$

$$\Rightarrow \int_{\hat{u}(k,0)}^{\hat{u}(k,z)} \frac{d\hat{u}}{\hat{u}} = -\frac{i}{2}\int_0^z \kappa^2(s)ds \Rightarrow \ln\hat{u}(\kappa,z) - \ln\hat{u}(\kappa,0) = -\frac{i}{2}\int_0^z \kappa^2(s)ds \Rightarrow$$

$$\Rightarrow e^{\ln\hat{u}(\kappa,z)-\ln\hat{u}(\kappa,0)} = e^{\frac{i}{2}\int_0^z \kappa^2(s)ds} \Rightarrow \hat{u}(\kappa,z) = \hat{u}(\kappa,0)e^{\frac{i}{2}\int_0^z \kappa^2(s)ds}$$

from where we finally conclude to

$$u(x,z) = \frac{1}{2\pi}\int_{-\infty}^{\infty} \hat{u}(k,0)e^{-\frac{i}{2}\int_0^z \kappa(s)^2ds)}e^{i\kappa(z)x}dk \tag{2.23}$$

We now assume an Airy type initial condition in the following formation:

$$u(x,z=0) = \mathrm{Ai}(\gamma^{\frac{1}{3}}x) \tag{2.24}$$

where γ is the width of the Airy wave. After calculating the *Fourier* transform of Eq. (2.24) we conclude to the following equation:

$$\mathrm{Ai}(\gamma^{\frac{1}{3}}x) = \int \frac{dp}{2\pi}e^{ip\gamma^{\frac{1}{3}}x}e^{i\frac{p^3}{3}}, \Rightarrow \mathcal{F}\left\{\mathrm{Ai}(\gamma^{\frac{1}{3}}x)\right\} = \int dx(3\gamma)^{-1}e^{-ik\gamma^{\frac{1}{3}}x\,\mathrm{Ai}(\gamma^{\frac{1}{3}}x)} =$$

$$= \int \frac{1}{3\gamma}dxe^{-ikx\gamma^{\frac{1}{3}}}\int \frac{dp}{2\pi}e^{ipx\gamma^{\frac{1}{3}}}e^{\frac{ip^3}{3}}\int dx\frac{1}{3\gamma}e^{i(p-k)x\gamma^{\frac{1}{3}}}\int \frac{dp}{2\pi}e^{\frac{ip^3}{3}} = \exp\left[\frac{ik^3}{3\gamma}\right]\frac{1}{\gamma^{\frac{1}{3}}}$$

which finally concludes to:

$$\hat{u}(k,z=0) = \frac{1}{\gamma^{\frac{1}{3}}}\exp\left[\frac{ik^3}{3\gamma}\right] \tag{2.25}$$

So if we substitute Eq. (2.24) to Eq. (2.22) we have

$$u(x,z) = \frac{1}{2\pi}\int_{-\infty}^{\infty}\frac{1}{\gamma^{\frac{1}{3}}}e^{\frac{ik^3}{3\gamma}-\frac{i}{2}\int_0^z \kappa(s)^2ds+i\kappa(z)x}dk \quad = \frac{1}{2\pi}\int_{-\infty}^{\infty}\frac{1}{\gamma^{\frac{1}{3}}}e^{\left[\frac{k^3}{3\gamma}-\frac{1}{2}\int_0^z \kappa(s)^2ds+k(z)x\right]}dk$$

So we have

$$\frac{k^3}{3\gamma} - \frac{1}{2}\int_0^z \kappa(s)^2 ds + \kappa(z)x \tag{2.26}$$

where we assume $F_2(z) = \int_0^z D^2(s)ds$ and $F_1(z) = \int_0^z D(s)ds$. Finally we assume $\kappa(s) = k - \frac{D(z)}{2}$ and Eq. (2.25) becomes

$$\frac{k^3}{3\gamma} - \frac{1}{2}\int_0^z \left(k^2 - kD(s) + \frac{D^2(s)}{4}\right) ds + \left(k - \frac{D(s)}{2}\right) x \Rightarrow$$

$$\Rightarrow \frac{k^3}{3\gamma} - \frac{1}{2}\left[\int_0^z k^2 ds - k\int_0^z D(s)ds + \frac{1}{4}\int_0^z D^2(s)ds\right] + \left(k - \frac{1}{2}D(z)\right) x$$

$$= \frac{k^3}{3\gamma} - \frac{1}{2}\left[\left(\int_0^z k^2 ds - kF_1(z) + \frac{1}{4}F_2(z)\right)\right] + \left(k - \frac{1}{2}D(z)\right) x$$

$$\Rightarrow \frac{k^3}{3\gamma} - \frac{1}{2}\left[k^2 z - kF_1(z) + \frac{1}{4}F_2(z)\right] + \left(k - \frac{1}{2}D(z)\right) x$$

$$\frac{k^3}{3\gamma} - \frac{1}{2}k^2 z + \frac{kF_1(z)}{2} - \frac{F_2(z)}{8} + \left(k - \frac{1}{2}D(z)\right) \tag{2.27}$$

where we assume $k = E + \frac{z}{2}\gamma$ and Eq. (2.26) becomes

$$\frac{1}{3\gamma}\left(E + \frac{z}{2}\gamma\right)^3 - \frac{1}{2}\left(E + \frac{z}{2}\gamma\right)^2 z + \frac{1}{2}\left(E + \frac{z}{2}\gamma\right) F_1(z) - \frac{1}{8}F_2(z)$$

$$+ \left(E + \frac{z - D(z)}{2}\right) x + \frac{1}{3\gamma}\left(E^3 + \frac{3}{2}E^2 z\gamma + \frac{3}{4}Ez^2\gamma^2 + \frac{z^3}{8}\gamma^3\right)$$

$$- \frac{1}{2}\left(E^2 + z\gamma E + \frac{z^2}{4}\gamma^2\right) z + \frac{1}{2}\left(E + \frac{z}{2}\gamma\right) F_1(z) - \frac{1}{8}F_2(z)$$

$$+ \left(E + \frac{z\gamma - D(z)}{2}\right) x = \frac{E^3}{3\gamma} + \frac{1}{2}E^2 z + \frac{1}{4}Ez^2\gamma + \frac{z^3}{24}\gamma + \frac{z^3}{24}\gamma^2$$

$$-\frac{1}{2}E^2 z - \frac{z^2\gamma E}{2} - \frac{z^3}{8}\gamma^2 + \frac{1}{2}EF_1(z) + \frac{z\gamma}{4}F_1 z - \frac{1}{8}F_2(z) + \left(E + \frac{z\gamma - D(z)}{2}\right) x$$

$$=\frac{E^3}{3\gamma}-\frac{1}{4}Ez^2\gamma-\frac{2z^3}{24}\gamma^2+\frac{1}{2}EF_1(z)+\frac{z\gamma}{4}F_1(z)-\frac{1}{8}F_2(z)+Ex+\left(\frac{z\gamma-D(z)}{2}\right)x$$

$$\phi=i\frac{\gamma F_1(z)z}{4}-i\frac{D(z)x}{2}-i\frac{F_2(z)}{8}+i\frac{\gamma zx}{2}-i\frac{\gamma^2z^3}{12} \tag{2.28}$$

$$\mu(x,z)=\frac{F_1(z)}{2}+x-\frac{\gamma z^2}{4} \tag{2.29}$$

Airy$'$ s trajectory is provided by $\mu(x,z)=0\Rightarrow$

$$x=-\frac{F_1(z)}{2}+\frac{\gamma z^2}{4} \tag{2.30}$$

2.5 Airy's Self-Healing properties

Beyond the free acceleration of an Airy beam an other exotic property of any diffraction free beam is it's ability to self-reconstruct through propagation. This property gets more and more important if the propagation of the beam is taking place through inhomogeneous media [72, 86]. It is also important to know under what circumstances this self-healing takes place. For example how the beam's wavelength, acceleration, intensity affect the self healing characteristic of a beam.

2.5.1 Mathematical representation of Self-reconstructing non-diffracting beams

To examine the self healing properties of a nondiffracting beam it was attempted to locate an obstacle at $z=0$ and see how the beam reacts. Of course this phenomenon can be explained from Babinet's principle [72, 87]. So if the non diffracting beam is disturbed by a finite energy perturbation called $\epsilon(x,y)$ i.e., then the given input field will be $\phi\left(x,y,z=0\right)=U_{ND}-\epsilon\left(x,y,z=0\right)$. Then we recall the propagation equation

$$i\frac{\partial\phi}{\partial\xi^2}+\frac{1}{2}\frac{\partial^2\phi}{\partial s^2}=0$$

where $s=\frac{x}{x_0}$, $\xi=\frac{z}{kx_0^2}$ and $k=\frac{2\pi n}{\lambda_0}$

Now if we directly substitute our input non diffracting field to the propagating equation it is easy to found $-ik\epsilon_z-\frac{1}{2}\bigtriangledown_\perp^2\epsilon=0\Rightarrow i\epsilon_z+\frac{1}{2k}\bigtriangledown_\perp^2\epsilon=0$.
This means that perturbation ϵ diffracts very rapidly as it was expected while on the other hand the nondiffracting wave remains invariant during propagation. As

a result $0 \lim_{z\to\infty} \epsilon(x,y,z) = 0$ which leads to $\phi(x,y,z) = U_{ND}(x,y,z)$ as $z \to \infty$ which concludes to that the non diffracting waves so as the Airy remain their undistorted properties.

2.6 Experimental methods for Self-healing properties of Nondiffracting Waves

To study those theoretical results mentioned above there is a number of experiments that are designed in order to see in practise those self-healing properties. To begin with a rectangular opaque obstacle used to block the Airy wave and see how it's self healing properties intrude to reconstruct Airy$'s$ undistorted propagation. A first set of experiments is designed so as to block the first lobe of an Airy accelerating wave. The first lobe is important because in there is included a large percentage of the wave energy. The experiments show that Airy$'s$ self healing properties are in this case strong enough to reconstruct the undistorted propagation of the beam.

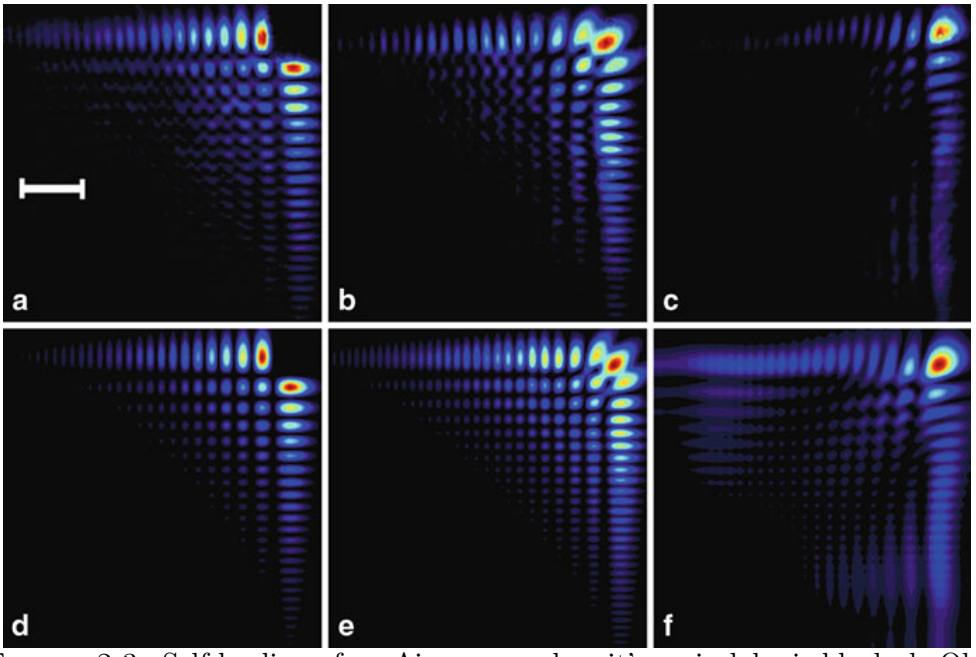

FIGURE 2.3: Self-healing of an Airy wave when it's main lobe is blocked. Observed intensity profile at (a) the input z=0, (b) z = 11 cm, and (c) z =30 cm. The corresponding numerical simulations are shown in (d–f)

Figure 2.3b depicts the reformation of this Airy beam after a distance of $z = 11cm$. The self-healing of this beam is apparent. The main lobe is reborn at

the corner and persists undistorted up to a distance of 30 cm Fig. 2.3c. Though an experiment that is designed to block a much bigger amount of Airy$'$ s energy rather than the first lobe will be far more interesting. Thus an experiment wich will lead us to very interesting results will be an experiment where we will block the whole internal structure of the Airy wave Fig. 2.4a. Even in this case the self healing properties of nondiffracting waves take place and the wave reconstruct its intensity profile.

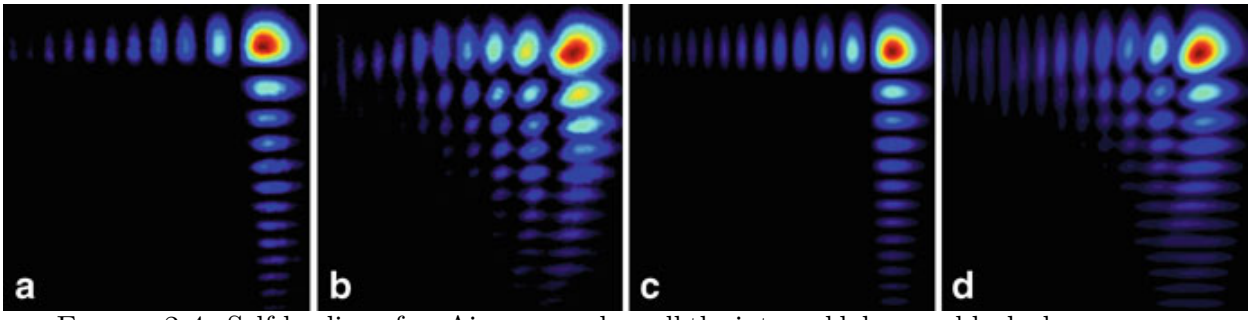

FIGURE 2.4: Self-healing of an Airy wave when all the internal lobes are blocked. Observed intensity profiles at (a) the input z =0 and (b) z = 16 cm. The corresponding numerical simulations are shown in (c) and (d)

Remarkably after z = 16 cm of propagation the wave self-heals and reconstructs in detail its fine intensity structure as depicted in Fig. 2.4b.
Figure 2.4c, d shows the corresponding calculated intensity profiles for these same distances.

Similar results occur when the obstacle is non symmetric. In this set of experiments the first three lobes of an Airy wave have been blocked. In this experiment apart from the arise of the self healing properties of non-diffracting waves it seems that the initially blocked lobes are reborn even brighter when compared to its surroundings. This is a clear manifestation of the nondiffracting character of the Airy wave. [72, 88].

2.7 The co-propagation of an Airy and a soliton pulse.

2.7.1 Nonlinear's effect contributions in the interaction of Airy with other pulses.

Recently the ability to manipulate optical waves with the usage of optical waves has been very promising while a lot of research has been done the last years to make this perspective more and more effective [89–92]. Thus the XPM nonlinearity is a very important variable in this exciting prospect. The existence of two pulses in order to control light's properties is ensured by the nature of XPM which in simple words is describing a kind of interaction between the two propagating pulses [1, 89]. This interaction is described while we induce third order nonlinearities in group velocity dispersion approximation. More particularly both the dynamics and the spectra of a signal can be manipulated by assuming proper characteristics of the control pulse such as amplitude, pulse width and walk-off between the signal and the pump pulse [89, 93, 94].

While we use a fundamental soliton for the signal the choice of the control pulse should be more careful. It is proposed that nondispersive wave packets such as Airy wave packet are able to control weaker in comparison with them signals at the optical event horizon region [89, 95]. Airy wave packet is preferred because compared with other nondispersive wave packets have a larger intensity due to its self healing properties.

Naturally a dispersive wave packet will lose it's intensity and would be disformed after the interaction with a high power soliton. Thus the dispersive character of such beams make it harder to control the evolution copropagating soliton. The advantage of Airy wave packet is due to it's ability to maintain it's intense even after the reaction with the fundamental soliton. Thus the interaction of the copropagating pulses will be increased.

Airy wave packets known as Self Accelerating Beams can propagate either on linear or nonlinear regime [96–98] . The case where the Airy is nonlinear is of particular interest because of it's high intensity non-dispersive pulse that is produced. While in the case where both soliton and Airy pulses have the same wavelength a lot of research has been done [99], in the case that the corresponding wavelengths are different wasn't investigated. A very recent study [89] shows that the Airy-soliton interactions with different wavelengths differ in a fundamental way from

what we observe in the case with the same wavelengths. More specifically while in the case with the same wavelengths as we mentioned before the nondispersive Airy wave packet gives us the possibility to obtain soliton manipulation, in the case with different wavelengths Airy beam is not capable to walk-off the soliton reconstructing an optical event horizon where Airy is frequence/time shifted.

Interestingly enough if Airy wave packet is substituted by an equal energy *Gaussian* pulse to play the role of the pump pulse the *Gaussian*-soliton interaction is not strong enough compared with the Airy-soliton one, and that's because Airy-soliton interaction is carrying higher levels of induced XPM nonlinearity . Thus the Airy wave packet has far more potentials in than the *Gaussian* in the field of signals control.

Relative stimulations show that by letting the soliton pulse propagate at the anomalous dispersion and the Airy wave packet in the normal we can observe the creation of XPM nonlinearity which is due to the interaction between the two pulses. The XPM acts by preventing as a natural barrier and does not let the Airy pulse to overlap the soliton. Because of it's dispersion free character Airy tends to freely accelerate while it's most energy is concentrated in the main lobe which is very important because it helps Airy not to distort while it's propagation. Because of the interaction between the Airy pulse and the soliton the most of the intensity of Airy reflects, leading to heavy effects on soliton. As we have seen in our stimulations the signal pulse tends to accelerate and follow a parabolic trajectory after the interaction with the Airy pulse.

The Airy pulse can also affect soliton's spectra [97]. As we have seen in our numerical results signal's acceleration is translated as a shift of signal's frequency toward the blue. For the realisation of the Airy a truncation constant is necessary. The smaller this constant is the higher power the Airy pulse carries. This aspect is very important because the more powerful is the Airy the stronger will be it's effects on the copropagating pulse which in our case is a signal.

When the truncation constant was bigger than 0.2 $Airy's$ total power was lower than a *Gaussian* pulse with the same peak intensity while with such a truncation constant oscillations in the trailing edge were significantly more, comparing with a much smaller truncation coefficient. In spite the fact that a significantly trunctated Airy pulse has less power than a *Gaussian* pulse with the same peak intensity Airy is able to shift both the soliton and it's spectrum components more than a *Gaussian* is able to.

In Figure 2.5 we depict both a low and highly truncated Airy. In the first row

we depict in figure (a) the propagation dynamics while in (b) is illustrated the intensity profile for the truncated Airy for $a = 0.01$. In second row we show the propagation dynamics in figure (c) while in (d) the corresponding intensity profile is illustrated. We see that the highly truncated Airy creates oscillation in the trailing edge which means that more energy is concentrated in this particular area and thus the peak intensity of the Airy is less and thus the energy in the main lobe is less compared with an Airy with $a = 0.01$. Thus the propagation of the Airy is distorted while it propagates. The difference in the low truncated Airy is that the peak intensity is concentrated in the main lobe, and thus Airy pulse retains it's shape and propagates following an accelerating trajectory.

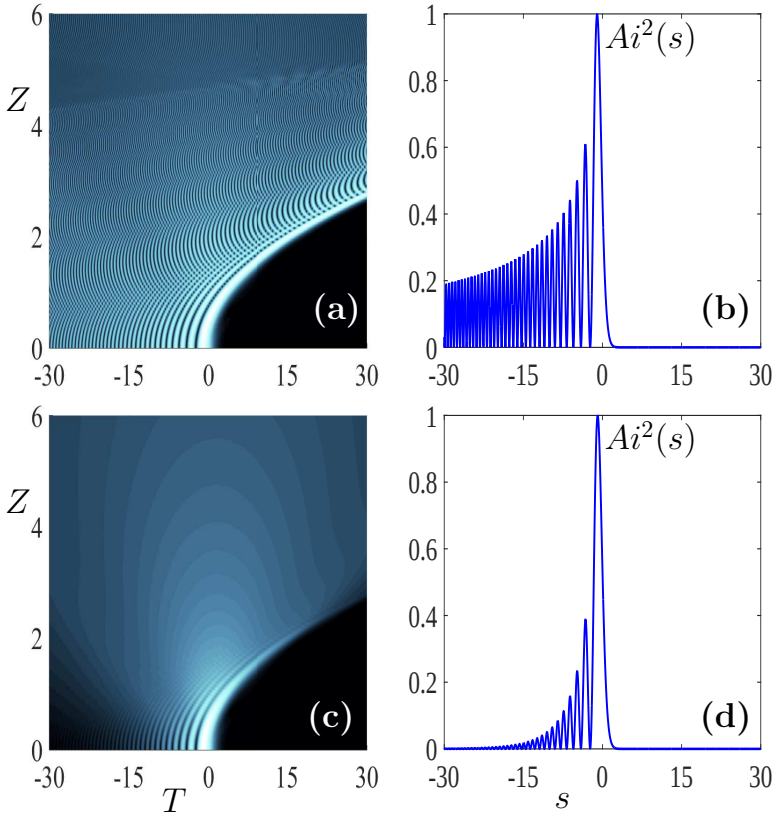

FIGURE 2.5: In the upper row we depict the propagation dynamics and the intensity profile of an infinite energy Airy with a small truncating constant $a = 0.01$ while in the second row we show the corresponding simulations for a large truncation constant $a = 0.1$

2.7.2 The pair of Nonlinear Schrödinger Equations

At this section we will study the principals that govern the propagation of a signal pulse along with an Airy pulse. Due to it's guiding features we will also call

Airy as a control pulse. Starting from the pair of NLS equation that govern the propagation of two optical pulses in a dispersive nonlinear media we obtain the two following equations

$$i\frac{\partial u}{\partial z} - \frac{\beta_u}{2}\frac{\partial^2 u}{\partial t^2} + \left(|u|^2 + 2|v|^2\right)u = 0 \tag{2.31}$$

$$i\frac{\partial v}{\partial z} - \frac{\beta_v}{2}\frac{\partial^2 v}{\partial t^2} + \left(|v|^2 + 2|u|^2\right)v = 0 \tag{2.32}$$

A slightly different system from Eqs. (2.31),(2.32) was first described by Manakov(1974) where z is the normalized distance along the waveguide and x is a traverse coordinate. By assuming that u governs the propagation of an Airy-(control) pulse while v governs the propagation of a signal pulse we can proceed with the following analysis:

To begin with terms β_u and β_v referred to the group-velocity dispersions for the u and v respectively.

Secondly for Eq. (2.31) terms $\left(|u|^2 + 2|v|^2\right)$ describe the nonlinear phenomena that occur during the propagation. For this equation term $|u|^2$ describes the SPM while term $2|v|^2$ is responsible for the XPM. Both of those nonlinear effects as well as the Chromatic Dispersion have been described in Chapter 1.

On the other hand in Eq. (2.32) terms $\left(2|u|^2 + |v|^2\right)$ describe the nonlinear effects occur while the propagation and related to the signal pulse. In contrast with Eq. (2.31) term $2|u|^2$ is now related with the XPM while term $|v|^2$ is now responsible for the SPM.

2.7.3 The initial conditions used

To continue our analysis we will mention the equations which describe the two copropagating pulses for u and v respectively.

$$u = \frac{d_2\,\mathrm{Ai}(d_3 t)\exp(at)}{0.535656} \tag{2.33}$$

$$v = d_4 d_5\,\mathrm{sech}((t - t_0)d_5) \tag{2.34}$$

As we can see Eq. (2.33) describes an Airy pulse where d_2 represents Airy$'s$ amplitude, d_3 stands for Airy$'s$ acceleration as well as width factor while α is the truncation coefficient which is necessary for the realization of the Airy. The constant at the denominator is used for normalization purposes. Heading now to

Eq. (2.34) where d_4 represents signal's pulse amplitude where d_5 is responsible for signal's width, while t_0 represents where the signal pulse is located.

While we always choose d_2 in such a way that the Airy has a nonlinear formation for d_4 we distinguish two cases where in the first one Eq. (2.34) describes a linear signal pulse while the other one a nonlinear signal pulse. Thus when $d_4 \ll 1$ we assume a linear formation while when $d_4 \approx 1$ a nonlinear form. An other essential point is t_0. In the procedure that follows depending on the formation of the Airy pulse we assumed, we locate the central of the signal pulse to be placed at Airy$'$ s local maxima or minima points. So beginning from Airy$'$ s main lobe where the first maximum is located we end up to Airy$'$ s second local minimum.

Finally depending on the sign of β_u and β_v we will distinguish four different cases. As we have mentioned in the first Chapter when the group velocity dispersion parameter is positive then the pulses propagates in the normal dispersion regime. On the other hand when this parameter is negative the pulse propagates in the anomalous dispersion regime where the creation of solitons is proposed.

2.7.4 Following Chapters Overview

In Chapter 3 we emphasize on the case that both pulses propagate in the normal dispersion regime under a self-defocusing nonlinearity. Basically as we mentioned before we distinguish two cases; the linear and the nonlinear while we assume every time a different focal point between the soliton and the Airy pulse. Starting from the linear propagation and Airy$'$ s first maximum we will end up to Airy$'$ s second minimum. Before we moved to the nonlinear propagation we test a special focal point where our goal is to examine Airy$'$ s pushing properties. After that moving to the nonlinear propagation where we begin again from Airy$'$ s first maximum to end up with Airy$'$ s second minimum. The same procedure follows with almost all the other cases .

In Chapter 4 Airy pulse propagates in the anomalous dispersion while the signal pulse propagates in the normal dispersion regime . As we mentioned before *Airy* propagating in the anomalous dispersion regime is not supposed to exhibit Airy$'$ s affect on the signal pulse although when it comes to the examine Airy$'$ s pushing properties we can see that the signal's manipulation is obtainable both in the linear and the nonlinear propagation.

In Chapter 5 Airy propagates in the normal dispersion regime while the signal pulse propagates in the anomalous dispersion regime . These conditions let Airy to exhibit its guiding features and manipulate the signal pulse so as to to follow

a parabolic accelerating trajectory no matter the linear or nonlinear formation of the signal pulse.

In Chapter 6 both pulses propagate in the anomalous dispersion regime . Thus the corresponding nonlinear effects along with the intense enough signal pulse that are taking place, make the affect of the Airy pulse on the signal pulse weak, that Airy almost past through the soliton pulse. This phenomenon is observed while we locate the center of the soliton pulse away from Airy$'s$ main lobe and especially in the nonlinear propagating signal pulse where high intensity signal pulses are interacting with the Airy pulse.

Chapter 3

Airy and signal evolution in the normal dispersion regime

3.1 Linear signal evolution

We will begin with the case where both of our pulses propagate in the normal dispersion regime while we assumed a linear formation for the signal pulse. At the same time as we mentioned in Chapter 2 we always assume a nonlinear formation for the control pulse. Due to the fact that both pulses propagate in the normal dispersion regime both β_u and β_v are positive. More analytically we assume $\beta_u = 2$ while $\beta_v = 1$. So by numerically solving Eqs. (2.31),(2.32) while using Eqs. (2.33),(2.34) for several values of t_0 which consist Airy$'$ s critical points (minima, maxima) we will now present the results we derive.

3.1.1 Signal localized at Airy's first maximum

We will begin by localizing the beam at Airy$'$ s first maximum $(t_0 = -1.019)$. Thus by recalling that β_v is positive we can conclude that the signal pulse is located at potential maximum point.
Figure (3.1) depicts the relative stimulation where we can see the affect of the Airy on the signal pulse as the signal is been manipulated to follow Airy$'$ s parabolic-accelerating trajectory. Although as anyone can see a part of the spectral components of the signal pulse still propagates invariant while an other spectral part accelerates along with the Airy pulse. Figure 3.1(b)depicts the spectra of the signal pulse. Signal's frequency is shifted towards the blue and that's due to the acceleration that the signal pulse is under. The split up that occurs between the Airy and the signal pulse is due to the fact that the focal point is set at signal's

potential maximum. But at last the bigger the gradient is formed the more the signal is accelerated.

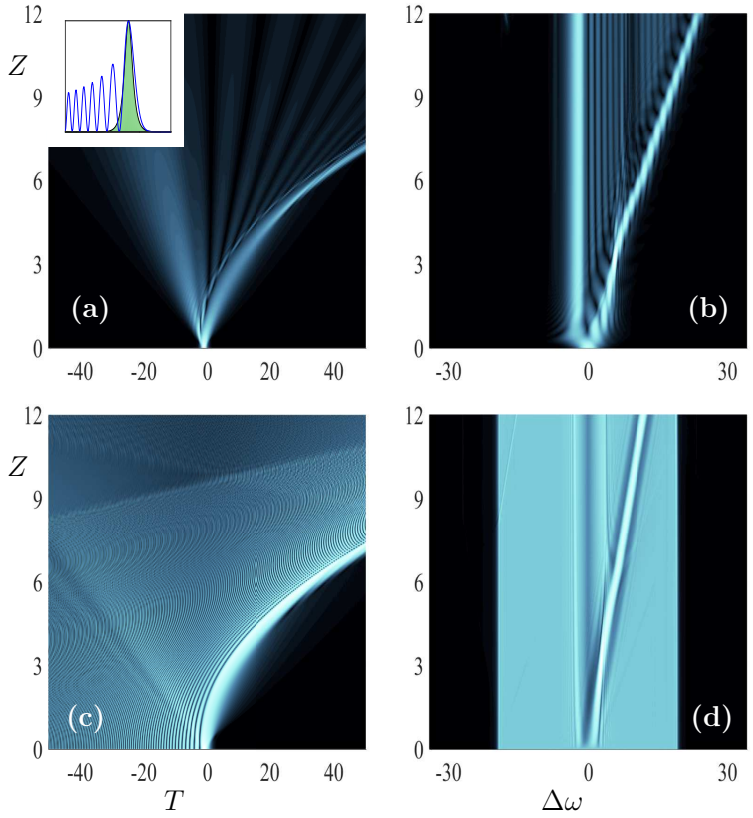

FIGURE 3.1: For the signal we assume: $d4 = 0.00001$,$d_5 = 2$ as for the control pulse : $d_2 = 2.5$, $d_3 = 1$ and $a = 0.001$. In the first column we show the dynamics of the signal/ control pulse respectively, while in the second column we show the corresponding spectra of the pulses. The inset in (a) shows the initial condition of the signal(green shaded)/ control pulse. The signal is magnified for illustration purposes.

3.1.2 Signal localized at Airy's first minimum

We will continue under the same initial conditions but the only change will be the center of the signal pulse. Now we will test the case where t_0 is located at a local minimum point of Airy at $t_0 = -2.3482$.

In Figure 3.2 as the central of the signal pulse is located at Airy′ *s* first minimum and the dispersion coefficient of u is positive we conclude that the signal pulse is located at a minimum point of the potential. Thus we expect the affect of Airy on the signal to be more intense. This practically means that the Airy pulse will be able to drag the signal pulse without the split-up that we observed in the case

before. As we can see in (b), compared with the Figure 3.1, Airy is capable of accelerating a lot more spectral components of the signal pulse although still a small part of them propagates invariant.

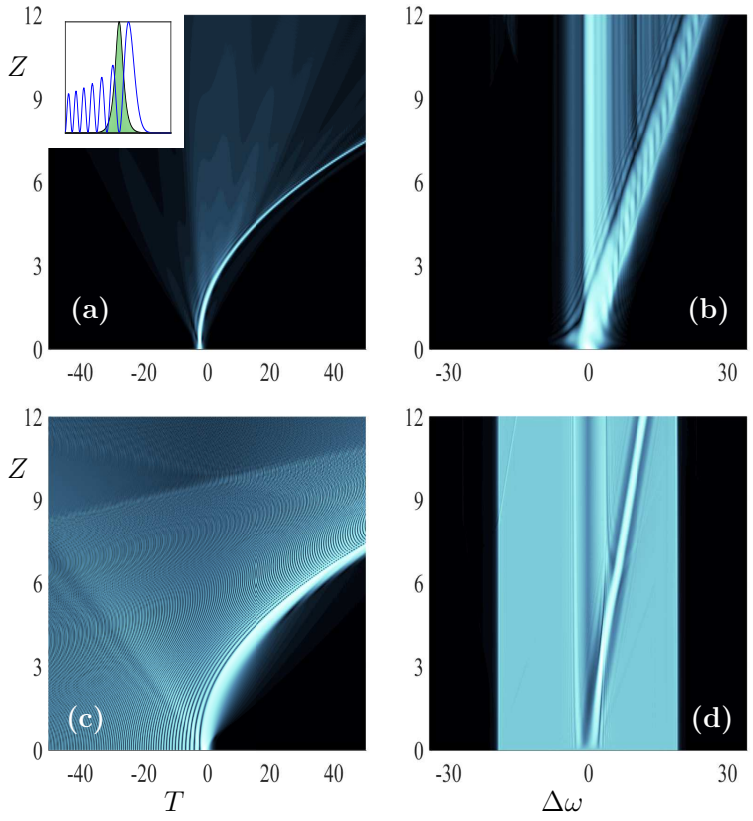

FIGURE 3.2: In the first column we show the dynamics of the signal/ control pulse respectively, while in the second column we show the corresponding spectra of the pulses. The inset in (a) shows the initial condition of the signal(green shaded)/ control pulse. The signal is magnified for illustration purposes.

3.1.3 Signal localized at Airy's second maximum

Now we will locate the center of the signal pulse at $t_0 = -3.227$ a local maximum of Airy′ *s* function and the relative stimulations are presented in Fig. 3.3 where it is obvious that the more the center of the signal pulse is localized away from Airy′ *s* first maximum the less the affect of the Airy is on the signal pulse. Thus more and more signal's components seem to ignore the acceleration and the parabolic trajectory of Airy. As a result more and more signal's components tend to form a pulse which propagates invariant through z. Again the focal point is located at a signal's potential maximum. Thus the split-up which we observe in

Figure 3.1 occurs again but this time more signal's components propagate invariant. Although *Airy′s* momentum is still able to manipulate part of the components of the signal to form an accelerating combined pulse.

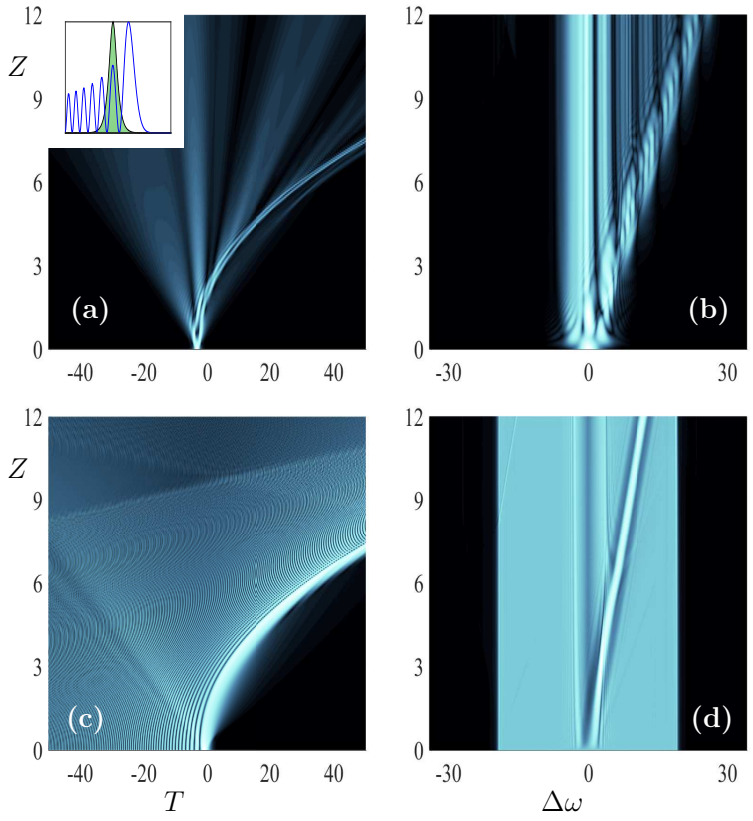

FIGURE 3.3: In the first column we show the dynamics of the signal/ control pulse respectively, while in the second column we show the corresponding spectra of the pulses. Thus the first/ second row corresponds to the signal/ control pulse. The inset in (a) shows the initial condition of the signal(green shaded)/ control pulse. The signal is magnified for illustration purposes.

3.1.4 Signal localized at Airy's second minimum

Just before we close the *Linear* sub case we will present now the results we got after locating the signal at $t_0 = -4.1309$.

In Figure 3.4 the center of the signal pulse is located at Airy′ *s* second minimum. Thus it might the affect of the Airy on the signal pulse be weaker but the main lobe of the signal pulse is caved at Airy′ *s* second minimum in a way that it tends to follow an accelerating, parabolic trajectory. Although comparing with the relative simulations of Figure 3.2, where the focal point is closer to Airy′ *s* main lobe, thus this particular lobe contains higher levels of energy, and the acceleration of the

pulse which is created in Figure 3.4 ,and can be observed from the gradient of the signal pulse, is less. From Figure 3.4(b) that shows the spectra of the signal pulse we can observe how the interaction between the signal and the control pulse affect signal's spectra. Signal pulse frequency experiences a shift towards the blue. The fact that the focal point is set at signal's potential minimum is essential for the phenomena described above.

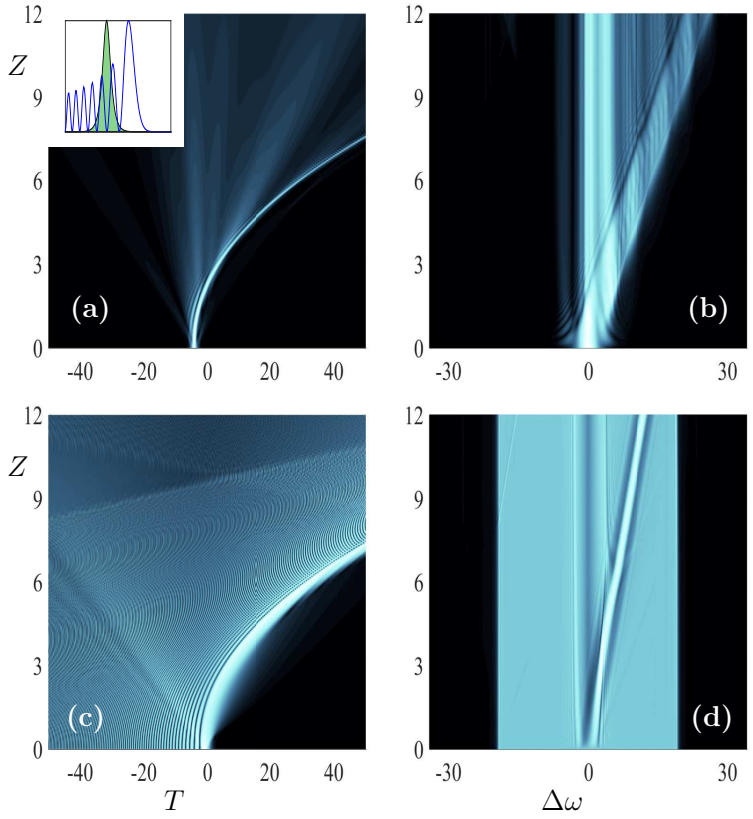

FIGURE 3.4: In the first column we show the dynamics of the signal/ control pulse respectively, while in the second column we show the corresponding spectra of the pulses. The inset in (a) shows the initial condition of the signal(green shaded)/ control pulse. The signal is magnified for illustration purposes.

3.1.5 Examining Airy's pushing properties

To examine the "*pushing*" properties of *Airy′s* function we will set $t_0 = 2.3842$ and we will reduce Airy′ *s* acceleration.

Figure 3.5 shows that if we locate the center of the signal pulse to be after Airy′ *s* main lobe, then we the affect of the Airy is much more intense. In this subcase we can observe the pushing features of Airy as Airy pushes the signal pulse to follow an accelerating trajectory from the moment that the control pulse collides

with the signal pulse. Signal's spectra is shifted towards the blue as a clear sign of the acceleration of the signal's pulse, while at the same time signal's spectra is compressed. In this subcase we reduced Airy′ *s* acceleration in order to make the effects of Airy more noticeable to the signal pulse. Although a slower accelerating Airy pulse may accelerate less the signal pulse, it may be easier to keep it in front of Airy′ *s* main lobe rather than to pass by.

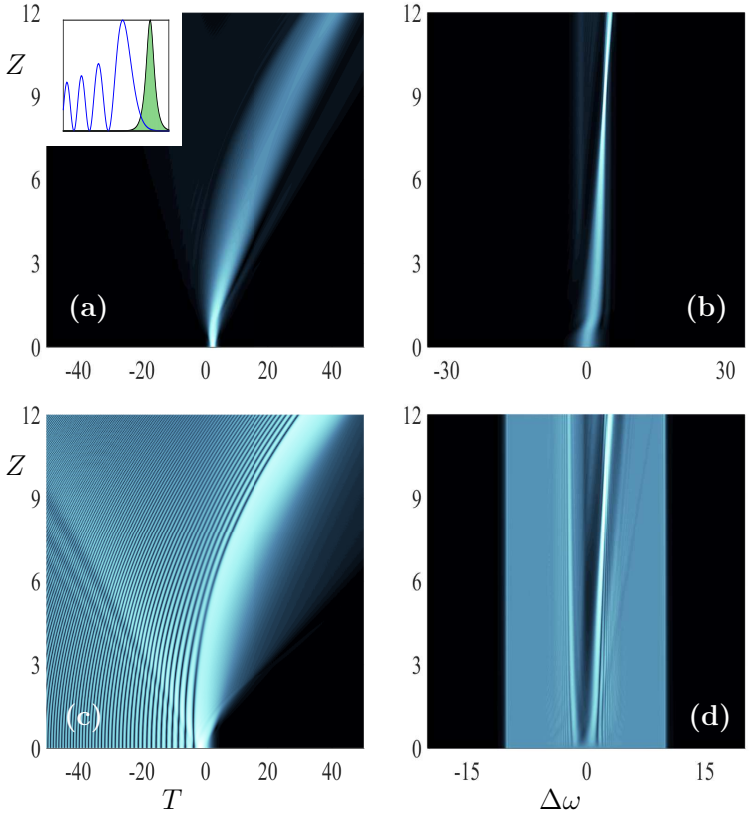

FIGURE 3.5: In the first column we show the dynamics of the signal/ control pulse respectively, while in the second column we show the corresponding spectra of the pulses. Thus the first/second row corresponds to the signal/ control pulse. The inset in (a) shows the initial condition of the signal(green shaded)/ control pulse. The signal is magnified for illustration purposes.

Before we proceed with the evolution of a nonlinear signal we should point out the advantage of the linear signal pulses against the nonlinear. Linear signals due to their low intensity can interact with a control pulse in a way that is easier for the control pulse to exhibit its own manipulating feature on the signal pulse. This does not means in any case that a nonlinear signal pulse is inappropriate for such dragging or pushing phenomena. Although as we will see in the chapter that follows the results while we use a linear signal pulse are better in comparison with those in the section of the nonlinear signal evolution.

3.2 Nonlinear signal evolution

At this section we will present the results we got by examining the *Nonlinear* case where the two initial conditions have the following form:

$$u = \frac{d_2\,\mathrm{Ai}(d_3 t)\exp(at))}{0.535656} \tag{3.1}$$

$$v = d_4 d_5\,\mathrm{sech}((t - t_0)d_5) \tag{3.2}$$

As we have mentioned before u describes an Airy pulse where d_2 represents Airy$'$ s amplitude, d_3 stands for Airy$'$ s acceleration as well as width factor, while α is the truncation coefficient which is necessary for the realization of the Airy. The constant at the denominator is used for normalization purposes. Heading now to v where d_4 represents signal's pulse amplitude where d_5 is responsible for signal's width, while t_0 represents where the signal pulse is located.
At this point it is important to examine how the nonlinearity affects the results we got above. As we mentioned before a nonlinear signal pulse will exhibit more resistance to Airy$'$ s accelerating property and thus the effect of the Airy pulse on the nonlinear signal pulse is not expected to be as intense as in the linear signal propagation. The higher intensity signal pulse that we assumed may lead us to more dispersive phenomena depending always the focal point that we examine.
To start with we will begin by examining our code by localizing the center of the signal at Airy$'$ s first maximum and we will continue with the rest of the points we tested before.

3.2.1 Signal localized at Airy's first maximum

So by assuming $t_0 = -1.019$ we locate the central of the signal pulse to be at Airy$'$ s first maximum.
Thus in Figure 3.6 we can see simulations that are pretty close to the linear case and that is because all the coefficients consisting u, v are the same with the linear case except from the intensity of the signal pulse. The nonlinearity of the signal pulse can lead to the creation of other pulses that propagate almost invariant. Even from this first local point we can observe that slight difference between the linear and nonlinear subcases. The fact that the focal point is set at signal's potential maximum along with the nonlinearity of the signal pulse leads to the split-up between the copropagating pulses and enhances the dispersive phenomena that are observed.

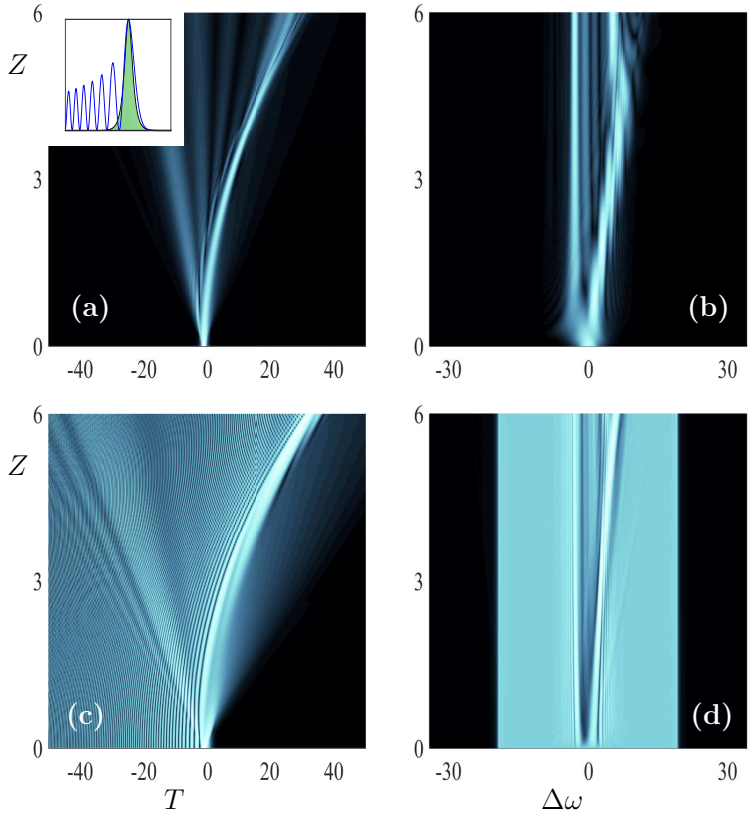

FIGURE 3.6: For the signal pulse we assume: $d4 = 1$,$d_5 = 2$ as for the control pulse : $d_2 = 2.5$,$d_3 = 1$ and $a = 0.005$. In the first column we show the dynamics of the signal/ control pulse respectively, while in the second column we show the corresponding spectra of the pulses. Thus the first/second row corresponds to the signal/ control pulse. The inset in (a) shows the initial condition of the signal(green shaded)/ control pulse. The signal is magnified for illustration purposes.

3.2.2 Signal localized at Airy's first minimum

So after examining the first value for t_0 we will now test our code for an other value of t_0. Now we will assume that $t_0 = -2.3482$ and the results we got are shown in Figure 3.7.

In Figure 3.7 the results after we have located the central of the signal pulse at Airy′ *s* first minimum are shown. As we have seen before in the linear subcase the first minimum seems to be a focal point were the intensity of Airy pulse seems to have a big effect on the signal pulse and that is because this particular critical point of Airy consists a signal's potential minimum point. As we can observe the gradient of the signal pulse in the spectral space is such that it is suggesting hard acceleration. Although a part of the signal pulse seem to ignore Airy′ *s*

accelerating feature and still propagating invariant. Despite that the focal point is set at a signal's potential minimum although the signal's intensity is enough to lead us to dispersive phenomena.

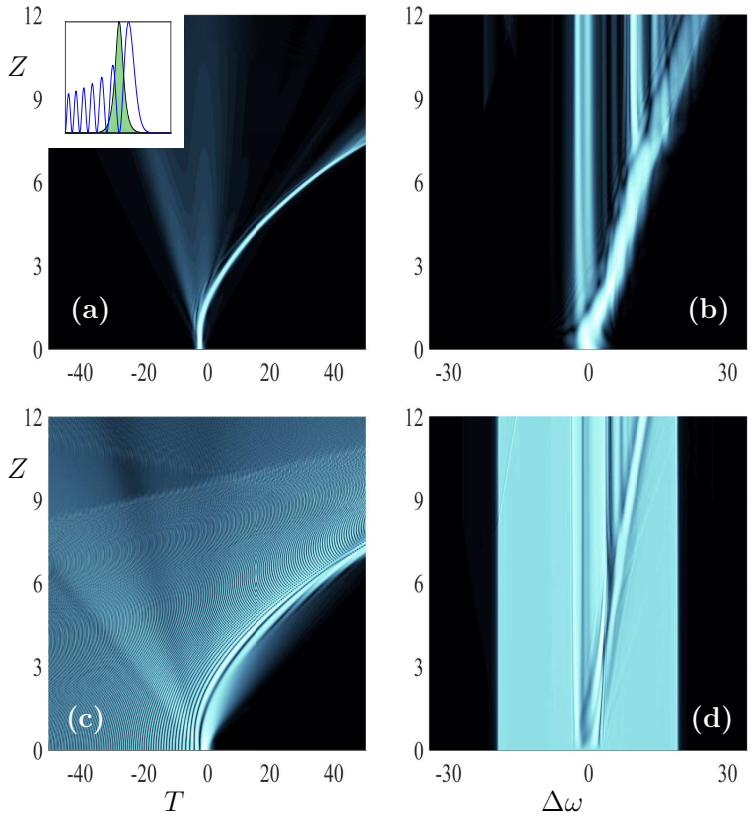

FIGURE 3.7: In the first column we show the dynamics of the signal/ control pulse respectively, while in the second column we show the corresponding spectra of the pulses. Thus the first/second row corresponds to the signal/ control pulse. The inset in (a) shows the initial condition of the signal (green shaded)/ control pulse. The signal is magnified for illustration purposes.

3.2.3 Signal localized at Airy's second maximum

Continuing with the next point we will set $t_0 = -3.227$ at Airy′ *s* second maximum and the results we got are presented in the following figure. In Figure 3.8 we locate the central of the signal pulse at Airy′ *s* second maximum. If we observe the dynamics of our simulation we will see that the signal pulse is heavily distorted while the Airy pulse drugs part of the signal to *Airy′s* first minimum. Thus the dragging effect of Airy is not as clear and that's because both the nonlinear effects and the "nature" of the focal point doesn't contribute to Airy′ *s* signal pulse guiding potential. In this subcase the focal point is set a signal's pulse

potential maximum. Thus as we cleared out before the signal pulse tends to move away from this focal point and cave itself at the first attractive focal point where signal's potential is minimum. Again a split-up between the copropagating pulses is taking place along with heavy dispersion phenomena.

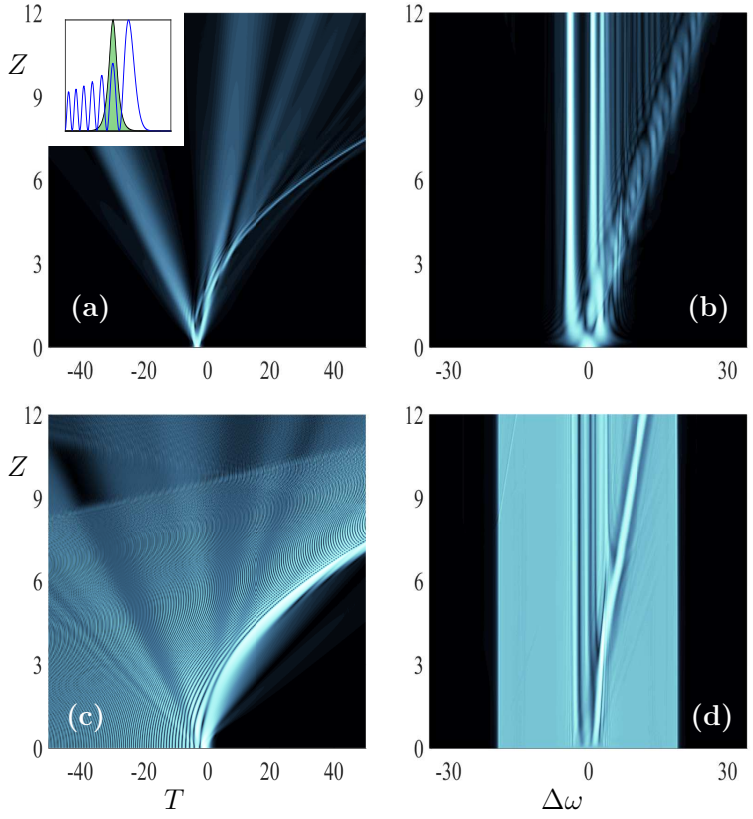

FIGURE 3.8: In the first column we show the dynamics of the signal/ control pulse respectively, while in the second column we show the corresponding spectra of the pulses. Thus the first/second row corresponds to the signal/ control pulse. The inset in (a) shows the initial condition of the signal(green shaded)/ control pulse. The signal is magnified for illustration purposes.

3.2.4 Signal localized at Airy's second minimum

Just before we close the *nonlinear* subcase we will present now the results we got after locating the pulse at $t_0 = -4.1309$; the second local minimum of Airy′ *s* function while our results are shown in Figure 3.9.

In Figure 3.9 even from the dynamics of the signal pulse shown in (a) we can see that other pulses that propagate invariant are created. In the spectra space those pulses can be represented in a more clear way as the signal and the control pulse propagate through z. The nonlinearity of the signal pulse along with the

nonlinearity of the Airy creates radiation that is translated in pulses that can not be drifted by the Airy pulse. As the center of the signal pulse is located at Airy′ *s* second minimum away from Airy′ *s* center the affect of Airy on the signal is expected to be less intense meaning that the signal pulse will exhibit some resistance to Airy′ *s* guiding capability. Although even in that case components of the signal pulse are clearly guided from Airy to follow a parabolic trajectory.

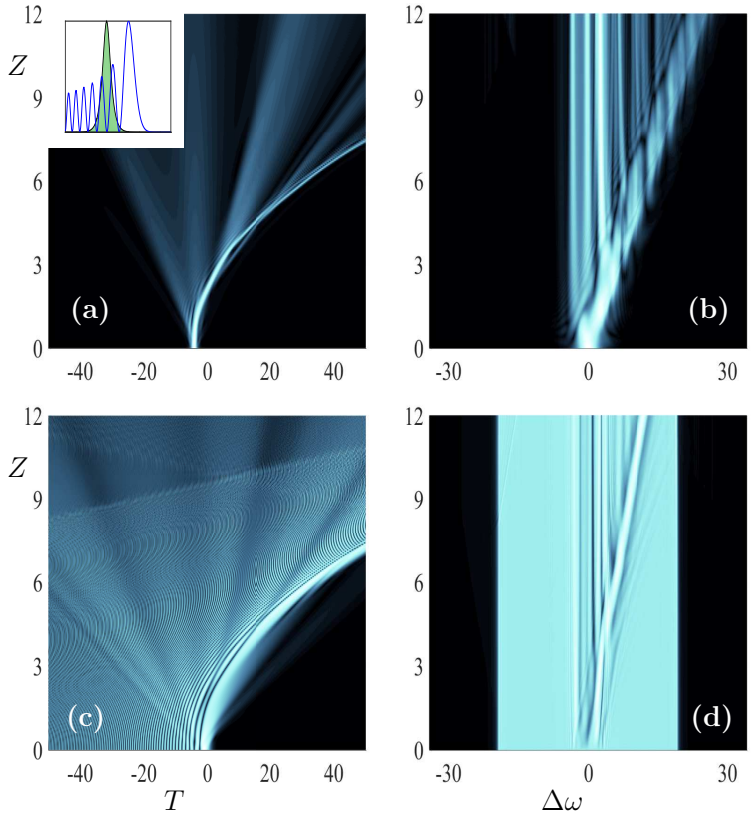

FIGURE 3.9: In the first column we show the dynamics of the signal/ control pulse respectively, while in the second column we show the corresponding spectra of the pulses. Thus the first/second row corresponds to the signal/ control pulse. The inset in (a) shows the initial condition of the signal(green shaded)/ control pulse. The signal is magnified for illustration purposes.

3.2.5 Examining Airy's pushing properties

To test again the "*pushing*" properties of the Airy pulse in the *nonlinear* propagation case we assume $x_0 > 0$ and be centred at $t_0 = 2.3482$ and the results we got are depicted in the Figure that follows:

In Figure 3.10 we test again the pushing properties of Airy. More specifically we locate the central of the signal pulse to be located after Airy′ *s* first maximum.

Thus as we can see from our simulations the main lobe of Airy where the most of Airy′ *s* energy is located will interact with the signal pulse, making the signal pulse to follow Airy on a parabolic trajectory. At this point we should mention that in this case too we slow down a bit Airy so as that the signal pulse will understand the reaction of Airy . As a result the signal is continuously pushed from Airy′ *s* main lobe. The reduction in Airy′ *s* acceleration is essential because in the case that Airy was very fast it will eventually pass by the signal without effecting it at all.

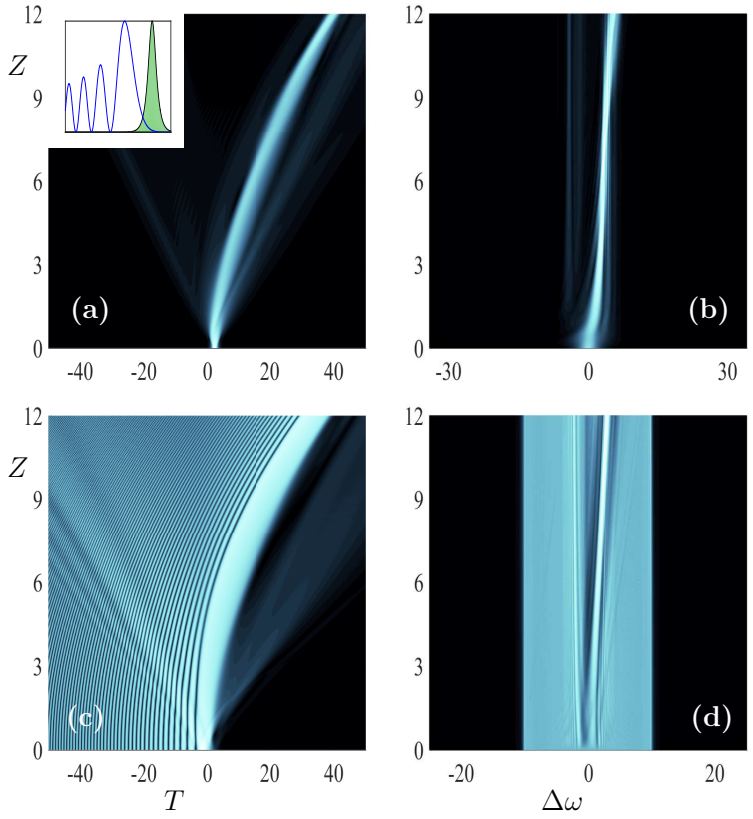

FIGURE 3.10: In the first column we show the dynamics of the signal/ control pulse respectively, while in the second column we show the corresponding spectra of the pulses. Thus the first/second row corresponds to the signal/ control pulse. The inset in (a) shows the initial condition of the signal probe(green shaded)/ control pulse. The signal is magnified for illustration purposes.

Chapter 4

Airy/signal evolution in the anomalous/normal dispersion regime

4.1 Linear signal evolution

After we have tested the case that both of the pulses propagate in the normal dispersion regime now we will proceed with the case that the Airy pulse propagates in the anomalous while the signal pulse in the normal dispersion regime. In order to make it clear we will write down the system of NLS equations that govern the propagation of those two pulses while the initial conditions we used are following next.

$$i\frac{\partial u}{\partial z} - \frac{\beta_u}{2}\frac{\partial^2 u}{\partial t^2} + (|u|^2 + 2|v|^2)u = 0 \tag{4.1}$$

$$i\frac{\partial v}{\partial z} - \frac{\beta_v}{2}\frac{\partial^2 u}{\partial t^2} + (2|u|^2 + |v|^2)v = 0 \tag{4.2}$$

where we substitute $\beta_u = -1$ and $\beta_v = \frac{1}{2}$. With regard to the initial conditions of the system above we take:

$$u = \frac{d_2\,\mathrm{Ai}(d_3 t)\exp(at))}{0.535656} \tag{4.3}$$

$$v = d_4 d_5\,\mathrm{sech}((t - t_0)d_5) \tag{4.4}$$

As we can see β_u is negative which corresponds to anomalous dispersion while β_v is positive which corresponds to normal dispersion. The fact that Airy pulse propagates in the anomalous dispersion regime indicates the creation of solitons

as at this regime the creation of solitons is proposed . Thus an Airy pulse with high intensity will lead to the creation of high intensity solitons. While for the control pulse we assumed a nonlinear form, for the signal pulse we will begin with a linear form and then we will proceed with the corresponding nonlinear.

4.1.1 Signal localized at Airy's first maximum

So we will test again both *linear* and *nonlinear* cases beginning with the first one. Now depending on the case the parameters d_2, d_3, d_4, d_5, x_0 will change. To start with we will locate the center of the signal pulse to be placed at Airy′ *s* first maximum and the results we got are the following:

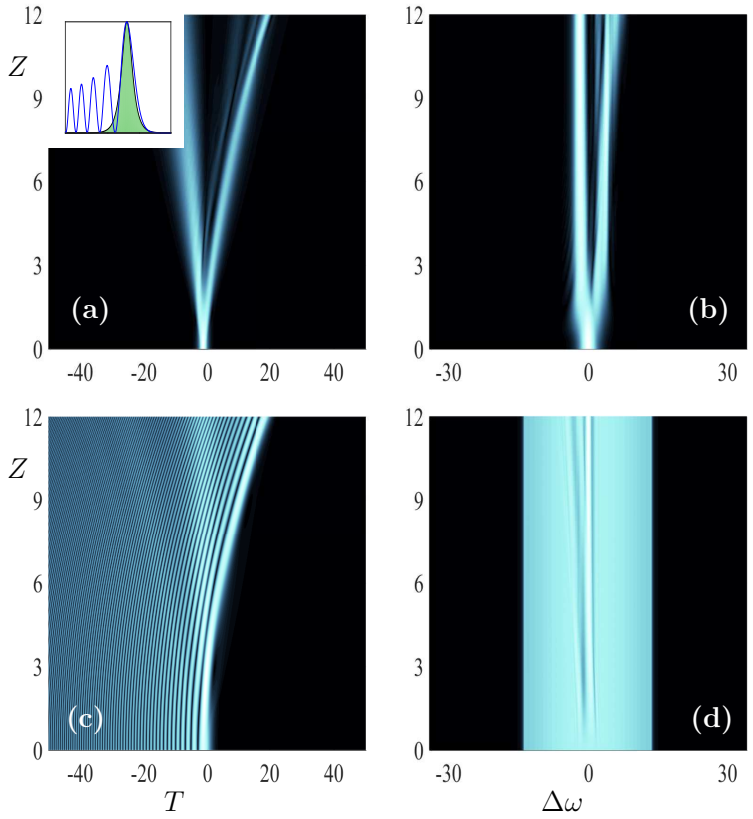

FIGURE 4.1: For the signal we assume: $d4 = 0.00001$,$d_5 = 1.5$ as for the control pulse : $d_2 = 0.8$,$d_3 = 0.8$ and $a = 0.005$. In the first column we show the dynamics of the signal/ control pulse respectively, while in the second column we show the corresponding spectra of the pulses. Thus the first/second row corresponds to the signal/ control pulse. The inset in (a) shows the initial condition of the signal(green shaded)/ control pulse. The signal is magnified for illustration purposes.

Figure 4.1 depicts the propagation of the two pulses we assumed in the real and spectral space. The focal point is set at *Airy′s* first maximum and due to the

positive sign of the dispersion coefficient of the signal pulse this focal point consists a signal's potential maximum. As a result the two pulses split-up and signal's part is totally ignoring Airy′ *s* acceleration and propagates invariant through z. On the other hand an other part of the signal pulse remains in front of Airy′ *s* main lobe and is constantly been pushed. Due to the anomalous dispersion regime that the control pulse is propagating we can see Airy′ *s* frequency been shifted toward the red while on the other hand the signal's frequency is shifted toward the blue.

4.1.2 Signal localized at Airy's first minimum

Now we will change the t_0 parameter assuming that the center of the signal is localized at an Airy′ *s* local minimum point. So we set $t_0 = -2.92982$ and the simulations we got using the same parameters above are the following:

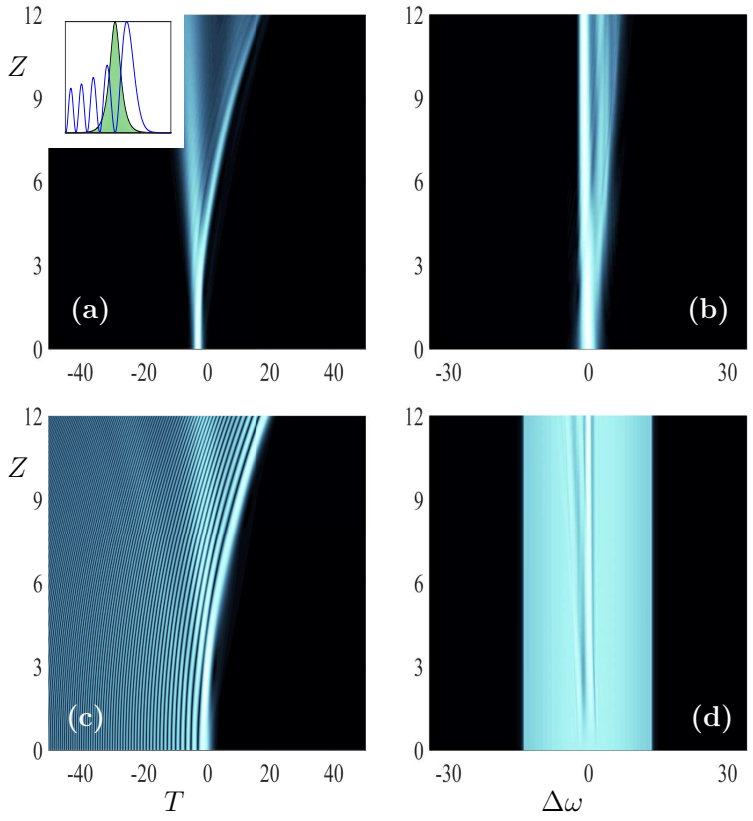

FIGURE 4.2: In the first column we show the dynamics of the signal/ control pulse respectively, while in the second column we show the corresponding spectra of the pulses. Thus the first/second row corresponds to the signal/ control pulse. The inset in (a) shows the initial condition of the signal(green shaded)/ control pulse. The signal is magnified for illustration purposes.

Figure 4.2 shows the evolution of the two copropagating pulses when the signal pulse is located ate Airy′ *s* first minimum. As we can see even though a part of the signal pulse is dragged from Airy the most intense part of the signal pulse remains invariant under the effects of Airy. That is shown from the high intensity pulses that are depicted in (b) while some components of the signal pulse were caved and accelerated from Airy. This minimum point is a signal's potential minimum. That dissuade the two pulses from splitting-up and contributes to the signal acceleration that is observed.

4.1.3 Signal localized at Airy's second maximum

Now we will change the t_0 parameter assuming that the center of the signal is localized at an Airy′ *s* local maximum point. So we set $t_0 = -4.03$ and the simulations we got are the following:

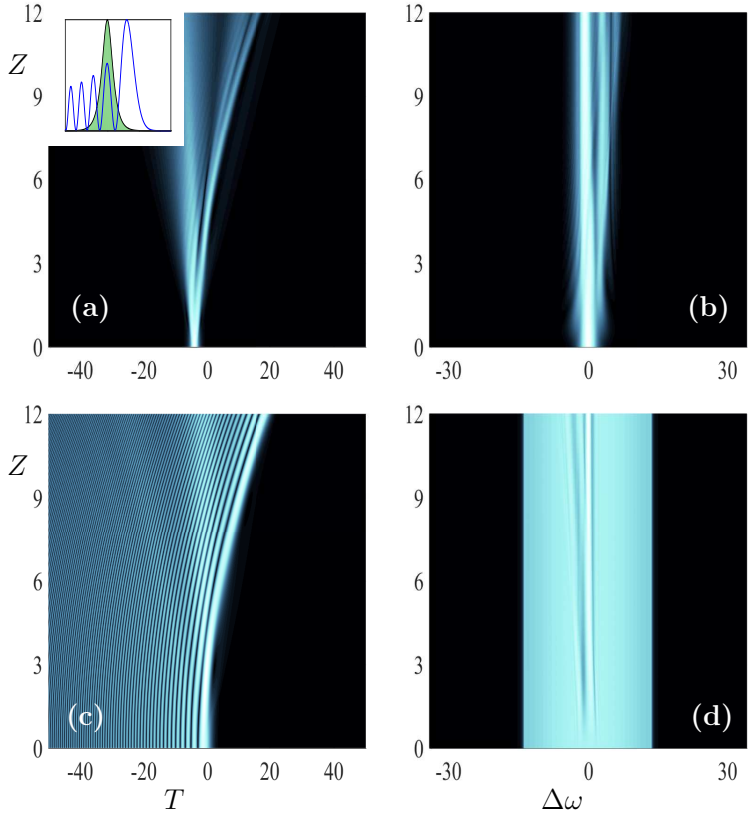

FIGURE 4.3: In the first column we show the dynamics of the signal/ control pulse respectively, while in the second column we show the corresponding spectra of the pulses. The inset in (a) shows the initial condition of the signal(green shaded)/ control pulse. The signal is magnified for illustration purposes.

In Figure 4.3 too, is clear that the intensity of the Airy pulse is not enough to guide the signal pulse at a parabolic trajectory entirely. Thus as we have seen before, some components of the signal pulse tend to accelerate with the Airy pulse although the most intense components of the signal pulse propagate invariant. Thus a high power pulse is emitted as we can see in (b) while the lower intensity components of the pulse differentiated from the high power signal pulse following a parabolic trajectory. The fact that the focal point is set a signal's potential maximum leads to the split-up that the two pulses are facing along with heavy dispersion phenomena.

4.1.4 Signal localized at Airy's second minimum

Just before we close the *linear* subcase we will present now the results we got after locating the signal at $x_0 = -5.0977$; the second local minimum of Airy′ *s* function:

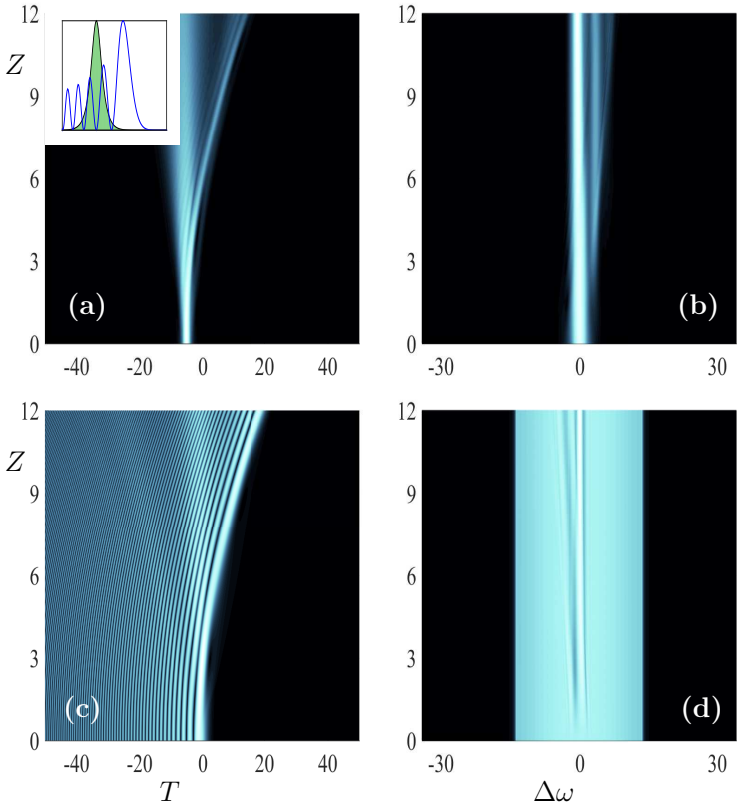

FIGURE 4.4: In the first column we show the dynamics of the signal/ control pulse respectively, while in the second column we show the corresponding spectra of the pulses. Thus the first/second row corresponds to the signal/ control pulse. The inset in (a) shows the initial condition of the probe(green shaded)/ Airy pulse. The signal is magnified for illustration purposes.

In Figure 4.4 we can clearly see that depending on how far we locate the central of the signal pulse from Airy′ *s* first maximum the less is the effect of Airy on the signal pulse. Thus the main lobe of Airy where the most of the Airy pulse energy is concentrated will be far enough to avoid to react with the signal pulse. Although again some components of the signal pulse are dragged from Airy, the biggest part of the signal pulse propagates invariant ignoring in practise Airy′ *s* accelearation. Thus a high intensity pulse is formed and propagating invariant as we can see from the spectral space of the signal pulse.

4.1.5 Examining Airy's pushing properties

In this case it worth to examine the "*pushing*" properties of the *Airy* pulse firstly for the *linear* case placing t_0 at $t_0 = 2.043$.

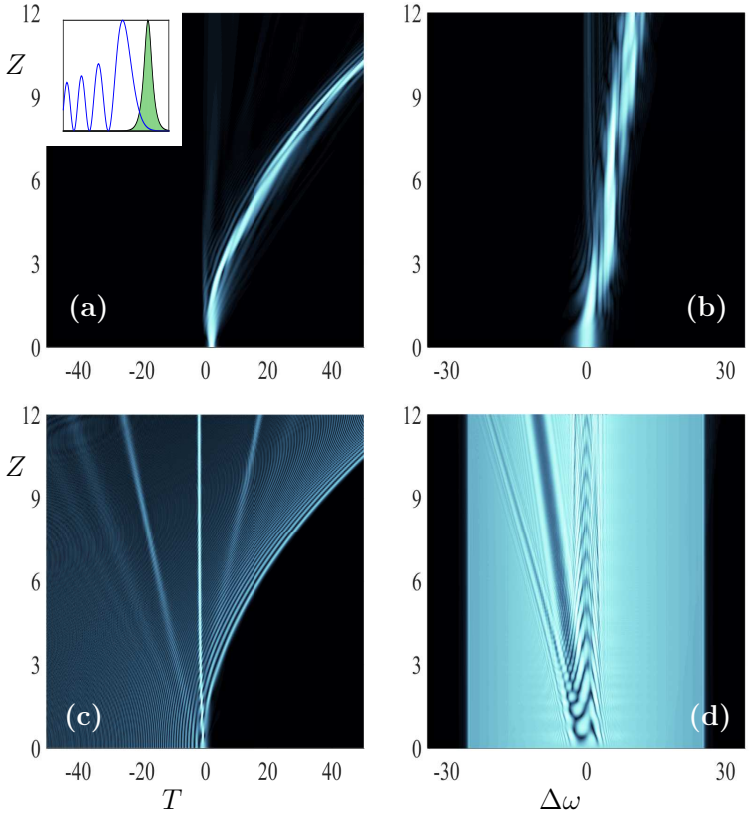

FIGURE 4.5: For the signal we assume: $d_4 = 0.00001$ and $d_5 = 2$ as for the control pulse : $d_2 = 2.5$, $d_3 = 0.65$, $a = 0.001$. In the first column we show the dynamics of the signal/ control pulse respectively, while in the second column we show the corresponding spectra of the pulses. The inset in (a) shows the initial condition of the signal(green shaded)/ control pulse. The signal is magnified for illustration purposes.

In this subcase we substitute $\beta_u = -2$ and $\beta_v = 1$ in Eqs. 4.1-4.2.
In Figure 4.5 we can see that due to the fact that Airy propagates in the anomalous dispersion regime in (c) there are some soliton emitted and that's due to the intensity of Airy. Although the intensity of the Airy pulse is enough that when it interacts with the signal pulse the main lobe of Airy constantly pushes the signal pulse which is as we can see in (a) follows a parabolic accelerating trajectory. As for the frequency of the signal pulse is shifted towards the blue as a clear sign of the acceleration that the signal pulse is under. Despite the fact that Airy was not capable of guiding the signal pulse effectively enough as we saw in the focal points we tested before at this point it exhibits clearly its manipulating features.

4.2 Nonlinear signal evolution

Now proceeding with the *nonlinear* subcase a question arise; how the nonlinearity will effect the copropagation of the two pulses. For this case we assumed $\beta_u = -1$ and $\beta_v = 1$. The form of the initial conditions remains the same as before while some coefficients that regulate the type of the signal pulse and characteristics of the Airy were changed.

$$u = \frac{d_2\,\mathrm{Ai}(d_3 t)\exp(at))}{0.535656} \tag{4.5}$$

$$v = d_4 d_5\,\mathrm{sech}((t - t_0)d_5) \tag{4.6}$$

As we have mentioned before u describes an Airy pulse where d_2 represents Airy$'s$ amplitude, d_3 stands for Airy$'s$ acceleration as well as width factor, while α is the truncation coefficient which is necessary for the realization of the Airy. The constant at the denominator is used for normalization purposes. Heading now to v where d_4 represents signal's pulse amplitude and d_5 is responsible for signal's width, while t_0 represents where the signal's center is located.

4.2.1 Signal localized at Airy's first maximum

So as we mentioned in the beginning we will start by locating beam at $t_0 = -1.2891$, Airy$'s$ first maximum. In Figure 4.6 we depict the real and the spectral space of the signal and the Airy pulse. It is obvious that the nonlinear form of the signal pulse makes signal pulses more intense, thus the reaction with the Airy pulse will not be such that the signal to follow the parabolic trajectory of Airy. In (a) the signal pulse is been diffracted under the existence of the nonlinear

effects. In comparison with the previous case where even part of the signal pulse pulse seemed to be accelerated from Airy in this case due to the strong nonlinear character of the signal pulse such phenomena are absent. Furthermore the location of the focal point at signal's potential maximum hampers the guidance of the signal pulse to a parabolic-accelerating trajectory.

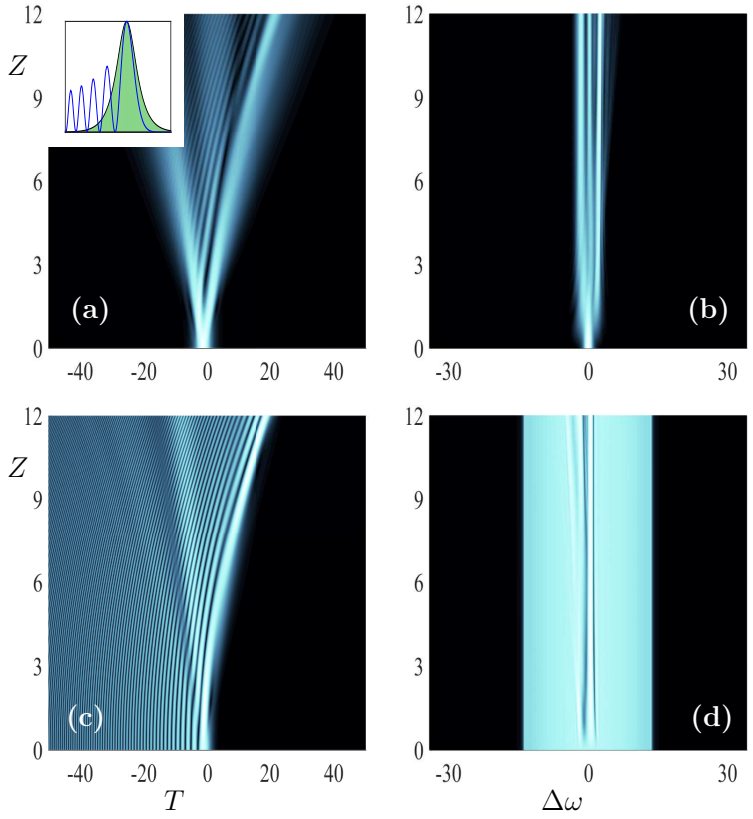

FIGURE 4.6: For the signal we assume: $d4 = 1$, $d_5 = 0.8$ as for the control pulse : $d_2 = 0.8$, $d_3 = 0.8$ and $a = 0.005$. In the first column we show the dynamics of the signal/ control pulse respectively, while in the second column we show the corresponding spectra of the pulses. Thus the first/second row corresponds to the signal/ control pulse. The inset in (a) shows the initial condition of the signal(green shaded)/ control pulse. The signal is magnified for illustration purposes.

4.2.2 Signal localized at Airy's first minimum

To continue we then tested the case that the t_0 is located at Airy′ s first minimum. In Figure 4.7 we depict the results we got at this focal point . As before the nonlinear formation of the signal pulse is of crucial importance as this is the main reason for the inability of the Airy pulse to drag the signal pulse at

its own parabolic trajectory. In (c) due to the propagation of the Airy in the anomalous dispersion regime the creation of solitons has an advantage.

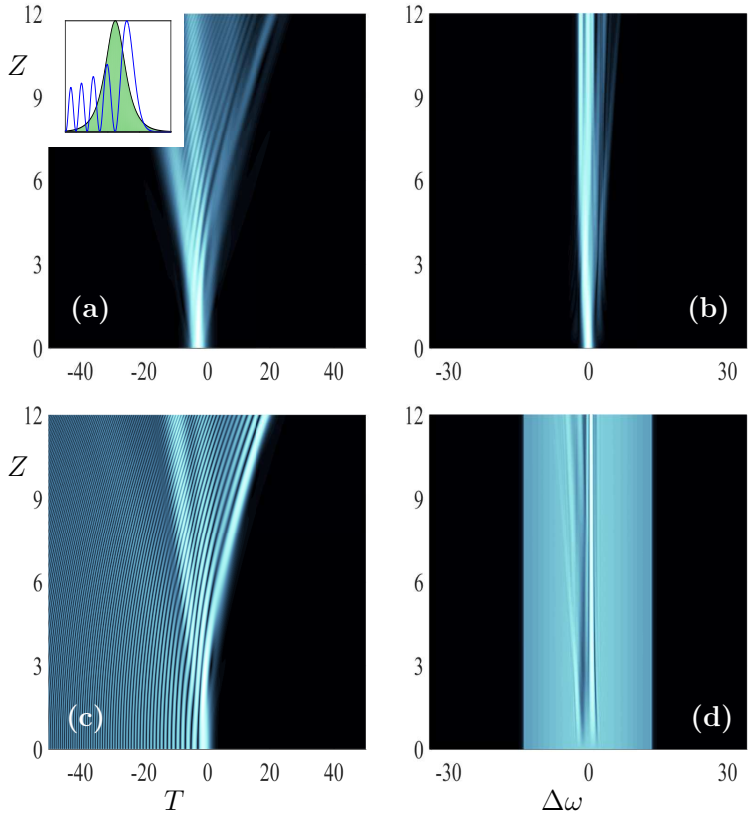

FIGURE 4.7: In the first column we show the dynamics of the signal/ control pulse respectively, while in the second column we show the corresponding spectra of the pulses. Thus the first/second row corresponds to the signal/ control pulse. The inset in (a) shows the initial condition of the signal(green shaded)/ control pulse. The probe is magnified for illustration purposes.

4.2.3 Signa localized at Airy's second maximum

Proceeding with the next point we will locate the center of the signal at Airy′ *s* second maximum by setting $t_0 = -4.043$. Figure 4.8 shows the corresponding simulations. Recalling that the signal pulse propagates in the normal dispersion regime we conclude that this point is signal's potential maximum again. Thus the signal pulse tends to be attracted from a point which its potential is getting minimized ; Airy′ *s* first minimum. Thus part of the signal pulse is been attracted by Airy′ *s* second lobe and been dragged through z. Although the most of the signal pulse ignores the acceleration of the Airy pulse and propagates almost invariant. The components of the signal pulse that propagates invariant form intense enough

pulses that resist *Airy′s* acceleration.This phenomena will not be different if we assumed an Airy pulse with higher nonlinearity because as Airy evolves in the nonlinear regime that would lead to soliton creation and as a result a less effective Airy at last.

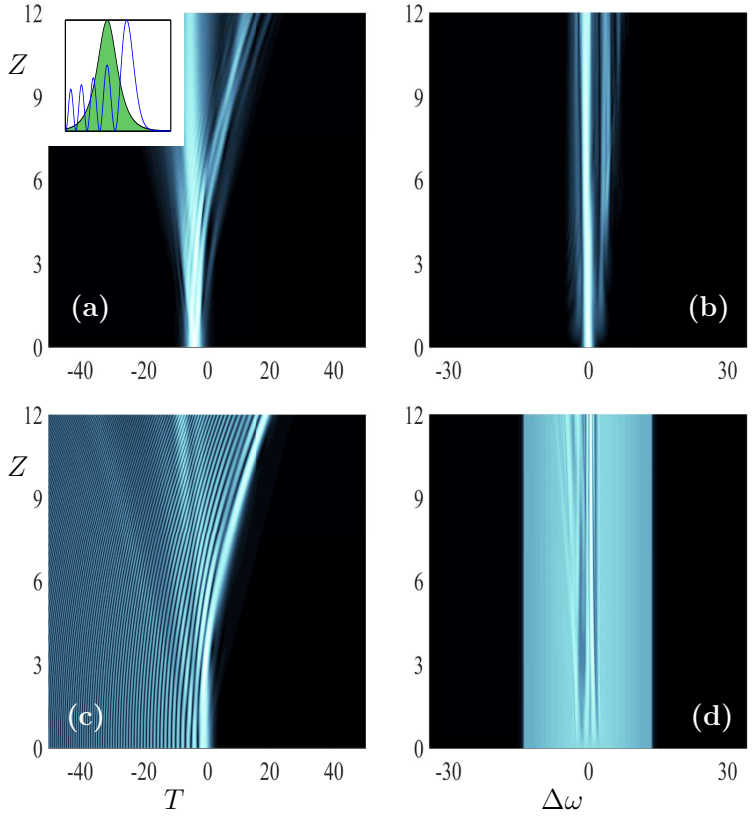

FIGURE 4.8: In the first column we show the dynamics of the signal/ control pulse respectively, while in the second column we show the corresponding spectra of the pulses. Thus the first/second row corresponds to the signal/ control pulse. The inset in (a) shows the initial condition of the signal(green shaded)/ control pulse. The signal is magnified for illustration purposes.

4.2.4 Signal localized at Airy's second minimum

Before we close the *nonlinear* subcase we will localize the center of the beam at Airy′ *s* second minimum .

In Figure 4.9 the relative simulations are shown. As anyone can conclude Airy in not capable of dragging the signal pulse due to signal's high nonlinearity. This nonlinearity acts like a preventing factor. The intensity of the signal pulse is such that Airy pass by the signal pulse without been able to accelerate even some components of the signal. Only a small fract of the signal pulse is drifted by

the Airy pulse and is propagating along with Airy′ *s* first attractive point ; the second lobe. Again an Airy with higher nonlinearity would not make the difference because the nonlinear regime that Airy propagates would just emit solitons from the high intensity of the Airy pulse.

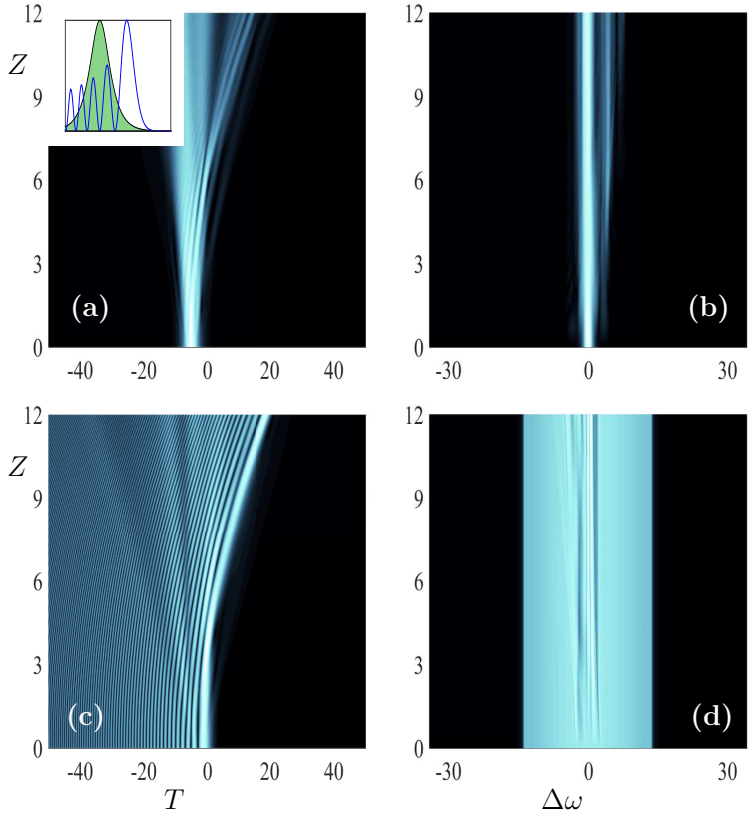

FIGURE 4.9: In the first column we show the dynamics of the signal/ control pulse respectively, while in the second column we show the corresponding spectra of the pulses. Thus the first/second row corresponds to the signal/ control pulse. The inset in (a) shows the initial condition of the signal(green shaded)/ control pulse. The signal is magnified for illustration purposes.

4.2.5 Examining Airy's pushing properties

To close all the subcases of the *nonlinear* subcase we will now examine the *pushing* properties of *Airy* function localizing the t_0 variable at $t_0 = 2.043$ under the following initial condition:

$$u = \frac{d_2 \,\mathrm{Ai}(d_3 t)\exp(at))}{0.535656} \tag{4.7}$$

$$v = d_4 d_5 \,\mathrm{sech}((t - t_0)d_5) \tag{4.8}$$

while $\beta_u = -2$ and $\beta_v = \frac{1}{2}$ and the results we got are the following:

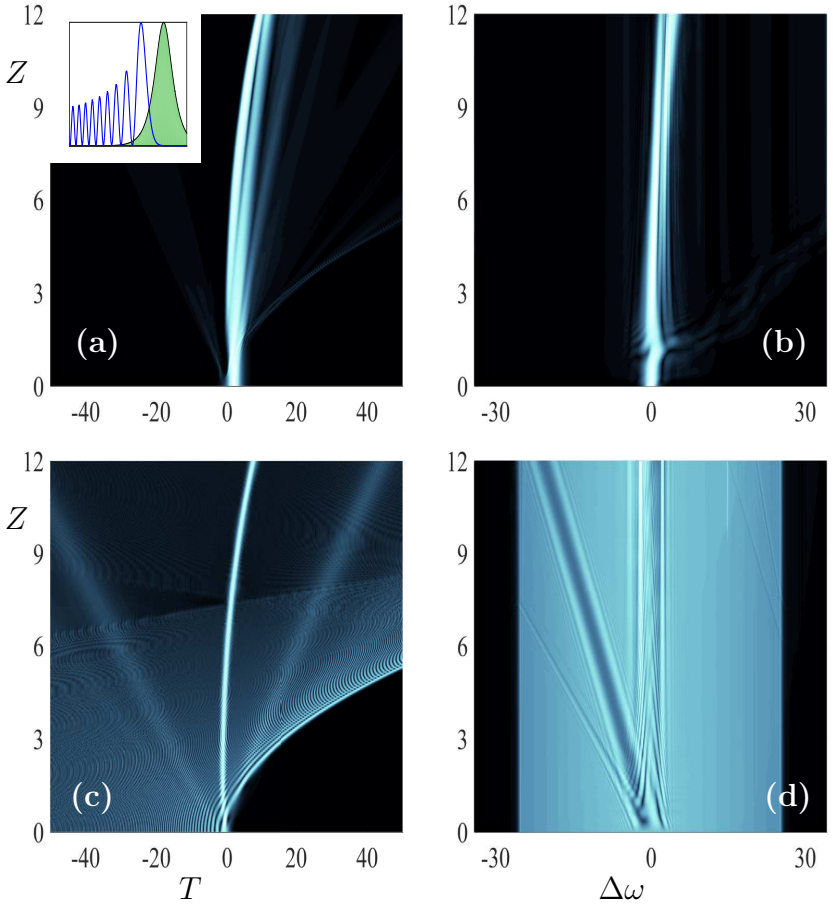

FIGURE 4.10: For the signal we assume: $d_4 = 1$ and $d_5 = 1$ as for the control pulse: $d_2 = 2.5$, $d_3 = 1.2$, $a = 0.001$. In the first column we show the dynamics of the signal/ control pulse respectively, while in the second column we show the corresponding spectra of the pulses. Thus the first/second row corresponds to the signal/ control pulse. The inset in (a) shows the initial condition of the signal (green shaded)/ control pulse. The signal is magnified for illustration purposes.

Figure 4.10 shows our simulations after we have tested the pushing properties of the Airy pulse while it propagates in the anomalous dispersion regime. The copropagating signal pulse propagates in the normal dispersion regime. Despite the fact that in the cases that we locate the focal point of the signal pulse to be located before Airy′ *s* main lobe, the results we got were not promising, although in this case where signal's focal point is located after Airy′ *s* main lobe we can see that Airy forces the signal pulse to follow a parabolic trajectory while it accelerates along with Airy through z. In the spectral space (b) the acceleration of the signal pulse becomes evident from the gradient of the pulse. In the spectral domain of the signal pulse (b) the frequency of the signal pulse is shifted toward the blue.

Chapter 5

Airy/signal evolution in the normal/anomalous dispersion regime

5.1 Linear signal evolution

After examining both *First* and *Second Cases* we will continue with the next; the *Third Case*. To begin with we will mention again the pair of *NLS* we are going to solve generally and then by substituting all the depending variables we will finally conclude to our *Third Case* which will be categorized in two subcases depending on the *linearity* or *nonlinearity* of the signal pulse.

$$i\frac{\partial u}{\partial z} - \frac{\beta_u}{2}\frac{\partial^2 u}{\partial t^2} + (|u|^2 + 2|v|^2)u = 0 \tag{5.1}$$

$$i\frac{\partial u}{\partial z} - \frac{\beta_u}{2}\frac{\partial^2 u}{\partial t^2} + (2|u|^2 + |v|^2)v = 0 \tag{5.2}$$

where $\beta_u = 1$ and $\beta_v = \frac{-1}{2}$.

In this case we assumed the following initial conditions for the functions u and v respectively:

$$u = \frac{d_2\,\mathrm{Ai}(d_3 t)\exp(at))}{0.535656} \tag{5.3}$$

$$v = d_4 \exp\left(-(t-t_0)^2/d_5^2\right) \tag{5.4}$$

To start with we assume a linear signal pulse to copropagate along with a nonlinear Airy pulse. In comparison with the previous cases we now use a Gaussian linear signal pulse represented by $exp(-x)^2$ instead of $sech(x)$ we assumed before.

5.1.1 Signal localized at Airy's first maximum

As Airy evolves in the normal and the signal pulse in the anomalous dispersion regime this focal point consists a signal's potential minimum. This means that this point is ideal to cave the signal pulse in Airy′ *s* main lobe and drag it through z.

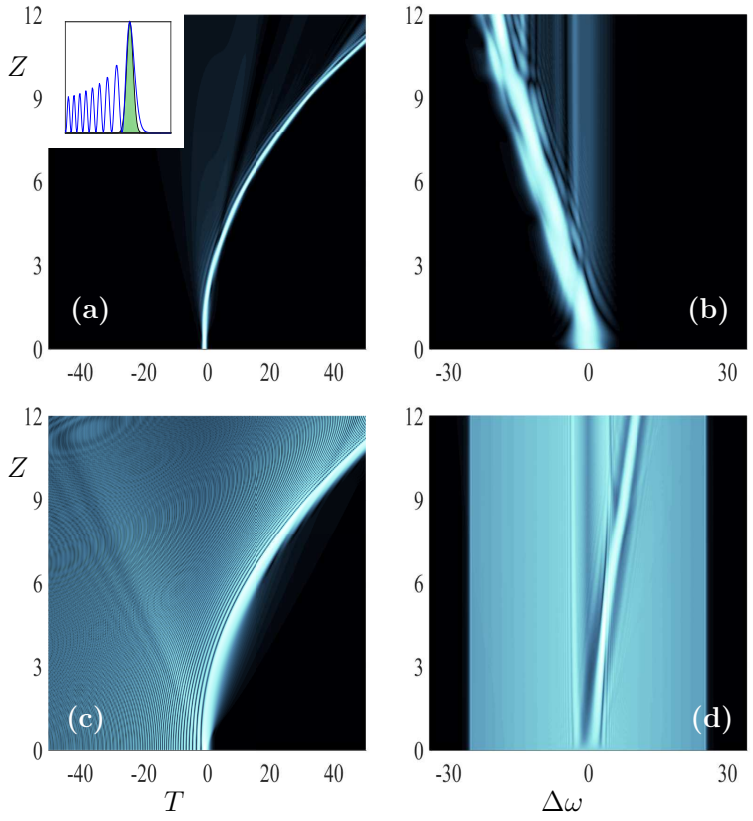

FIGURE 5.1: For the signal we assume: $d_4 = 0.00001$ and $d_5 = 0.651$ as for the control pulse we set : $d_2 = 2$, $d_3 = 1.2$, $a = 0.0001$. In the first column we show the dynamics of the signal/ control pulse respectively, while in the second column we show the corresponding spectra of the pulses. Thus the first/second row corresponds to the signal/ control pulse. The inset in (a) shows the initial condition of the signal(green shaded)/ control pulse. The signal is magnified for illustration purposes.

Beginning from Airy′ *s* first maximum we locate the focal point of the signal pulse to be placed at $t_0 = -0.8789$. Now Airy is propagating at the normal dispersion regime while the signal pulse is propagating at the anomalous dispersion regime and as a result Airy′ *s* first maximum consists a signal's potential minimum point. As a result the regime where Airy propagates allow to express it's dynamics without producing solitons as in the previous case, while in the anomalous dispersion regime that the signal pulse is evolving the creation of soliton is proposed.

What we should mention in Figure 5.1 is that as the signal pulse propagates in the anomalous dispersion regime, red shifted phenomenon occurs for the frequency of the signal pulse as we can see in (b) as the spectral components of the signal pulse are accelerating toward the left side . The signal pulse is caved in Airy′ *s* main lobe and it's dragged as long as the two pulses co-propagate.

5.1.2 Signal localized at Airy's first minimum

Proceeding with the next focal point we will use the initial conditions we show above but using an other value of variable t_0. Now we will set $t_0 = -1.9336$ in order to locate the center of the signal pulse at Airy′ *s* first minimum, which consists a signal's potential maximum point, and the simulations we got are the the following :

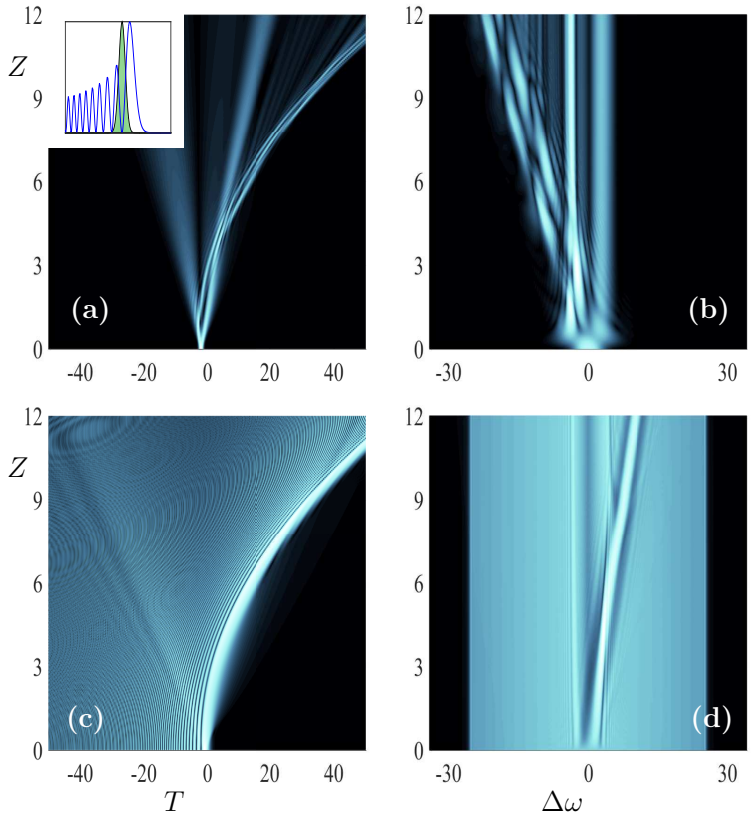

FIGURE 5.2: In the first column we show the dynamics of the signal/ control pulse respectively, while in the second column we show the corresponding spectra of the pulses. Thus the first/second row corresponds to the signal/ control pulse. The inset in (a) shows the initial condition of the signal(green shaded)/ control pulse. The signal is magnified for illustration purposes.

Continuing with this focal point which simulations presented in Figure 5.2 by comparing (a) and (b) the real and spectral spaces we can see that due to the fact that the signal pulse propagates in the anomalous dispersion regime there are high power pulses that are created which remain invariant as the signal pulse interacts with the Airy pulse . Although Airy$'$ *s* intensity is capable of drifting away with the less intense spectral components of the signal pulse that are attracted by signal's potential minimum (Airy$'$ *s* main lobe) and guide them through a parabolic-accelerating trajectory.

5.1.3 Signal localized at Airy's second maximum

To continue with the next focal point we will locate the center of the signal pulse at Airy$'$ *s* second maximum by assuming $t_0 = -2.6367$. As we can see in Figure 5.3 Airy$'$ *s* intensity is such that the signal pulse is caved in Airy$'$ *s* second maximum and it's dragged. Due to the fact that the signal pulse evolves in the anomalous dispersion regime this second maximum point consists an attractive point as it is a signal's potential minimum. In (b) signal's frequency accelerated to the left experiencing the red-shifted phenomenon.

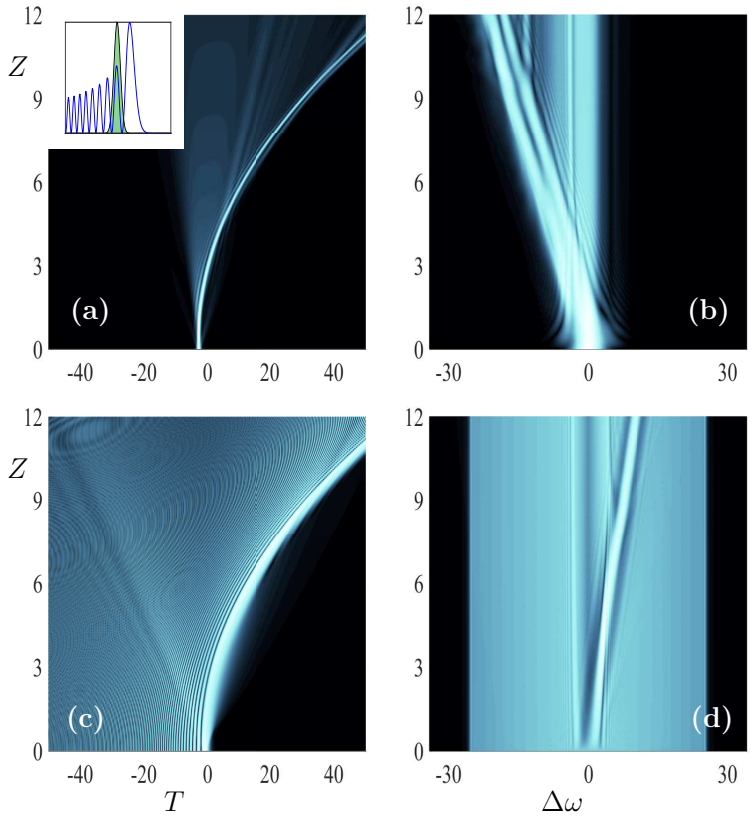

FIGURE 5.3: In the first column we show the dynamics of the signal/ control pulse respectively, while in the second column we show the corresponding spectra of the pulses. Thus the first/second row corresponds to the signal/ control pulse. The inset in (a) shows the initial condition of the signal(green shaded)/ control pulse. The signal is magnified for illustration purposes.

5.1.4 Signal localized at Airy's second minimum

In order to close the *linear* subcase of the *Third Case* we will locate the center of the beam at Airy′ *s* second minimum by substituting $t_0 = -3.2477$ and we got the following results:

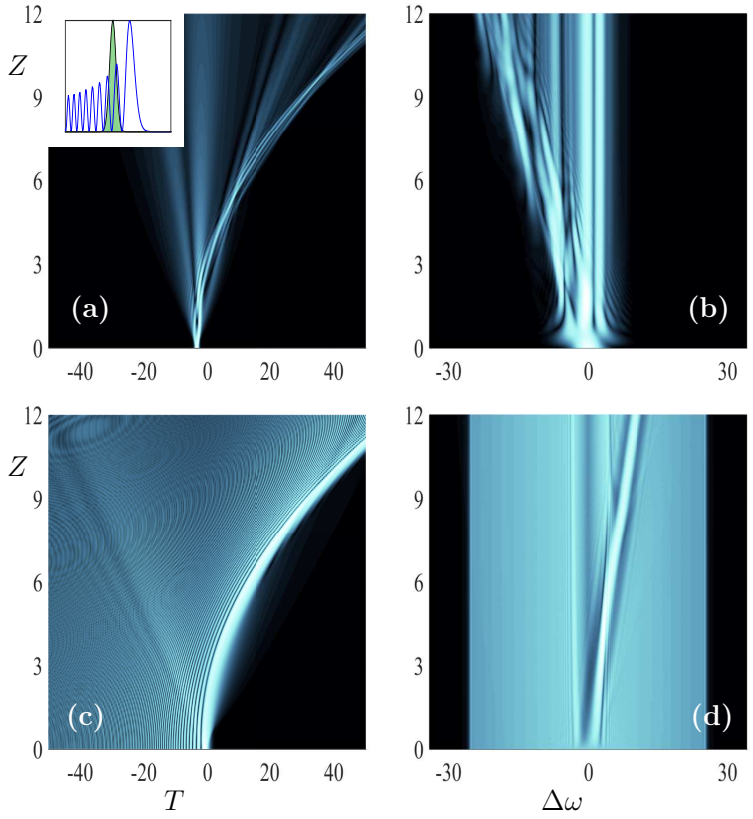

FIGURE 5.4: In the first column we show the dynamics of the signal/ control pulse respectively, while in the second column we show the corresponding spectra of the pulses. Thus the first/second row corresponds to the signal/ control pulse. The inset in (a) shows the initial condition of the signal(green shaded)/ control pulse. The signal is magnified for illustration purposes.

In Figure 5.4 we depict our simulations for placing the center of the signal pulse at Airy′ *s* second minimum. Part of the signal pulse is caved at this focal point although the signal pulse tends to reach Airy′ *s* main lobe and be dragged. Although because this particular lobe that the signal pulse is located at is less effective than the others because its lack of energy, thus the signal pulse tends to emit high intensity pulses that propagate invariant, ignoring Airy′ *s* acceleration. Furthermore the fact that this focal point is a signal's potential maximum point contributes to the split-up between the two copropagating pulses.

5.1.5 Examining Airy's dragging properties

To close the *linear* subcase of the *Third Case* we will locate the beam between the first maximum and the first minimum of Airy′ *s* function. More specifically we will set $t_0 = -1.2305$ and the results we got are depicted in Figure 5.5.
In the dynamics of this case we can see that the signal pulse is attracted by Airy′ *s* main lobe and is dragged from there, forced to follow an accelerating parabolic trajectory. By placing the signal pulse so close to it's potential minimum point we achieve that the signal pulse will jump fast enough to it's closest potential minimum point (Airy′ *s* main lobe) and forced to follow a parabolic-accelerating trajectory.

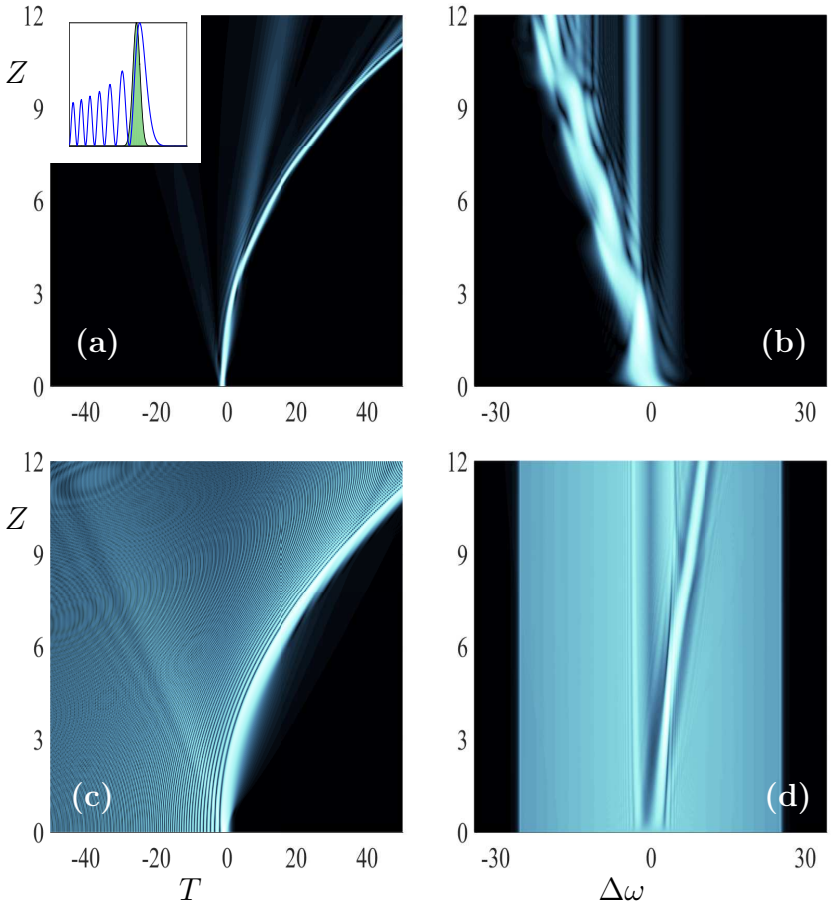

FIGURE 5.5: In the first column we show the dynamics of the signal/ control pulse respectively, while in the second column we show the corresponding spectra of the pulses. Thus the first/second row corresponds to the signal/ control pulse. The inset in (a) shows the initial condition of the signal(green shaded)/ control pulse. The signal is magnified for illustration purposes.

5.2 Nonlinear signal evolution

Proceeding with the *nonlinear* subcase of the third case we will assume a *nonlinear* formation of the signal pulse and see how this nonlinearity will affect the results we got above.

5.2.1 Signal localized at Airy's first maximum

We will begin this subcase by locating the central of the signal pulse at Airy′ *s* first maximum assuming $t_0 = -0.8789$ and the simulations we got are the following:

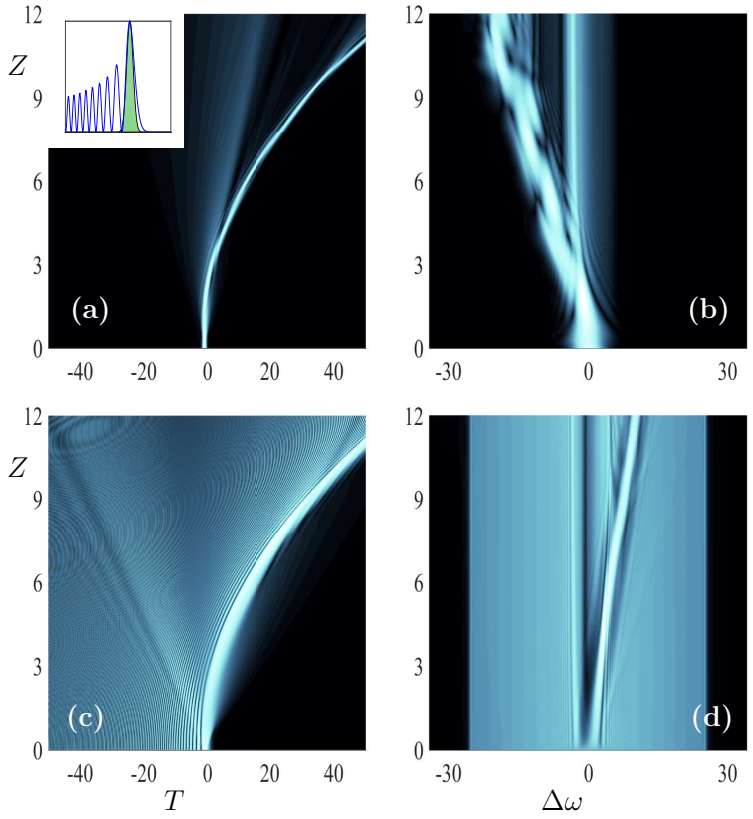

FIGURE 5.6: For the signal we assume: $d_4 = 0.8$ and $d_5 = 0.651$ as for the control pulse we set : $d_2 = 2$, $d_3 = 1.2$, $a = 0.001$. In the first column we show the dynamics of the signal/ control pulse respectively, while in the second column we show the corresponding spectra of the pulses. Thus the first/second row corresponds to the signal/ control pulse. The inset in (a) shows the initial condition of the signal(green shaded)/ control pulse. The signal is magnified for illustration purposes.

In Figure 5.6 the propagation of the signal and the Airy pulse are depicted both in the real and the spectral space. For the control pulse we assumed an

intense nonlinear Airy pule. In this way we create a high intensity Airy pulse which will be able to guide the signal pulse in a parabolic trajectory as seen in (a) along with a significant acceleration as seen from the gradient formed in the spectral space of the signal pulse (b). Although some high intensity components of the signal pulse due to high nonlinearity tend to propagate invariant forming high intensity pulses that ignore Airy′ *s* acceleration.

5.2.2 Signal localized at Airy's first minimum

Now proceeding with the next point we will locate the center of the signal at Airy′ *s* first minimum by assuming $t_0 = -1.9336$, and we will present the simulations we got:

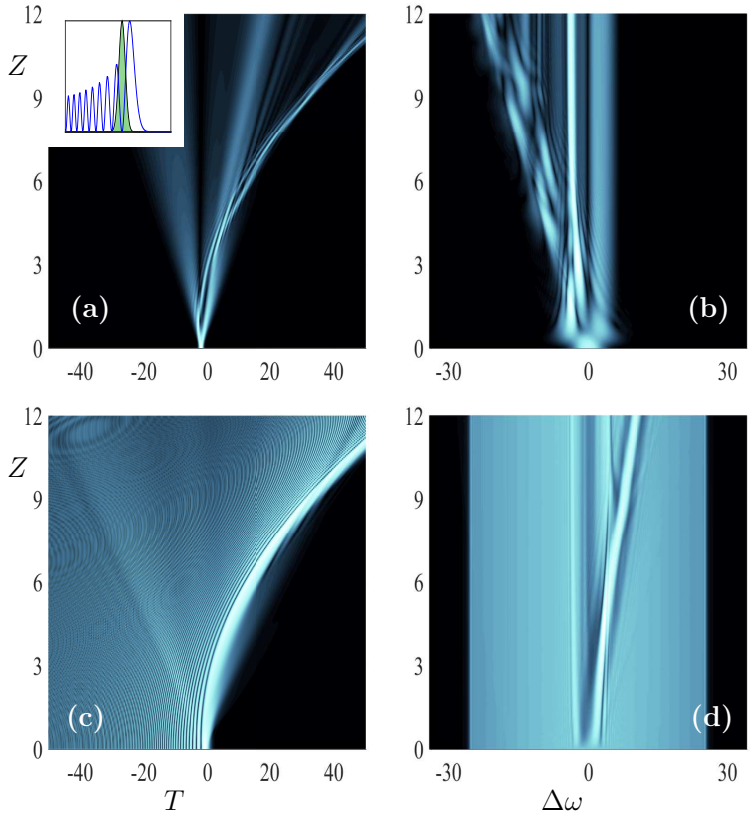

FIGURE 5.7: In the first column we show the dynamics of the signal/ control pulse respectively, while in the second column we show the corresponding spectra of the pulses. Thus the first/second row corresponds to the signal/ control pulse. The inset in (a) shows the initial condition of the signal(green shaded)/ control pulse. The signal is magnified for illustration purposes.

In Figure 5.7 we locate the focal point to be placed at Airy′ *s* first minimum. Due to the fact that this focal point consists a signal's potential maximum point the

signal pulse tends to jump to a potential minimum point. The closest potential minimum point is Airy′ *s* main lobe. As a result a part of the signal pulse is attracted from Airy′ *s* main lobe and it is dragged through z. As we can see in the spectral space part of the signal's pulse that is dragged from Airy′ *s* main lobe is shifted toward the red experiencing the red-shifting phenomenon due to the anomalous dispersion that the signal is propagating.

5.2.3 Signal localized at Airy's second maximum

This time we will locate the center of the signal pulse at Airy′ *s* second maximum assuming $t_0 = -2.6367$ and we got the following simulations:

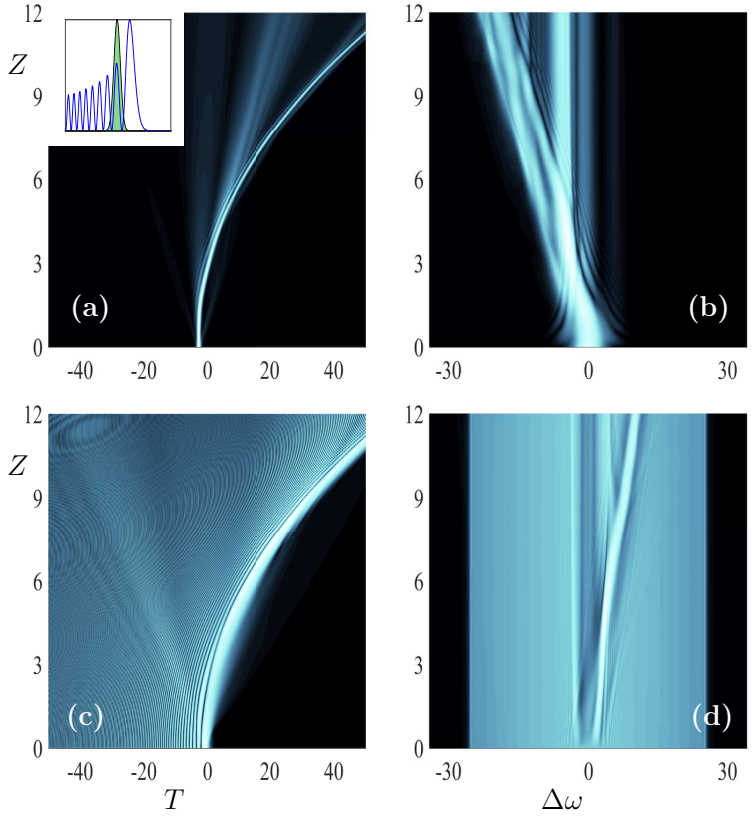

FIGURE 5.8: In the first column we show the dynamics of the signal/ control pulse respectively, while in the second column we show the corresponding spectra of the pulses. Thus the first/second row corresponds to the signal/ control pulse. The inset in (a) shows the initial condition of the signal(green shaded)/ control pulse. The signal is magnified for illustration purposes.

In Figure 5.8 we depict the real and spectral space of the evolution of both control and signal pulse. As we can see from (a) the signal pulse is forced to follow a parabolic-accelerating trajectory due to the interaction between the Airy and

the signal pulse. Moreover due to the fact that Airy′ *s* second maximum consists a signal's potential minimum point and thus the signal pulse is caved at this focal point and is constantly been accelerated. The spectra space of the signal pulse is shifted toward the red as a clear sign of the acceleration that the signal pulse is under.

5.2.4 Signal localized at Airy 's second minimum

Just before we close the *nonlinear* subcase of the *Third Case* we will localize the center of the signal pulse at Airy′ *s* second minimum by setting $t_0 = -3.2477$ and the results we got are the following:

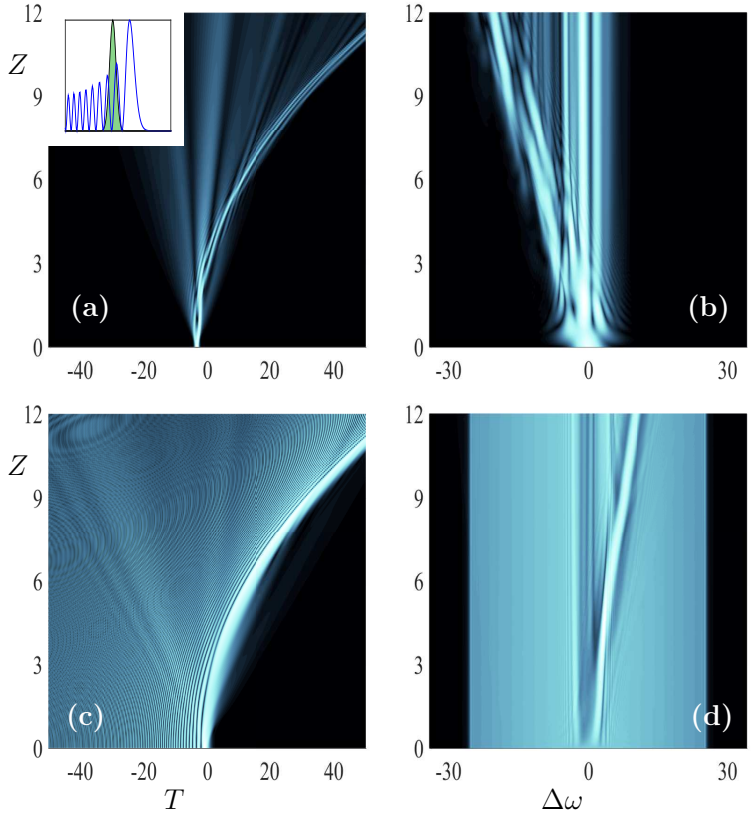

FIGURE 5.9: In the first column we show the dynamics of the signal/ control pulse respectively, while in the second column we show the corresponding spectra of the pulses. Thus the first/second row corresponds to the signal/ control pulse. The inset in (a) shows the initial condition of the signal(green shaded)/ control pulse. The signal is magnified for illustration purposes.

Figure 5.9 shows the evolution of the copropagating pulses in the real and the spectral space. As we can see from the real space of the signal pulse (a) part the signal pulse is following the Airy at a parabolic trajectory but with some losses

translated as high intensity pulses that differ from the parabolic trajectory and forming invariant pulses that ignore Airy′ *s* acceleration and can be seen in (b). This focal point consists a signal's potential maximum. That means that the signal pulse tends to jump to the closest potential minimum point in order to be dragged from the Airy pulse. That's why the split up between the two copropagating pulses occurs. Due to the anomalous dispersion regime that the signal pulse is propagating the frequency of the signal pulse is shifted toward the red as a clear sign of the acceleration that the signal pulse is under.

5.2.5 Examining Airy's dragging properties

To close the *nonlinear* subcase of the *Third Case* we will locate the signal pulse between the first maximum and the first minimum of Airy.

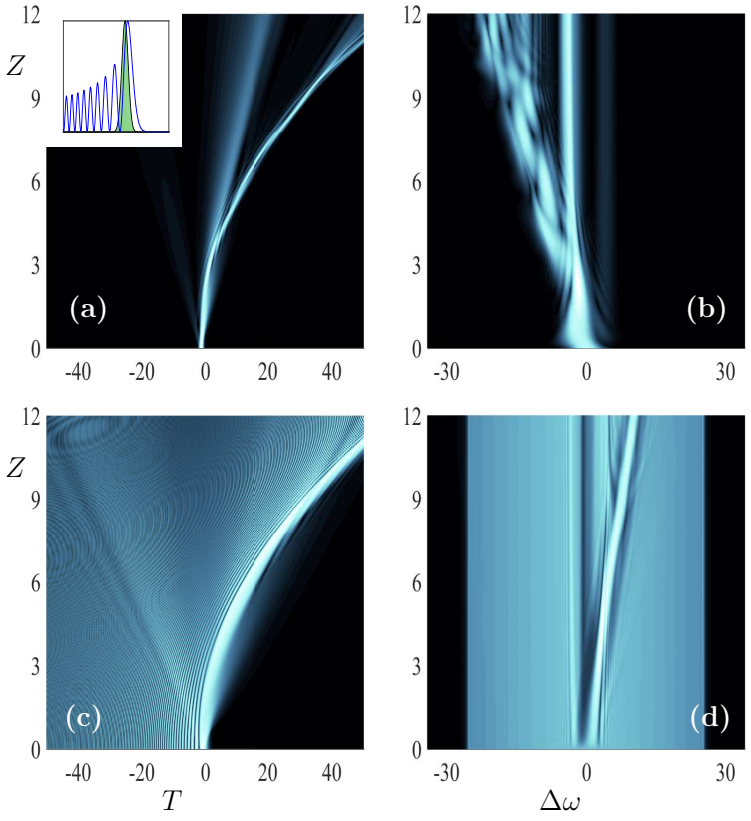

FIGURE 5.10: In the first column we show the dynamics of the signal/ control pulse respectively, while in the second column we show the corresponding spectra of the pulses. Thus the first/second row corresponds to the signal/ control pulse. The inset in (a) shows the initial condition of the signal(green shaded)/ control pulse. The signal is magnified for illustration purposes.

Figure 5.10 shows the results when the focal point is placed between the first maximum and minimum of Airy. The nature of this focal point forces the signal pulse to jump to the signal's potential minimum (Airy′ *s* main lobe) in order to be dragged from the Airy pulse. That transition due to the high nonlinearity of the signal pulse is resulting some high intensity pulses that evolve invariant ignoring Airy′ *s* acceleration. Although fron (b) we can see that most components of the signal pulse are guided by the Airy pulse and signal's frequency is shifted toward the red.

Chapter 6

Airy and signal evolution in the anomalous dispersion regime

6.1 Linear signal evolution

At this point and after having tested three cases there is only one case remaining to examine depending on the sign of the parameters β_u and β_v. Now in *Fourth Case* we will examine the case that our system of NLS equations

$$i\frac{\partial u}{\partial z} - \frac{\beta_u}{2}\frac{\partial^2 u}{\partial t^2} + (|u|^2 + 2|v|^2)u = 0. \tag{6.1}$$

$$i\frac{\partial u}{\partial z} - \frac{\beta_u}{2}\frac{\partial^2 u}{\partial t^2} + (2|u|^2 + |v|^2)v = 0 \tag{6.2}$$

where variables β_u and β_v are both negative and $\beta_u = -1.5$, $\beta_v = -0.55$

Firstly we will need to mention the *initial conditions* we used in this case:

$$u = \frac{d_2\,\mathrm{Ai}(d_3 t)\exp(at))}{0.535656} \tag{6.3}$$

$$v = d_4 d_5\,\mathrm{sech}((t - t_0)d_5) \tag{6.4}$$

To start with we will assume a linear signal pulse propagating along with a nonlinear Airy pulse and then in the next section we will test a nonlinear signal pulse copropagating with an Airy pulse. Due to the fact that the signal and the Airy pulse propagate in the anomalous dispersion regime the creation of solitons is supported.

As for the initial conditions Eqs. (6.3), (6.4) in this case too u describes an Airy pulse where d_2 represents Airy$'s$ amplitude, d_3 stands for Airy$'s$ acceleration as well as width factor, while α is the truncation coefficient which is necessary for the

realization of the Airy. The constant at the denominator is used for normalization purposes. Heading now to v where d_4 represents signal's pulse amplitude where d_5 is responsible for signal's width, while t_0 represents where the signal's center is located. Due to the fact that the signal pulse is evolving in the Anomalous Dispersion regime the existence of solitons is supported.

6.1.1 Signal localized at Airy's first maximum

So by assuming $t_0 = -1.035$ we will locate the central of the signal pulse at a signal's potential minimum, and we will present you the results we got after solving our system under the *intial conditions* above for the *linear* subcase of the *Fourth Case*.

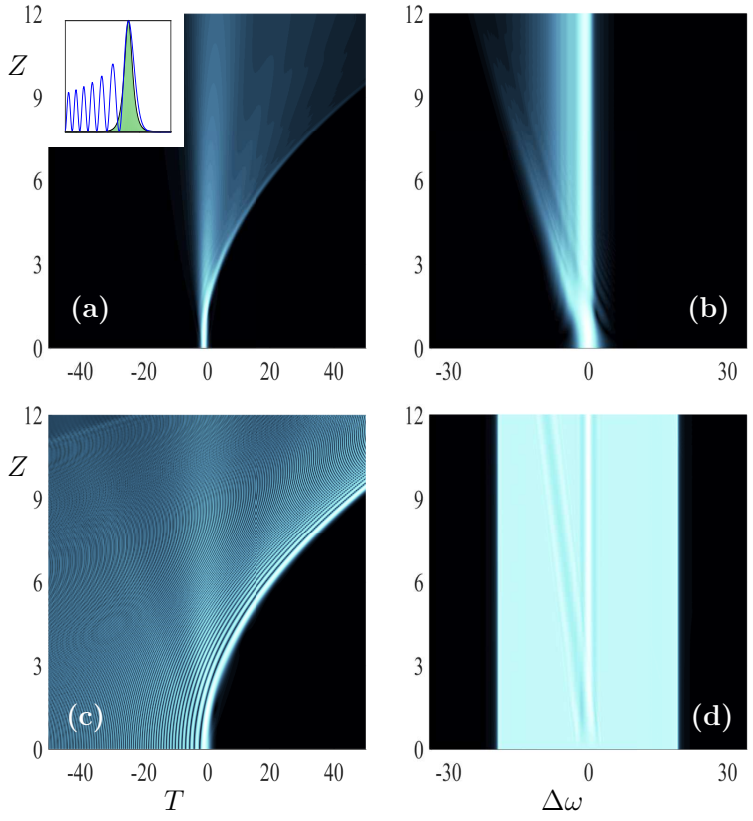

FIGURE 6.1: For the signal pulse we assume: $d_4 = 0.00001$ and $d_5 = 2$ as for the control pulse we set: $d_2 = 1$, $d_3 = 1$, $a = 0.001$. In the first column we show the dynamics of the signal/ control pulse respectively, while in the second column we show the corresponding spectra of the pulses. Thus the first/second row corresponds to the signal/ control pulse. The inset in (a) shows the initial condition of the signal(green shaded)/ control pulse. The signal is magnified for illustration purposes.

In Figure 6.1 the central of the pulse is located at Airy′ *s* first maximum. While the signal pulse is caved in Airy′ *s* main lobe and dragged the signal pulse is splitting and a high intensity pulse is created. As we can see in (b) the high intensity pulse which propagates invariant is depicted clearly along with the spectral components of the signal pulse that are guided from Airy to follow a parabolic trajectory and thus to be accelerated. Part of the signal's frequency is shifted toward the red as a clear sign of the acceleration of the signal pulse.

6.1.2 Signal localized at Airy's first minimum

Continuing with the next value of t_0 we will assume that t_0 is located at a local minimum of Airy function. So we setted $t_0 = -2.373$ and the simulations we got are the following:

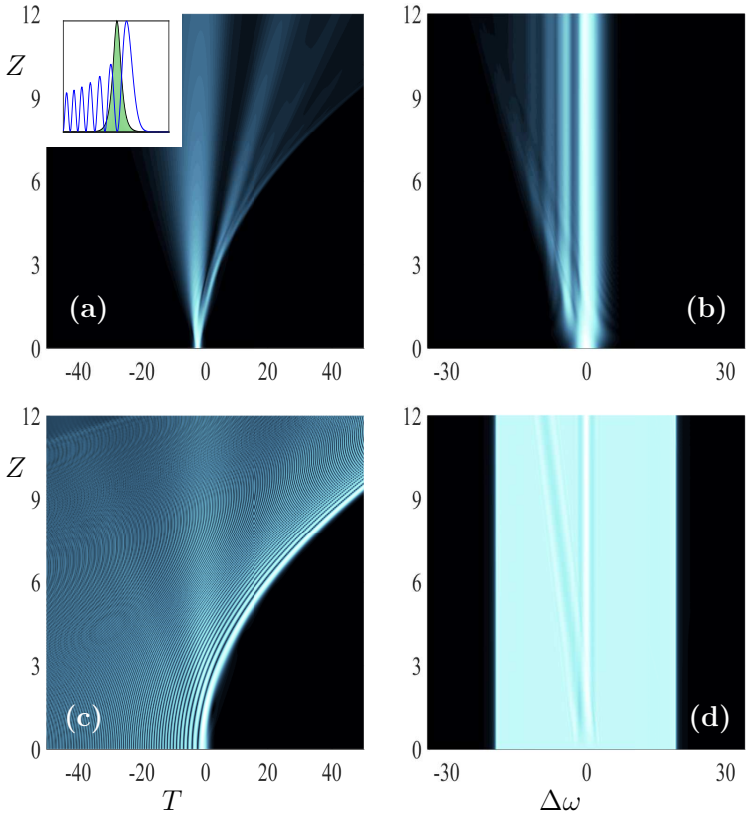

FIGURE 6.2: In the first column we show the dynamics of the signal/ control pulse respectively, while in the second column we show the corresponding spectra of the pulses. Thus the first/second row corresponds to the signal/ control pulse. The inset in (a) shows the initial condition of the signal(green shaded)/ control pulse. The signal is magnified for illustration purposes.

In Figure 6.2 the central of the signal pulse is located at Airy′ *s* first minimum point, just before the main lobe. Airy′ *s* main lobe attracts the signal pulse and components of the signal pulse dragged from Airy′ *s* main lobe. However due to the fact that this focal point consists a signal's potential maximum point it is easy to see that in (a) the two copropagating pulses split-up. A part of the soliton pulse is caved in Airy′ *s* main lobe and forced to follow a parabolic- accelerating trajectory. Although the most of the signal pulse ignores Airy′ *s* acceleration. In (b) some spectral components of the signal pulse are accelerated thus we can see a frequency shift to the left.

6.1.3 Signal localized at Airy's second maximum

Just before we close the *linear* subcase we will assume $t_0 = -3.253$ which is a local maximum of ours Airy function and we will present now our results for this case:

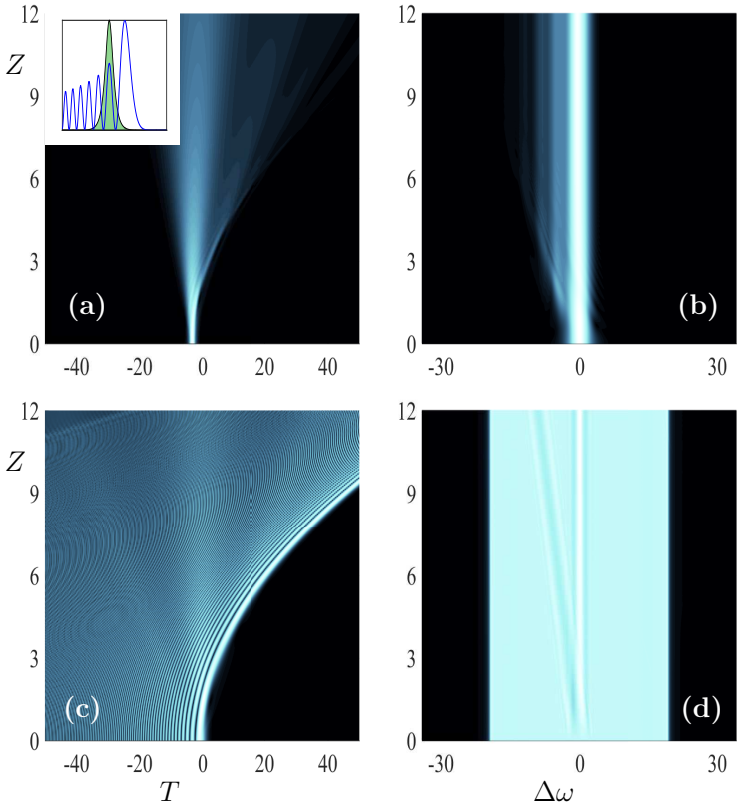

FIGURE 6.3: In the first column we show the dynamics of the signal/ control pulse respectively, while in the second column we show the corresponding spectra of the pulses. Thus the first/second row corresponds to the signal/ control pulse. The inset in (a) shows the initial condition of the signal (green shaded)/ control pulse. The signal is magnified for illustration purposes.

In Figure 6.3 we depict the propagation of a signal and an Airy pulse both in the spectral and in the real space. This focal point consists a signal's potential minimum point. As a result part of the signal pulse is caved at Airy′ *s* second maximum and been dragged through z. Although the fact that Airy is propagating in the anomalous dispersion regime along with the fact that the signal propagates in the anomalous dispersion regime too, means that Airy is not capable to exhibit its dynamics to guide the signal pulse. Thus a high intensity pulse is evolving, invariant ignoring in practise Airy′ *s* acceleration.

6.1.4 Signal localized at Airy's second minimum

To close the *linear* subcase of the *Fourth Case* we will finally locate the center of the signal pulse at Airy′ *s* second minimum and we got the following results:

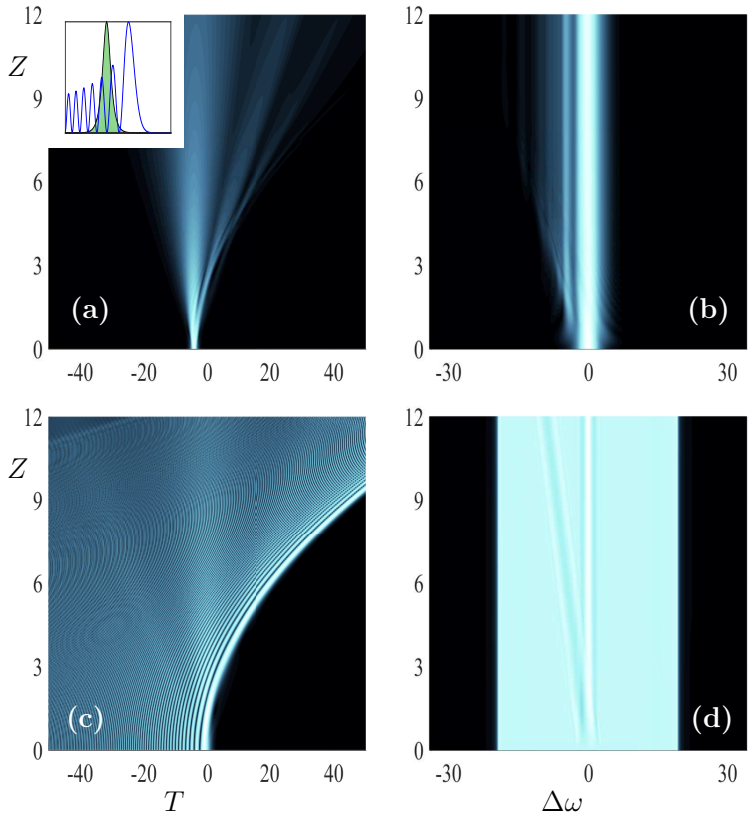

FIGURE 6.4: In the first column we show the dynamics of the signal/ control pulse respectively, while in the second column we show the corresponding spectra of the pulses. Thus the first/second row corresponds to the signal/ control pulse. The inset in (a) shows the initial condition of the signal(green shaded)/ control pulse. The signal is magnified for illustration purposes.

At this point we should remind that both pulses propagate in the anomalous dispersion regime where the formation of solitons is proposed. Thus as we can see in Figure 6.4 the more away from Airy′ *s* main lobe we place the center of the signal pulse the less are the effects of Airy on this signal pulse. Thus what we can see is an almost pass by of the Airy through the signal pulse and that's due to the high intensity of the signal pulse. Although during this pass by Airy drags some components of the signal pulse as we can see in (b) and accelerates them as frequency shift toward the red is noticable. Although the high intensity pulse stands out us in the previous focal points.

6.2 Nonlinear signal evolution

We will now proceed with the *nonlinear* evolution of a signal pulse. We will assume an other set of *initial conditions* and β_u, β_v and we will see how the difference in the group velocity dispersion will affect the previous results along with the nonlinearity we assumed for the signal pulse . Moreover we will assume Eqs. (6.2)-(6.3) while $\beta_u = -1.2$ and $\beta_v = -2$ along with the other coefficients that are specifying the features of the two pulses.
As for the initial conditions Eqs. (6.3), (6.4) in this case too u describes an Airy pulse where d_2 represents Airy′ *s* amplitude, d_3 stands for Airy′ *s* acceleration as well as width factor, while α is the truncation coefficient which is necessary for the realization of the Airy. The constant at the denominator is used for normalization purposes. Heading now to v where d_4 represents signal's pulse amplitude where d_5 is responsible for signal's width, while t_0 represents where the signal's center is located.

6.2.1 Signal localized at Airy's first maximum

To start with we will locate the center of the signal at Airy′ *s* first maximum by substituting $t_0 = -1.0124$ and the results we got are the following:
In Figure 6.5 we depict our simulations for the nonlinear subacase of this fourth case after we have locate the signal's pulse center at Airy′ *s* first maximum. The main difference in comparison with the linear subcase is that we have induced a nonlinearity to the signal pulse. Due to this high nonlinearity of the signal pulse the signal pulse interacts with the Airy pulse in a way that degenerates the Airy pulse. Although some of the components of the signal pulse seem to be dragged from the Airy pulse and forced to follow a parabolic-accelerating trajectory.

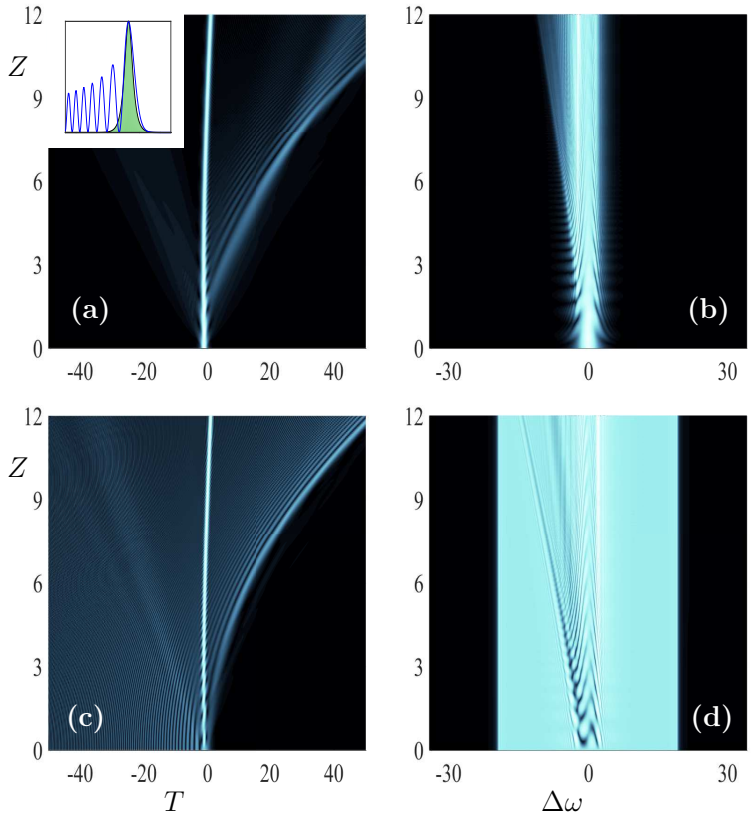

FIGURE 6.5: For the signal we assume: $d_4 = 1$ and $d_5 = 2$, as for the control pulse: $d_2 = 1$, $d_3 = 1$, $a = 0.001$. In the first column we show the dynamics of the signal/ control pulse respectively, while in the second column we show the corresponding spectra of the pulses. The inset in (a) shows the initial condition of the signal(green shaded)/ control pulse. The signal is magnified for illustration purposes.

6.2.2 Signal localized at Airy's first minimum

Then for the next point we assume $t_0 = -2.3010$ which is a local minimum for our Airy function and the results we got are the following:
In Figure 6.6 the center of the signal pulse is placed just before Airy′ *s* main lobe. After a while the signal pulse is attracted from Airy′ *s* main lobe and the extraordinary phenomenon is that Airy is distorted in a way that Airy′ *s* main lobe is no more propagating. Practically the Airy pulse pass through the signal pulse which due to it's high intensity and the anomalous dispersion regime that is propagating develops full resistant to Airy′ *s* acceleration. Thus it propagates invariant interacting with the Airy but no evidence proves the guidance of the signal pulse by the Airy pulse.

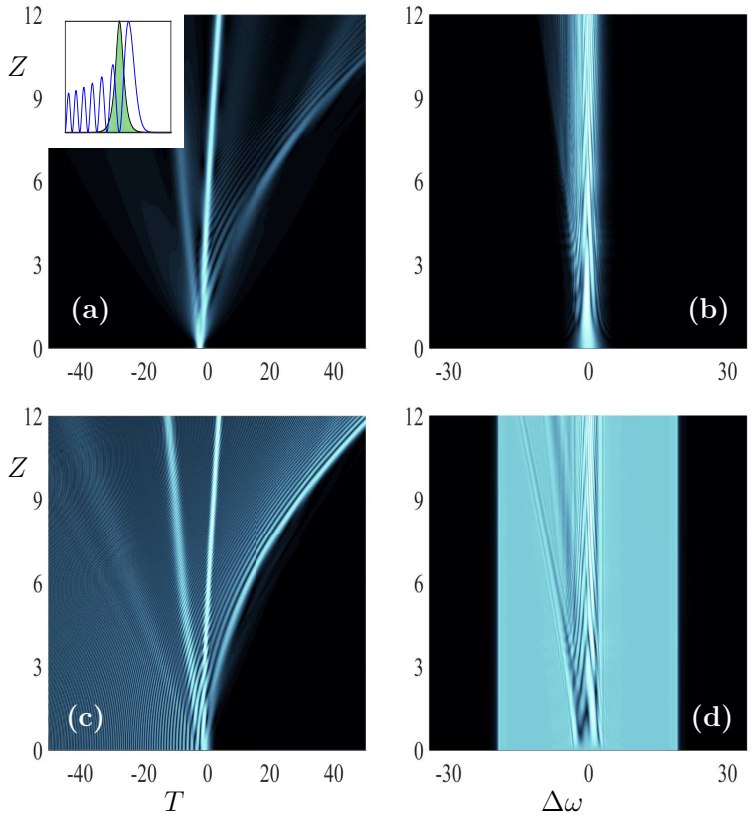

FIGURE 6.6: In the first column we show the dynamics of the signal/ control pulse respectively, while in the second column we show the corresponding spectra of the pulses. Thus the first/second row corresponds to the signal/ control pulse. The inset in (a) shows the initial condition of the signal(green shaded)/ control pulse. The signal is magnified for illustration purposes.

6.2.3 Signal localized at Airy's second maximum

Just before we end the *nonlinear* subcase of the *Fourth Case* we will place the center of the beam at Airy′ *s* second maximum at $t_0 = -3.2214$.
In Figure 6.7 we depict the propagation of the signal and the control pulse both in the real and the spectral space. Again the control pulse is facing a high power soliton pulse that is kind of blocking Airy′ *s* accelerating features. Airy′ *s* main lobe is interacting with the signal pulse without any further accelerating phenomena taking place . The soliton pulse interact with the Airy in a way that forces Airy to emit intense solitons under the contribution of the anomalous dispersion regime that Airy is evolving too.

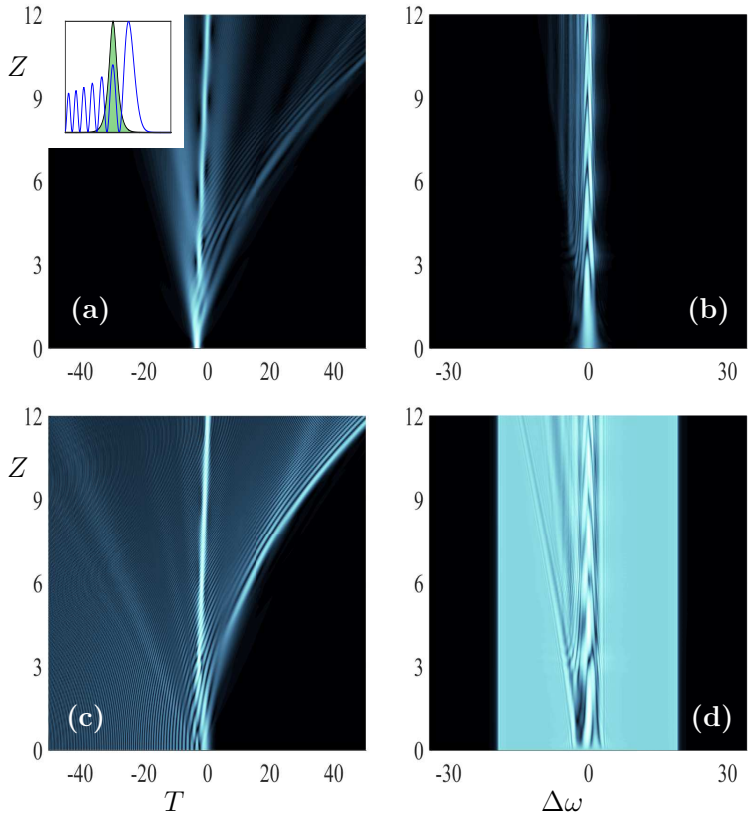

FIGURE 6.7: In the first column we show the dynamics of the signal/ control pulse respectively, while in the second column we show the corresponding spectra of the pulses. Thus the first/second row corresponds to the signal/ control pulse. The inset in (a) shows the initial condition of the signal(green shaded)/ control pulse. The signal is magnified for illustration purposes.

6.2.4 Signal localized at Airy's second minimum

To close this case too we will finally position the center of the signal at Airy′ *s* second minimum by substituting $t_0 = -4.0977$ and we got the following simulations:

In Figure 6.8 the center of the signal pulse is locate at Airy′ *s* second minimum. That means that due to the anomalous dispersion regime that the signal pulse is evolving this particular focal point is charachterized as a signal's potential maximum point. As a result the signal pulse is attracted from this particular focal point. The results in this focal point are not different. The high intensity signal pulse that we assumed dominates in comparison with the incapable to exhibit its dynamics Airy pulse. As a result the signal pulse evolves invariant totally ignoring

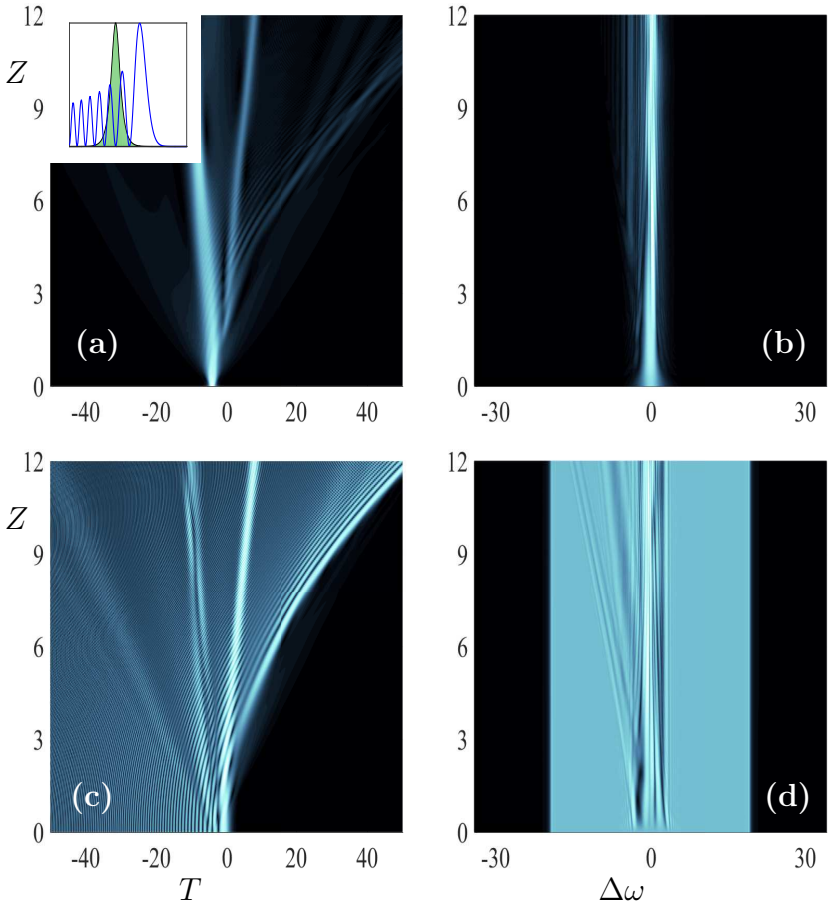

FIGURE 6.8: In the first column we show the dynamics of the signal/ control pulse respectively, while in the second column we show the corresponding spectra of the pulses. Thus the first/second row corresponds to the signal/ control pulse. The inset in (a) shows the initial condition of the signal(green shaded)/ control pulse. The signal is magnified for illustration purposes.

Airy′ *s* acceleration. This is a very characteristic case of a walk-off phenomena we mentioned in Chapter 1.

Chapter 7

Conclusion

The purpose of this thesis is to examine how a signal's guidance from an Airy pulse is possible. We have tested a variety of cases were both of those pulses are propagating in the same or different regime in order to conclude if this assumption is possible and under what circumstances. The results that we have shown above are sufficient enough to prove this argument while the exact propagating regime along with exact specifications that characterize each pulse are defined clearly. The guided pulse (signal) can be found to follow exactly the path of the guiding pulse (Airy).

Beginning from the linear case where the signal pulse is in a linear formation we assumed next a nonlinear formation for the Airy pulse depending the propagation regime . Proceeding with a variety of focal points that place the signal pulse in Airy$'s$ critical points. In particular interest is the regime that the signal and the Airy pulse are evolving and that's because signal's potential minima or maxima points are in direct correlation with the evolving regime. Some extra cases were added where it was necessary to examine how the the signal pulse will react with an Airy pulse if we place the signal after Airy$'s$ main lobe. The parabolic trajectories that we observed are a clear sign of affect of Airy on the signal pulse.

What we can exclude from this work is that we can use an Airy pulse in order to control the properties of a weak or even strong signal pulse. Signal's properties can vary as long as we vary Airy$'s$ parameters. Coefficients such as Airy$'s$ amplitude, truncation coefficient and the relative phase, play an essential role in the results we mentioned before.

References

[1] G. P. Agrawal, *Nonlinear Fiber Optics*. California 92101-4495,USA: Academic Press,Elsevir, fourth ed., (2007).

[2] H. H. Hopkins and N. S. Kapany, "A flexible fibrescope, using static scanning," *Nature*, vol. 173,1, no. 39-41, (1954).

[3] A. C. S. van Heel, "A new method of transporting optical images without aberrations," *Nature*, vol. 173, no. 39, (1954).

[4] A. Hasegawa and F. Tappert *Appl. Phys. Lett*, vol. 23, no. 142, (1973).

[5] L. F. Mollenauer and R. H. Stolen *Opt. Lett*, vol. 9, no. 13, (1984).

[6] L. F. Mollenauer, J. P. Gordon, and M. N. Islam *IEEE J. Quantum Electron*, vol. 22, no. 157, (1986).

[7] J. D. Kafka and T. Baer *Opt. Lett.*, vol. 12, no. 181, (1987).

[8] M. N. Islam, L. F. M. amd R. H. Stolen, J. R. Simpson, and H. T. Shang *Opt. Lett*, vol. 12, no. 814, (1987).

[9] A.S.Gouveia-Neto, A. S. L. Gomes, and J. R. Taylor *Opt. Quantum Electron*, vol. 20, no. 165, (1998).

[10] E. Desuvire, D. B. B. Desthieux, and S. Bigo, *Erbium-Doped Fiber Amplifiers: Device and System Development*. New York: Wiley, (2002).

[11] C. Headley, G. P. Agrawal, and Eds, *Raman Amplification in Fiber Optical Communication Systems*. Boston: Academic Press, (2005).

[12] A. Hasegawa and M. Matsumoto, *Optical Solitons in Fibers*. New York: Springer, (2002).

[13] Y. S. Kivshar and G. P. Agrawal, *Optical Solitons: From Fibers to Photonic Crystals*. Boston: Academic Press, (2003).

[14] N. Akhmediev and E. A. Ankiewicz, *Dissipative Solitons*. New York: Springer, (2005).

[15] L. F. Mollenauer and J. P. Gordon, *Solitons in Optical Fibers: Fundamental and Applications*. Boston: Academic Press, (2006).

[16] P. Diament, *Wave Transmission and Fiber Optics*. New York: Macmillan, (1990).

[17] Y. R. Shen, *Principles of Nonlinear Optics*. New York: (Wiley, (1984).

[18] M. Schubert and B. Wilhelmi, *Nonlinear Optics and Quantum Electronics*. New York: Wiley, (1986).

[19] P. N. Butcher and D. N. Cotter, *The Elements of Nonlinear Optics*. Cambridge, UK: Cambridge University Press, (1990).

[20] P. M. Morse and H. Feshbach, *Methods of Theoretical Physics*. New York: McGraw-Hill, (1953).

[21] D. Marcuse, *Light Transmission Optics*. New York: Van Nostrand Reinhold, (1982).

[22] G. P. Agrawal and M. J. Potasek *Phys. Rev*, vol. A 33, no. 1765, (1986).

[23] E. R. R. Alfano, *The Supercontinuum Laser Source*. New York: Springer, (1989).

[24] R. H. Stolen, E. P. Ippen, and A. R. Tynes *Appl. Phys. Lett.*, vol. 20, no. 62, (1972).

[25] R. G. Smith *Appl. Opt.*, vol. 22, no. 294, (1973).

[26] E. P. Ippen and R. H. Stolen *Appl. Phys. Lett.*, vol. 21, no. 539, (1972).

[27] J.-H. Lee, *Analysis and Characterization of Fiber Nonlinearities with Deterministic and Stochastic Signal Sources*. PhD thesis, Virginia Polytechnic Institute and State University, Blacksburg, Virginia, February 2000.

[28] R. H. Stolen and C. Lin *Phys. Rev*, vol. A 17, no. 1448, (1978).

[29] A. Hasegawa and F. Tappert *Phys. RevAppl. Phys. Lett.*, vol. 23, no. 142, (1973).

[30] V. I. Karpman and E. M. Krushkal *Sov. Phys. JETP*, vol. 28, no. 1997, (1971).

[31] N. Yajima and A. Outi *Prog. Theor. Phys*, vol. 45, no. 1997, (1971).

[32] R. H. Hardin and F. D. Tappert *SIAM Rev. Chronicle*, vol. 15, no. 423, (1973).

[33] R. A. Fisher and W. K. Bischel *Appl. Phys. Lett*, vol. 23, no. 661, (1973).

[34] R. A. Fisher and W. K. Bischel *J. Appl. Phys*, vol. 46, no. 4921, (1975).

[35] M. J. Ablowitz and J. F. Ladik *Stud. Appl Math.*, vol. 55, no. 213, (1976).

[36] I. S. Greig and J. L. Morris *J. Comput. Phys*, vol. 20, no. 60, (1976).

[37] B. Fornberg and G. B. Whitham *Phil. Trans. Roy. Soc.*, vol. 289, no. 373, (1978).

[38] M. Delfour, M. Fortin, and G. Payre *J. Comput. Phys*, vol. 44, no. 277, (1981).

[39] T. R. Taha and M. J. Ablowitz *J. Comput. Phys*, vol. 55, no. 203, (1984).

[40] D. Pathria and J. L. Morris *J. Comput. Phys*, vol. 87, no. 108, (1990).

[41] L. R. Watkins and Y. R. Zhou *J. Lightwave Technol*, vol. 12, no. 1536, (1994).

[42] M. S. Ismail *Int. J. Comput Math*, vol. 62, no. 101, (1990).

[43] K. V. Peddanarappagari and M. Brandt-Pearce *J. Lightwave Technol*, vol. 15, no. 2232, (1997).

[44] K. V. Peddanarappagari and M. Brandt-Pearce *J. Lightwave Technol*, vol. 16, no. 2046, (1998).

[45] E. H. Twizell, A. G. Bratsos, , and J. C. Newby *Math. Comput. Simul*, vol. 43, no. 67, (1997).

[46] W. P. Zeng *J. Comput. Math*, vol. 133, no. 17, (1999).

[47] I. Daq *Comput. Methods Appl. Mech. Eng*, vol. 247, no. 174, (1999).

[48] A. G. Shagalov *Int. J. Mod. Phys. C*, vol. 10, no. 967, (1999).

[49] Q. S. Chang, E. H. Jia, , and W. Sun *J. Comput. Phys*, vol. 148, no. 397, (1999).

[50] W. Z. Dai and R. Nassar *J. Comput. Math*, vol. 18, no. 123, (2000).

[51] S. R. K. Iyengar, G. Jayaraman, , and V. Balasubramanian *Comput. Math. Appl*, vol. 40, no. 1375, (2000).

[52] S. R. K. Iyengar, G. Jayaraman, and V. Balasubramanian *Comput. Math. Appl*, vol. 40, no. 1375, (2000).

[53] Q. Sheng, A. Q. M. Khaliq, , and E. A. Al-Said *J. Comput. Phys*, vol. 16, no. 1095, (2001).

[54] J. B. Chen, M. Z. Qin, , and Y. F. Tang *Comput. Math. Appl*, vol. 43, no. 1095, (2002).

[55] J. I. Ramos *Appl. Math. Comput*, vol. 133, no. 1, (2002).

[56] X. M. Liu, B. Lee, and I. Photon *Technol. Lett*, vol. 15, no. 1549, (2003).

[57] W. T. Ang and K. C. Ang *Num. Methods Partial Diff. Eqs*, vol. 20, no. 843, (2004).

[58] M. Premaratne *IEEE Photon. Technol. Lett*, vol. 1304, no. 16, (2004).

[59] G. M. Muslu and H. A. Erbay *Math. Comput. Simulation*, vol. 581, no. 67, (2005).

[60] O. V. Sinkin, R. Holzlohner, J. Zweck, and C. R. Menyuk *J. Lightwave Technol*, vol. 61, no. 21, (2003).

[61] T. Kremp and W. Freude *J. Lightwave Technol*, vol. 1491, no. 23, (2005).

[62] M. Berry and N. L. Balazs *Am. J. Phys.*, vol. 47, no. 264, (1979).

[63] D. Greenberger *Am. J. Phys.*, vol. 48, no. 256, (1980).

[64] K. Unnikrishnan and A. Rau *Am. J. Phys.*, vol. 64, no. 1034, (1996).

[65] J. Durnin *J. Opt. Soc. Am.*, vol. A 4, no. 651, (1987).

[66] J. Durnin, J. Miceli, and J. Eberly *Phys. Rev. Lett.*, vol. 58, no. 1499, (1987).

[67] J. Gutierrez-Vega, M. Iturbe-Castillo, and S. Chavez-Cerda *Opt. Lett.*, vol. 25, no. 1493, (2000).

[68] D. McGloin and K. Dholakia *Contemp. Phys.*, vol. 46, no. 15, (2005).

[69] R. Stutzle *Phys. Rev. Lett.*, vol. 95, no. 110405, (2005).

[70] L. Schiff, *Quantum Mechanics*. New York, NY: McGraw-Hill, 3rd ed., (1968).

[71] G. Siviloglou and D. Christodoulides *Opt. Lett.*, vol. 32, no. 979, (2007).

[72] N. K. Efremidis and I. Chremmos, "Caustic design in periodic lattices," *Opt. Lett.*, vol. 37, no. 1277, (2012).

[73] G. A. Siviloglou, A. D. J. Broky, , and D. N. Christodoulides *Phys. Rev. Lett.*, vol. 99, no. 213901, (2007).

[74] J. Baumgartl, M. Mazilu, , and K. Dholakia *Nat. Photon.*, vol. 2, no. 675, (2008).

[75] P. Polynkin, M. Kolesikc, J. V. Moloney, G. A. Siviloglou, and D. N. Christodoulides *Science*, vol. 324, no. 229, (2009).

[76] A. Salandrino and D. N. Christodoulides *Opt. Lett.*, vol. 35, no. 2082, (2010).

[77] P. Zhang, S. Wang, Y. Liu, X. Yin, C. Lu, Z. Chen, , and X.Zhang *Opt. Lett.*, vol. 36, no. 3191, (2011).

[78] A. Minovich, A. E. Klein, N. Janunts, T. Pertsch, D. N.Neshev, and Y. S. Kivshar *Phys. Rev. Lett.*, vol. 107, no. 116802, (2011).

[79] A. Chong, W. H. Renninger, D. N. Christodoulides, and F. W. Wise *Nat. Photon.*, vol. 4, no. 103, (2010).

[80] D. Abdollahpour, S. Suntsov, D. G. Papazoglou, and S. Tzortzakis *Phys. Rev. Lett.*, vol. 105, no. 253901, (2010).

[81] I. Chremmos, N. K. Efremidis, and D.N.Christodoulides *Opt. Lett.*, vol. 36, no. 1890, (2011).

[82] E. Greenfield, M. Segev, W. Walasik, , and O. Raz *Phys. Rev Lett.*, vol. 106, no. 213902, (2011).

[83] M. V. Berry and C. Upstill, *Progress in Optics*, vol. XVIII. E. Wolf, north-holland ed., (1980).

[84] Y. A. Kravtsov and Y. I. Orlov, *Caustics, Catastrophes and Wave Fields*. Springer, (1999).

[85] Z. Ye, S. Liu, C. Lou, P. Zhang, Y. Hu, D. Song, J. Zhao, and Z. Chen *Opt. Lett.*, vol. 36, no. 3230, (2011).

[86] V. Garces-Chavez, D. McGloin, H. Melville, W. Sibbett, and K. Dholakia *Nature*, vol. 419, no. 145, (2002).

[87] Z. Bouchal, J. Wagne, and M. Chlup *Opt. Commun.*, vol. 151, no. 207, (1998).

[88] C. Hwang, D. Choi, K. Kim, and B. Lee *Opt. Exp.*, vol. 18, no. 23504, (2010).

[89] W. Cai, M. S.Mills, D. N.Christodoulides, and S. Wen *Opt. Comm.*, vol. 316, no. 127-131, (2014).

[90] D. Miller *Nat.Photonics*, vol. 4, no. 3, (2010).

[91] T.A.Ibrahim, K.Amarnath, L. andR.Grover, V.Van, and P.-T.Ho *Opt.Lett.*, vol. 29, no. 2779, (2004).

[92] V. Almeida, C.A.Barrios, R.R.Panepucci, and M.Lipson *Nature*, vol. 431, no. 1081, (2004).

[93] V. Perlin and H.G.Winful *IEEEPhotonicsTechnol.Lett.*, vol. 13, no. 960, (2001).

[94] A. S. Wabnitz, Y.Kodama *Opt.FiberTechnol.*, vol. 1, no. 187, (1995).

[95] A.Demircan, S.Amiranashvili, and G.Steinmeyer *Phys.Rev.Lett.*, vol. 106, no. 163901, (2011).

[96] T.Ellenbogen, N.Voloch-Bloch, A.Ganany-Padowicz, and A.Arie *Nat.Photonics*, vol. 3, no. 395, (2009).

[97] Y. Hu, Z. Sun, D. Bongiovanni, D. Song, C. Lou, J. Xu, Z. Chen, and R. Morandotti *Opt.Lett.*, vol. 37, no. 3201, (2012).

[98] J. IdoKaminer, Nemirovsky, and M. Segev *Opt.Express*, vol. 20, no. 18827, (2012).

[99] A.Rudnick and D.M.Marom *Opt.Express*, vol. 19, no. 25570, (2011).